ProQuest LLC.
789 East Eisenhower Parkway
P.O. Box 1346
Ann Arbor, MI 48106 – 1346

Intumescent Mechanisms of Fire-Retarding Polyurethane Systems and Development of Graphite/Polymer Nano-composites

Qingchun Yuan

A report submitted in fulfilment of the requirements of
The Nottingham Trent University for the degree of Doctor of Philosophy

This research was carried out in
The Polymer Engineering Centre, College of Science & Technology,
The Nottingham Trent University,
Burton Street, Nottingham, NG1 4BU, UK

September 2004

This thesis is classified.

Abstract

As an effective and environmentally friendly fire retarding approach, intumescence has been applied to design better fire retarding polymer systems for different applications. However, intumescent mechanisms have not been well understood. This has hindered the further development of intumescent fire retarding polymer systems. This research investigated the intumescent mechanisms of three commercial fire retarding polyurethane products and developed a new generation of fire retarding products based on graphite/polymer nanocomposites.

The three commercial products were studied using a single direction well-ventilated natural burning method and a series of intumescent char characterisation techniques developed in this research. The natural burning method was designed to show the protection and protection efficiency of intumescent chars. The protection efficiency was measured by the difference of char yields between natural burning and furnace burning. The intumescent chars produced by natural burning were investigated for their char structures, gas permeability, bulk strength and reactivity using microscopic methods, open porosity, durometer hardness and X-ray diffraction, respectively. Experimental results show that the three commercial products contain inert inorganic additives. The charring ability of the polymers is important in producing integrated chars by binding the inert additives together, and in strengthening the chars. An integrated char with lower open porosity has higher protection efficiency. The lower porosity also results in the char with higher strength.

Graphite/polymer nanocomposites were synthesised by solution intercalation and *in situ* polymerisation methods. Five graphites were modified into graphite oxides (GO) by oxidation. A chosen GO was intercalated with a polyethylene oxide (PEO), polyethylene glycol Mn1500 (PEG1500) or polyvinyl pyrrolidone (PVP) in water. The GO and its PEG1500 or PVP intercalated compounds as nano-structured graphites were used in the synthesis of polyurethane nanocomposites. The nanostructured graphites were intercalated with the polyol polyethylene glycol Mn300 (PEG300), and then polymerised with the tolylene diisocyanate (TDI). The graphite/polyurethane nanocomposites synthesised contain 5.0 wt.% of GO or equivalent.

The fire retardant study of all the nanocomposites showed a non-dripping and slow burning process. The burning produced integrated chars with improvement in not only char morphology but also char yield. The chars have graphitised structure, which is ideal in terms of anti-oxidation of the char. Graphite/polymer nanocomposites are a new generation of intumescent fire retarding polymer systems.

Acknowledgements

The author wishes to thank the following people and organisations for their respective contribution in preparing this thesis.

Firstly, I would like to express my appreciation to my supervisors Dr. Fengge Gao, Head of Polymer Engineering Centre, and Professor Barry Hull, Dean of the faculty of Construction, Computing and Technology, for their support and guidance throughout my PhD study.

Special thanks go to the Hilti A.G., which sponsors the project of this PhD study, Dr. Arne Reiheimer and Dr. Antje Wenzel, who came to meet and discuss the progress of the project from the Hilti A.G..

No words can describe my gratitude to Miss Judith Kipling for her true friendship, encouragement, discussion, support and correcting the English.

Special thanks go to my husband, daughter for encouraging me to undertake this study and their generous support. Deep love and respect go to my parents and siblings for their understanding and encouragement.

I also thank the fellow students who were involved in the polymer materials research and who worked in the FRI.

List of Symbols and Abbreviations

Aldrich-F	Graphite flake from Aldrich
Aldrich-GO	Graphite oxide made from Aldrich-P
Aldrich-P	Graphite powder from Aldrich
APP	Ammonium polyphosphate
BDH-GO	Graphite oxide made from BDH-P
BDH-P	Graphite powder from BDH
CY	Char yield
Db	Bulk density
DSC	Differential scanning calorimeter
GC-MS	Gas chromatography mass spectrometry
GO	Graphite oxide
Hd	Durometer hardness
HRR	Heat release rate
Hv	Vicker hardness
LUH-GO	Graphite oxide made from LUH-P
LUH-P	Graphite powder from LUH A.G.
MDI	4,4'-methanediphenyldiisocyanate
Nano-structured graphite	Interlayer spacing expanded graphite products
NGS-GO	Graphite oxide made from NGS-P
NGS-P	Graphite powder from NGS A.G.
NMR	Nuclear magnetic resonance
OI	Oxygen index
Organo graphite oxide	Polymer intercalated graphite oxide
PAN	Polyacrylonitrile
PEG1500	Polyethylene glycol with a number average molecular weight of 1500
PEG300	Polyethylene glycol with a number average molecular weight of 300
PEO	Polyethylene oxide
PMMA	polymethymethacrylate
Po	Open porosity
PS	Polystyrene

PU	Polyurethane
PVA	Polyvinyl alcohol
PVC	Polyvinyl chlorine
PVP	Polyvinyl pyrrolidone
Py-MS	Pyrolysis mass spectrometry
SEM	Scanning electron microscopy
TDI	Tolylene diisocyanate
TEM	Transmission electron microscopy
TGA	Thermo gravimetric analysis
TPU	Thermoplastic polyurethane
XRD	X-ray diffraction
50%GO+PEG1500	50 wt.% of PEG1500 intercalated graphite oxide
50%GO+PVP	50 wt.% of PVP intercalated graphite oxide

Contents

Chapter 1

Introduction

1.1 Background for the research

Since the 1950's, synthetic polymer materials in the form of rubbers, plastics and fibres have gradually replaced conventional cellulose materials and even metals until, at the present time, they represent a large proportion of the materials used. These synthetic pure polymers are often inflammable and have poor mechanical properties. A lot of research on polymers has been dedicated to producing polymer materials with lower flammability and better mechanical properties.

Research on the fire retardancy of polymers has shown that char-forming polymers have lower flammability [1] and release heat more slowly than non-char-forming polymers.[2] The char has been designed to occur in the form of intumescent or swollen chars on the surface of the burning polymers. This process is called Intumescence, it is more and more widely used as a polymer fire retardant mechanism. The carbonaceous char formed on the polymer surface acts as a physical barrier to inhibit the diffusion of the decomposed flammable volatiles into the flame region and to protect the polymer underneath the char from heat. Such a condensed phase action can significantly reduce the evolution of toxic species and hence has become a popular solution for developing environmentally friendly fire retarding polymer materials. This has been regarded as the most successful approach of all the traditional fire retarding mechanisms. [3]

However, little work has been done on the intumescent char formation mechanisms. Effective techniques for the characterisation of intumescent chars have not been developed.[4,5] This lack of knowledge has hindered not only the understanding of intumescent mechanisms, but also the design of better fire retarding polymer systems. Developing characterisation techniques for intumescent chars and understanding intumescent mechanisms and their relation to the efficiency of fire retardancy is essential for designing better intumescence systems.

Furthermore, the conventional intumescent fire retarding approach normally needs more than 40% of fire retardants to meet the requirements of increasingly stringent

legislation, which usually results in a reduction of mechanical properties by about 20%.[5] The addition of a large amount of fire retardants also causes processing difficulties and migration of the fire retardants during applications. The invention of clay/nylon 6 nanocomposites has shown that these problems can be overcome.[6] The clay/nylon 6 nanocomposites not only have improved thermal stability and char formation, but also have significantly enhanced mechanical properties by adding just 5% of clay. Due to the low amount of clay added and the interaction between the clay layers and nylon 6, the addition of clay should not cause any processing or migration problems.

Graphite not only has a similar two-dimensional layered structure to clay, its graphite sheets also have both excellent mechanical properties and an ideal structure of carbonaceous chars. Graphite/polymer nanocomposite technology is a promising approach to produce less flammable and stronger polymer materials.

1.2 Aims and Objectives

As discussed above, the mechanism of intumescence is not well understood, whilst nano-technology has shown to be a promising approach to improve a wide range of engineering properties of polymers. Based on this information and the requirement of Hilti A. G., the sponsor of this project, this project is aimed at acquiring an understanding of intumescent mechanisms of existing polyurethane based fire stopping products and to use the knowledge obtained to design a new generation of fire retarding products using a graphite/polymer nanocomposite approach.

To achieve the project goals, the following objectives have been investigated.

- Development of experimental techniques for the characterisation of intumescent chars,
- Mechanistic studies of char formation during combustion of polymer systems and their relation to fire resistance properties,
- Modification of natural and synthetic graphites for the manufacture of nanocomposites,
- Exploration of synthetic methods to produce graphite/polymer nanocomposites,

- Investigation of the relationships between the nano-structure of the composites and fire resistance.

Based on the completion of the objectives, this thesis is arranged in eight chapters. Following this introduction, a literature review on polymer fire retardancy, carbon fibre polymer composites and clay and graphite/polymer nanocomposites is given. After the literature review, a chapter on experimental techniques used in this research follows. The experimental results are presented and discussed in Chapters 4 to 7. Chapter 4 is about development of methodologies for the characterisation of intumescent chars. In Chapter 5, the characterisation techniques developed in the previous chapter are applied to examine the intumescent mechanisms of three existing commercial fire stopping polyurethane products. Chapters 6 and 7 are on the development of graphite/ polyurethane nanocomposites. In Chapter 6, graphite is modified into nano-structured graphite, which is used in the synthesis of graphite/polyurethane nanocomposites in Chapter 7. Finally, Chapter 8 ends with conclusions drawn from this study and suggestions for further work.

Chapter 2
Literature Review

The aims of this project are to understand the intumescent mechanisms of fire retarding polymer systems and to synthesise nanocomposites from graphite and polyurethanes with improved fire retardancy without affecting other properties. The literature review, therefore, covers the fire retardancy of polymers, graphite-structured carbon fibre polymer composites and clay or graphite polymer nanocomposites as well as their fire retardancy. The chapter is arranged in three sections. Firstly, fundamentals of the fire retardancy of polymers are discussed, especially their thermal decomposition, also conventional fire-retarding of polyurethanes and current research on intumescent fire retardancy. The second section deals with graphite-structured carbon fibre polymer composites, including the structure and properties of graphite and carbon fibres, carbon fibre polymer composites and their fire retardancy. Finally, the development in the synthesis, properties and fire retardancy of clay or graphite/polymer nanocomposites is examined.

2.1 Fundamentals of polymer combustion and fire retardancy

Polymers are inflammable. In terms of fire safety, the major interest in the polymer industry is not the fact that their products burn but how to render them less likely to ignite and, if they are ignited, to burn much less efficiently. This phenomenon is termed Fire Retardance. By understanding polymer combustion process, a few fire-retarding approaches have been developed, which have been used to design fire retardant polymer systems.

2.1.1 Polymer combustion process and current fire retarding approaches

2.1.1.1 Polymer combustion process

The polymer combustion process occurs in the same way as a candle flame. The flame produces the major heat to maintain the burning, while the condensed phase supplies

fuel to the flame. Provided the supply of fuel and the release of heat exceed the energy required for combustion, the combustion proceeds at an increasing rate until an explosion occurs. If the energy supply is constant and equals the demand, a stationary equilibrium will be established, this is, a steady burning occurs. If the available energy is lower than that required to maintain this equilibrium, the rate of combustion will then decrease until the flame extinguishes.[5] A model describing the steady burning process, mass and heat transfer of polymer combustion in a real fire is shown in Figure 2.1.

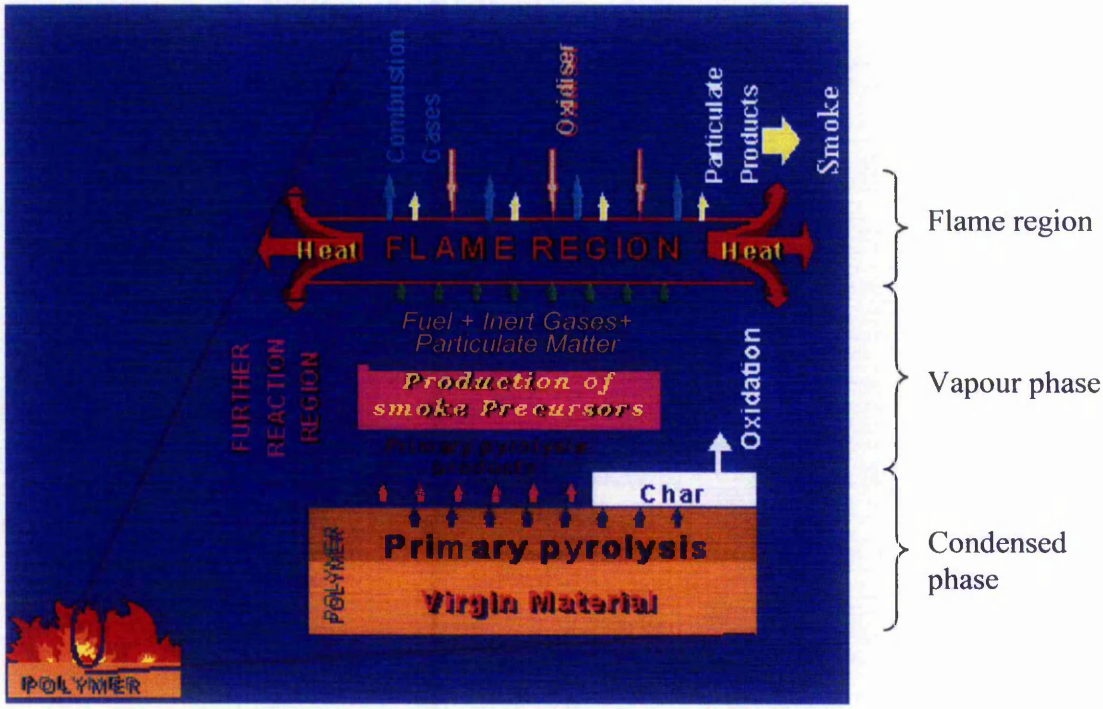

Figure 2.1 A model of polymer combustion in a real fire[7]

The polymer, in the condensed phase, decomposes producing volatiles and residues on the surface of the condensed phase. The decomposed volatiles are released from the condensed phase, passing a vapour phase and then burning in a flame region. In the flame region, the combustion carries out in free radical exothermic reactions. The reactions are maintained by internally generated free radicals and heat. The heat released from the flame partially transfers back through the vapour phase to the condensed phase, which allow more polymer to decompose. This process maintains the supply of fuel to the flame region. The volatiles immediately decomposed from the polymer are called primary pyrolysis products. The primary pyrolysis products will react further in the vapour phase, producing secondary or further pyrolysis products and smoke precursors. These products react with oxygen from the air and burn to generate

heat and combustion products in the flame region. The combustion process is sustained in a cycle as described in Figure 2.2.

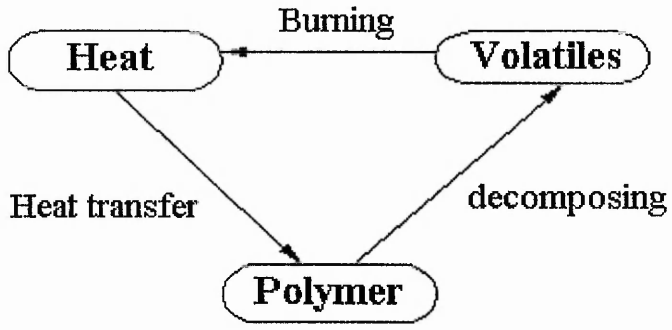

Figure 2.2 Polymer combustion process

The decomposition of polymers generates fuel. The fuel moves to the flame region and burns. The burning produces heat. The heat transfers back to the polymer maintaining the decomposition. When any of these factors in this cycle are weakened, the self-sustaining burning will be retarded or stopped. In accordance with polymer burning processes, the following fire retarding approaches have been developed to improve the fire resistance of polymers:

- Modifying the backbone structure of polymers to improve the thermal stability and reduce the decomposition,
- Adding materials that will inhibit burning in the gas phase,
- Adding materials that decompose endothermically to lower the temperature of the burning polymer,
- Adding materials that decompose into non-flammable volatiles to dilute the combustible gases,
- Adding materials to promote char formation at the burning polymer surface acting as a barrier to hinder heat transfer from the flame to the polymer and mass transfer of the decomposed volatiles of the polymer to the flame.

Among the above five approaches, the first one enhances the thermal stability of polymers by modifying their chemical structure via such as incorporating silicon-

containing units or aromatic rings into the polymer backbones. This approach is more expensive than additive approaches. For commodity polymers, the low cost of the materials requires that the fire retarding approach should also be of low cost. This limits the applicable solutions primarily to the additive methods. One fire retardant may have more than one function during combustion. The commonly used fire retardants work mainly in one of the following three ways: vapour phase fire retarding, endothermic fire retarding and char forming fire retarding.

2.1.1.2 Vapour phase fire retarding

Vapour phase fire retarding is achieved by adding materials that scavenge reactive free radicals, decreasing the free radical propagation both in the vapour phase and the flame region, finally resulting in incomplete combustion and reducing the burning rate of polymers. Compounds containing bromine and chlorine are particularly effective because their gaseous intermediates scavenge more active flame propagating free radicals, for example hydrogen radicals and hydroxyl radicals, thereby reducing the combustion rate of the flame. The most important scavenging reactions are as follows:

$$H\cdot + HX \rightleftharpoons H_2 + X\cdot \qquad \text{Reaction 2.1}$$

$$OH\cdot + HX \rightleftharpoons H_2O + X\cdot \qquad \text{Reaction 2.2}$$

The halogen free radicals tend to recombine to become relatively stable halogen molecules. Reaction 2.1 is found to be about twice as fast as Reaction 2.2. The high value of the ratio H/OH in the flame front indicates that Reaction 2.1 is the main inhibiting reaction. The radical trapping is the most important but not the only activity of the halogenated fire retardants. The physical factors such as the density and mass of the halogen and its heat capacity also have a profound influence on fire retardancy. [5,8]

Bromine is the most effective and widely used halogen element in fire retardants. It performs most of its flame retardant function in the vapour phase by means of two mechanisms: redirection or termination of the chemical reactions involved in combustion; the evolution of heavy bromine-containing gases which tend to protect the condensed phase by inhibiting access of oxygen and heat transfer. This results in the reduction of the heat released by combustion and the heat feeding back from the flame to the burning polymer surface. [8]

Chlorine is believed to perform its flame retardant function in both the vapour and condensed phases. In the gaseous phase, it functions in the same way as bromine. In the condensed phase, it redirects the chemical reactions involved in decomposition. The chemical reactions may involve halogenation followed by dehydrohalogenation, to yield a polymeric residue rich in double bonds that is then converted to char.[8]

The statistical data shows that halogen-containing fire retardants account for nearly half of the global consumption of fire retardants in 1997. However, the use of some traditional halogenated fire retardants caused concern due to the possible formation of toxic halogenated dioxins or dibenzofurans.[9] Recycling of halogen-containing waste is also difficult. The future of halogen based fire retardants is not promising due to increasingly stringent environmental legislation.

2.1.1.3 Endothermic fire retarding

Endothermic fire retarding occurs when materials are added to polymers, which decompose endothermically to lower the temperature of burning polymers. Typical endothermic fire retardants are aluminium trihydroxide, $Al(OH)_3$, and magnesium hydroxide, $Mg(OH)_2$. Aluminium trihydroxide, for example, contains 34.6% of chemically bound water that is released when exposed to heat. The release of water commences at approximately 180-200°C accompanied by an increase in enthalpy of 1300 KJ/kg. The relatively low decomposition temperature restricts the use where processing temperatures are above 180°C. The major endotherm and water liberation occur at the temperatures between 270 and 320°C, Reaction 2.3: [10]

$$2Al(OH)_3 \xrightarrow{180\text{-}330^{\circ}C} Al_2O_3 + 3H_2O - 203KJ \qquad \text{Reaction 2.3}$$

Magnesium hydroxide is more attractive than aluminium trihydroxide in that it begins to decompose at much higher temperatures, 300-320°C, and has an increase in enthalpy of decomposition of 1450 KJ/kg. This allows its use in thermoplastics that are processed at temperatures too high for aluminium trihydroxide.

2.1.1.4 Char forming fire retarding

Char forming fire retardants operate mainly in the condensed phase. They promote the formation of a layer of char on burning polymer surfaces. The formed char layer

provides both thermal insulation to reduce the decomposition of the underlying polymer and a mass transport barrier to prevent or delay the escape of decomposed volatiles as fuel into vapour phases.

Char forming fire retardants are mainly phosphorus containing compounds. They increase the amount of carbonaceous char by redirecting the chemical reactions of polymer decomposition in favour of forming solid carbon materials.

Lyons has proposed that phosphorus compounds such as polyphosphate as fire retardants decompose to acid fragments under heating. These acids form polymeric species which act as effective dehydrating and esterifying agents. The following reactions represent the reactions. [11]

i. Formation of phosphorus acid by heat:

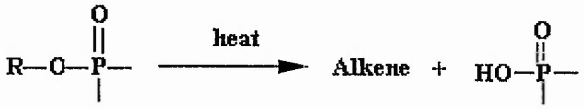

ii. Polymerization to form polyacids:

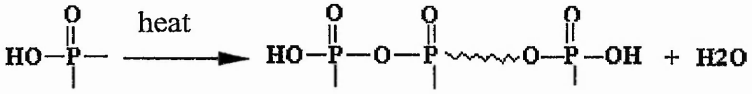

iii. Esterification with char promoter, for example an alcohol, followed by dehydration

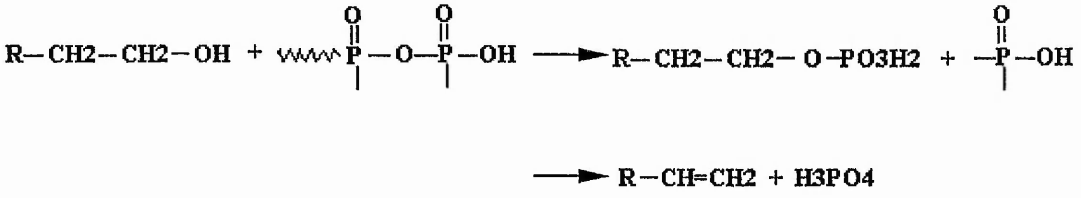

The resulting compounds may then undergo cross-linking or other reactions to form char.

The action of phosphorus containing compounds is particularly desirable as they are effective in the stage of decomposition in condensed phases rather than in the stages of ignition or combustion in gaseous phases. This increases the probability of arresting the

burning process at an earlier stage. By comparison of relative effectiveness of phosphorus and bromine indicates that 1% of phosphorus is equivalent to approximately 6% of bromine in polyolefins and polystyrene, 4-5% of bromine in polyesters and 5-7% of bromine in polyurethanes. The char forming fire retardants are more effective in char forming polymers than in non-char forming polymers. [8]

2.1.1.5 The assessment of fire retarding polymer systems

The efficiency of fire retardant polymers can be assessed by different burning tests. However, the burning process of polymers varies not only with the difference in the form of polymers (fibres, coatings, plastics) but also with fire scales. For scientific study, laboratory-scale assessments are adopted. In terms of fire resistance, ignitability and burning efficiency are the most important issues. Studies on the fire retarding behaviour of polymers generally include following aspects: ignitability, fire propagation and heat output.

The ignitability of polymers is usually evaluated by oxygen index (ASTM D 2863-87) to assess how readily a polymer will catch fire in a specified controlled atmosphere. An apparatus of the oxygen index is shown in Figure 2.3.

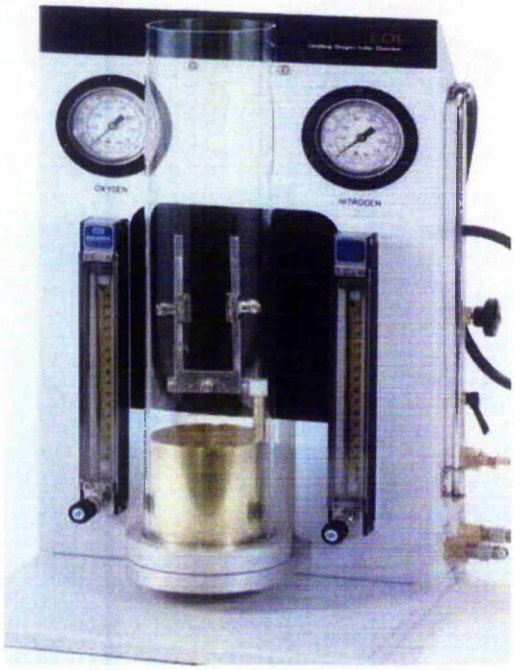

Figure 2.3 An apparatus used to determine the oxygen index[12]

A prepared sample is fixed vertically on the sample holder in the cylinder. Oxygen and nitrogen are metered separately and flow through the cylinder from the base up. A gas flame is applied to ignite the sample at the top and removed once ignition has occurred. The lowest oxygen concentration in the inflow gases of oxygen and nitrogen is determined in terms of just supporting sustained burning to reach the minimum burning length criterion. This lowest oxygen concentration is defined as the oxygen index (OI), that is

$$OI = \frac{[O_2]}{[O_2]+[N_2]} \times 100 \qquad \text{Equation 2.1}$$

where $[O_2]$ and $[N_2]$ are the minimum oxygen concentration and the corresponding nitrogen concentration in the inflow gases, respectively.

The minimum burning length criterion typically takes either a length of material being burned or a minimum length of time for the sample to burn before it self-extinguishes.

Since air is comprised of approximately 21 vol.% of oxygen, any material with an oxygen index less than 21 will burn readily in the ambient environment. In contrast, a polymer with an oxygen index greater than 21 will be less ignitable and will have a lower tendency to propagate a fire. Consequently, the material is defined as highly flammable when its OI is less than or equal to 21, while the polymers with oxygen index between 21 and 28 are referred as being slow-burning. Materials with an oxygen index greater than 28 are generally self-extinguishing.[13,14] The effectiveness of fire retardants is measured by the change in the oxygen index.

The fire propagation and heat output can be measured by a Cone Calorimeter (ASTM E1354), which was developed in the 1980s at the National Bureau of Standards.[15,16] The principle of Cone Calorimeter is shown in Figure 2.4.

The Cone Calorimeter applies a radiative heat source to heat a sample one-dimensionally and uniformly. During the measurement a sample is exposed to an external heat flux at either 35 kw/m^2 or 40 kw/m^2 in air. The ignition time, heat release rate, heat of combustion, mass loss rate as well as the components of the exhaust gases are measured during the experiment to describe the fire properties of polymers. The Cone Calorimeter is accepted as a bench-scale fire test.

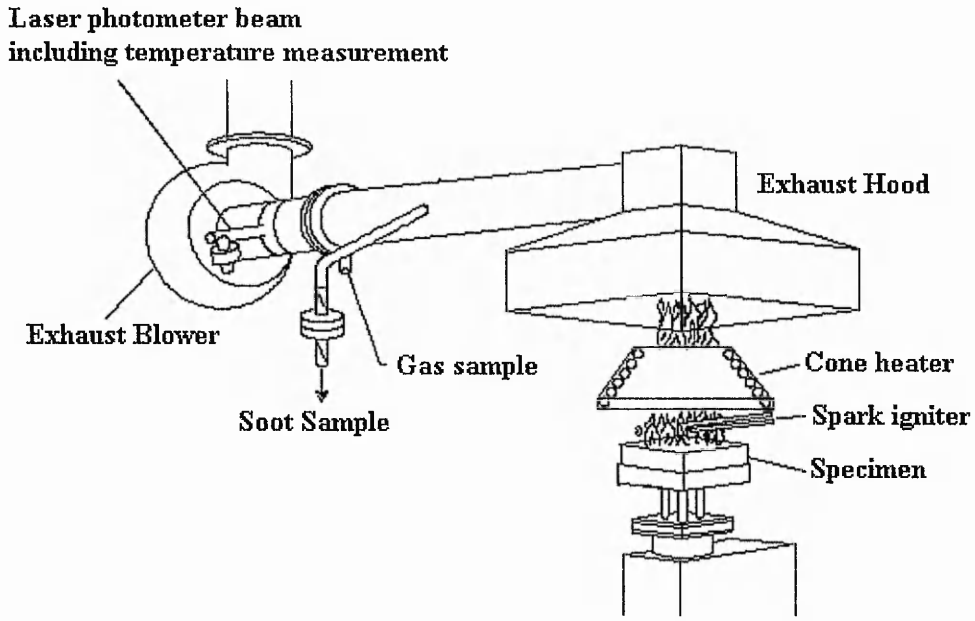

Figure 2.4 The principles of the Cone Calorimeter[17]

2.1.2 General decomposition mechanisms of most polymers

Combustible volatiles from decomposed polymers fuel the polymer combustion, as described in Figure 2.1. The decomposition performance of polymers, therefore, has a vital influence on the flammability of polymers and the selection of their fire retarding methods. The chemical structure of polymers plays the most important role in their thermal stability and char formation. In terms of char formation polymers can be classified into non-char-forming polymers and char-forming polymers.

Non-char-forming polymers undergo almost complete degradation and produce little char. In thermal degradation, these polymers decompose into small fragments by random- or end-chain scissions, or sometimes by a mixture of these mechanisms.

The reactions consist of random- or end-chain initiated free radical scissions, propagation, intermolecular or intramolecular transfer and termination of radicals. Polyethylene and polypropylene are typical examples of polymers that undergo random-chain scission yielding smaller molecular fragments but only a very small amount of monomers. Polymers undergoing end-chain scission produce mainly monomers. For example, Polymethymethacrylate, PMMA, undergoes a reversal of the polymerisation reaction and yields 91-98% monomer. Polymethacrylonitrile, poly-α-methystyrene and polytetrafluoroethylene also depolymerise when heated. Polystyrene decomposes by a

mixture of random- and end-chain scissions, yielding up to 50% monomer together with some oligomeric fragments. [18]

The char-forming polymers produce a lower amount of volatiles and a char by thermal decomposition. These polymers have reactive side groups attached to their backbones and degrade initially by releasing these reactive side groups through chain-stripping and cross-linking reactions. The former reaction results in the formation of π-bonds in the residue. Polyvinylchloride and polyvinyl alcohol, for example, decompose by releasing hydrogen chloride and water, respectively, in the initial stage. The π-bonds in the residue then break down into smaller fragments. The conjugated alkene fragments react further through cyclization, aromatisation, cross-linking and condensation to form a char.[18]

Polyacrylonitrile is a typical example, it undergoes mainly cyclization at lower temperatures followed by aromatizaton (dehydration) at higher temperatures, as shown schematically in Reaction 2.4, and ultimately carbonisation into condensed aromatic structures at elevated temperatures.[19] For this reason, polyacrylonitrile has been used in the production of carbon fibres.

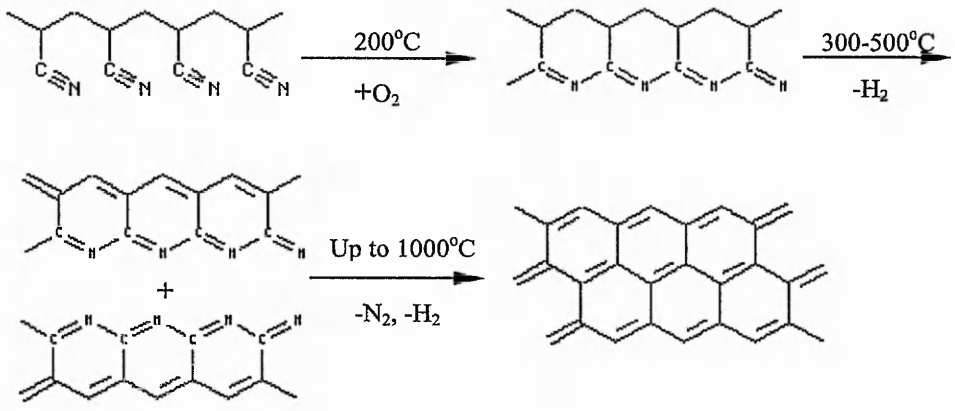

Reaction 2.4

Polyurethanes, diene polymers, aromatic and heterocyclic backbone polymers can also form chars.

2.1.3 Progress in the fire retarding study of polyurethanes

The major investigation in this project is related to the synthesis, decomposition and charring of polyurethanes. The polyurethane chemistry, the understanding thermal decomposition of polyurethanes in the vapour phase and the charring behaviour in the condensed phase, therefore, will be reviewed.

2.1.3.1 Polyurethane chemistry [20-22]

Polyurethanes are formed by reacting a polyol (an alcohol with two or more reactive hydroxyl groups per molecule) with a diisocyanate or a polymeric isocyanate in the presence of suitable catalysts and additives. The general addition reaction is shown in Reaction 2.5.

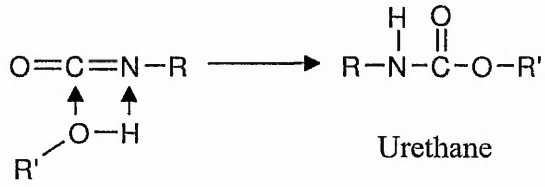

Reaction 2.5

where R and R'are the rest parts of the diisocyanate or the polyol, respectively.

The isocyanate groups are also able to react with the newly formed urethanes or other functional groups that have active hydrogen if the isocyanate groups are in excess compared to the hydroxyl groups in the reaction system. The isocyanate group reacts with the urethane group and forms allophanates, Reaction 2.6. These reactions can be utilised to obtain crosslinked structures.

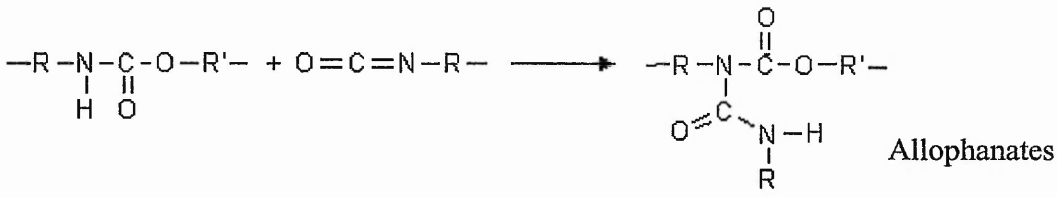

Reaction 2.6

Isocyanates react readily with water producing unstable carbanicacids which then decompose to amines and carbon dioxide, as shown in Reaction 2.7. The carbon dioxide is liberated as a gas and causes foaming.

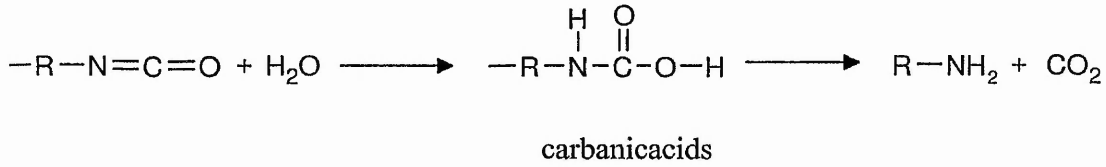

Reaction 2.7

The amines formed in the above reaction react with isocyanate groups forming biurets, Reaction 2.8.

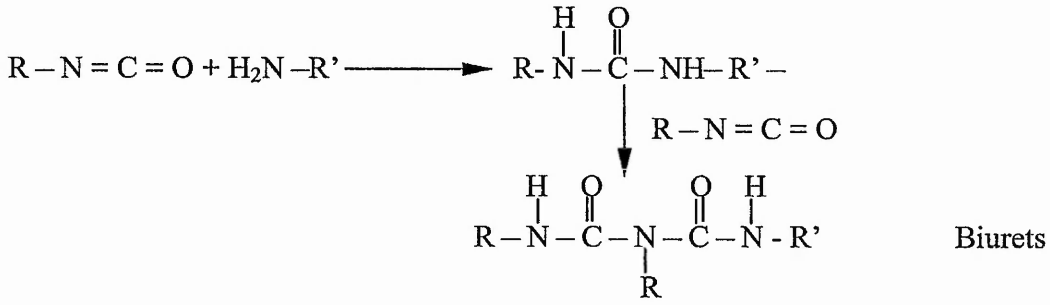

Reaction 2.8

Isocyanate groups can also react with each other to produce uretidinediones by dimerization and isocyanurates by trimerization, as shown in Reaction 2.9 and 2.10.

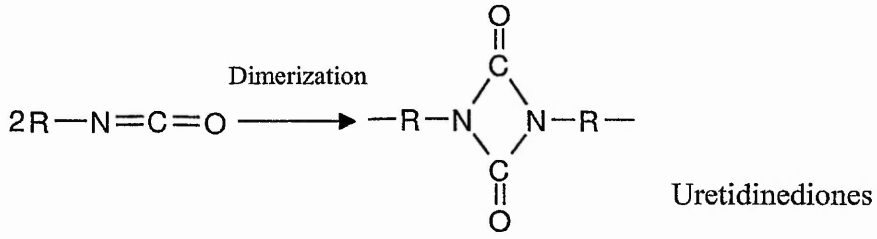

Reaction 2.9

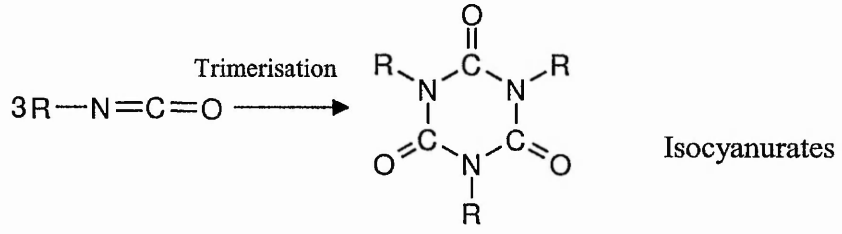

Reaction 2.10

The isocyanate-polyol stoichiometry, which is expressed as Isocyanate Index, plays an important role in determining the structure and thermal properties of polyurethanes. The isocyanate index is defined as the amount of isocyanate used in the synthesis of polyurethane relative to the theoretical equivalent amount of diols, i.e.,

$$\text{Isocyanate Index} = \frac{\text{The amount of isocyanate used}}{\text{The theoretical amount of isocyanate required}} \times 100$$

Equation 2.2

Polyurethanes can be synthesised into very different and useful products such as thermoplastics, flexible foams and rigid foams, by adjusting the isocyanate index, the chemistry of the raw materials and formulations.

Thermoplastic polyurethanes, noncrosslinked polyurethanes, are synthesised by using linear diol compounds, which have two hydroxyl groups, and excess diisocyanate to form a prepolymer. The prepolymer is then reacted with a chain extender in exact molar proportions calculated from the free isocyanate present. Chain extenders are low molecular weight difunctional compounds containing active hydrogen, such as 1,4 butane diol. They are often used to cure prepolymers, and their role is to increase the molecular weight of urethane polymers without affecting elongation at break for elastomer or plastic products.

Flexible polyurethane foams have open-cell structures that allow free movement of air throughout the foams when compressed. Flexible polyurethane foams are produced typically by reacting tolylene diisocyanate (TDI, Figure 2.5) with a polyol, and have an isocyanate index close to 100.

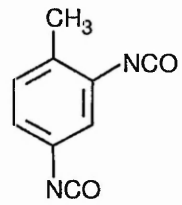

2,4-Tolylene diisocyanate

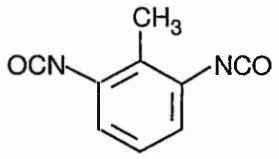

2,6-Tolylene diisocyanate

Figure 2.5 The chemistry structures of tolylene diisocyanates

Carbon dioxide is the principal blowing agent for flexible polyurethane foams. It is usually produced by the reaction between an excess of diisocyanate with water. Sometimes liquid carbon dioxide can also be used.

Rigid polyurethane foams are highly cross-linked polymers with a closed cell structure - each bubble within the material has closed walls so that gas movement is not possible. These materials have good structural strength in relation to their weight and outstanding thermal insulation properties. This has led to their widespread use as insulants in buildings and refrigerators.

A polymethylene polyphenylisocyanate (polymeric MDI) containing 4,4'-methane-diphenyldiisocyanate (MDI) and a polyol, both having functionality higher than 2, are normally used to produce cross-linked polyurethanes. The chemical structures of MDI and polymeric MDI are shown in Figure 2.6.

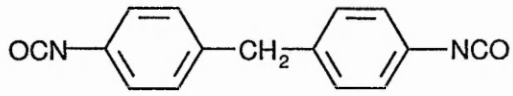

4,4'-methanediphenyldiisocyanate (MDI)

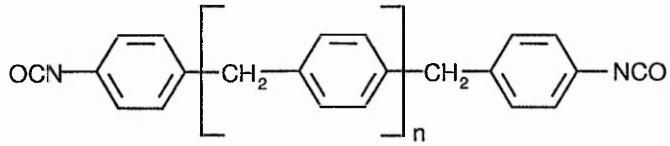

polymeric MDI

Figure 2.6 The chemical structures of MDI and polymeric MDI

The isocyanate index of rigid polyurethane foams may be much higher than 100. As a result of the considerable excess of isocyanate, the foams may have considerable amounts of isocyanurate structures that impart deformation resistance and thermal stability to the foam. Hydrofluorocarbons or other blowing agents are usually contained within the cells. As these substances have a much lower thermal conductivity than air, such cell-closed foams have a significantly lower conductivity than open-celled foams. To retain this low thermal conductivity the gas must not leak out. Consequently, rigid polyurethane foams for insulation applications must have at least 90% closed cells.

Catalysts are required to facilitate polyurethane formation, although isocyanates react readily with linear polyols, but the rate of reaction decreases rapidly as the size of the substituents on the alcohols increases. Mild and strong bases are used for the isocyanate and alcohol reactions. Commonly used catalysts are tertiary amines, for example, tri-ethylene diamine, 1,4-diazo(2,2,2)bicyalooctane (DABCO) and Ti(II) caprylate.

2.1.3.2 The decomposition of polyurethanes

The decomposition of polyurethanes has been studied by analysing the pyrolytic vapour products of the polymers. In early studies, decomposed volatiles were trapped in liquid nitrogen. The products collected were analysed using various characterisation techniques. [23-27] On-line techniques such as pyrolysis mass spectrometry (Py-MS) [28-34] and gas chromatography mass spectrometry (GC-MS) [35] methods have been used over the last few decades to obtain information on the pyrolysis reactions. Recently, laser-pyrolysis time-of-flight mass spectrometry has been used to simulate real fire situations to investigate the primary pyrolysis reactions of polyurethanes and its derivatives.[34] According to these research findings, the decomposition of polyurethanes may be involved in one or more of the following mechanisms:

i. Depolymerisation: polyurethanes are decomposed into their precursors: the isocyanates and polyols.

Reaction 2.11

ii. Dissociation into a primary amine, an olefin and carbon dioxide via putative six-membered ring transition states.

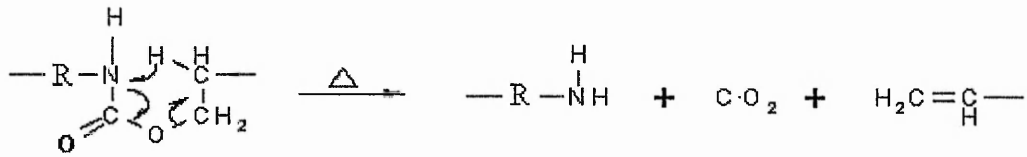

Reaction 2.12

iii. Dissociation into a secondary amine and carbon dioxide through a four-membered ring transition state:

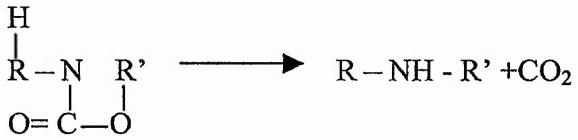

Reaction 2.13

Many researchers have reported that depolymerisation is a major route for the polyurethane decomposition. However, by the trapping method, Woolley[23,24] succeeded in recovering only 1% of the TDI from the decomposition vapour phase of commercial flexible foams at 200-300°C. Polyol type materials have been confirmed in the residue of linear polyurethanes[25,26] and commercial PU foams,[23] but such residues, although very similar to, were not exactly identical to the source polyols.

According to Reaction 2.13, the decomposition should yield CO_2 as the only volatile material at low temperatures. All the nitrogen should remain in the non-volatile residue, which should produce a residue with nitrogen content higher than that of the original foam. The experimental findings did not support this mechanism.[23] The foam structure collapsed on heating, and this was accompanied by a loss of one third of the foam weight. The residue contains little or no nitrogen. Therefore, if Reaction 2.13 is involved at all, it might play only a very minor role.

Although the decomposed products obtained by trapping can give an insight into the decomposition mechanisms of polyurethanes, the information can not exactly show the primary decomposition. Woolley reported that virtually all of the nitrogen, originally in the foam, reappeared in the form of a yellow smoke formed during heating.[23] This indicates that the primary decomposed products have reacted with each other forming other materials.

The research group at Universutà di Catania in Italy studied the thermal decomposition of different types of polyurethane by Py-MS in the 1980s [30-33]. These results showed that the primary thermal degradation of the polyurethane they examined was significantly influenced by the molecular structure of the polyurethanes. N-monosubstituted polyurethanes undergo a quantitative depolymerization process by a

low-energy hydrogen transfer from the nitrogen atom at a temperature of 170°C (see Reaction 2.11).

The thermal decomposition of N, N'- disubstituted polyurethanes, which contain an aliphatic chain linked to the oxygen atom, occurs selectively in a six-membered cyclic transition state with the transfer of the β-hydrogen of the aliphatic chain to the nitrogen. These reactions (see Reaction 2.12) occur at around 220°C producing secondary amines, olefins and carbon dioxide.

N, N'-disubstituted polyurethanes without a β-hydrogen linked to the oxygen atom, for example, a totally aromatic polyol, form cyclic oligomers via an ester exchange mechanism in their primary thermal fragmentation reactions, yielding cyclic compounds (Reactions 2.14 & 2.15).

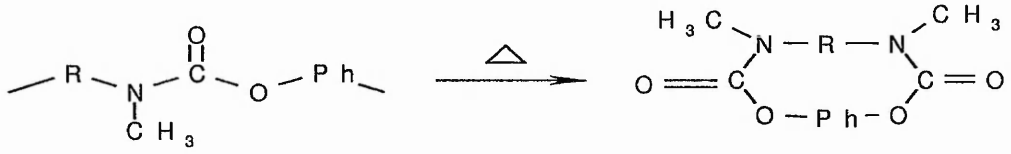

Reaction 2.14

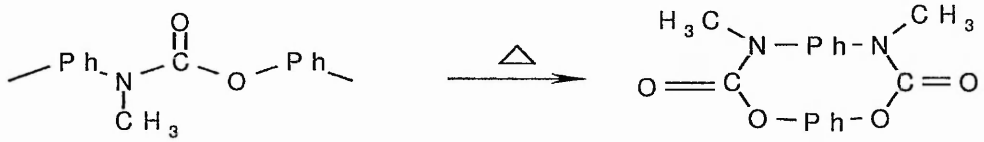

Reaction 2.15

These above results focus only on the urethane structures. Commercial polyurethane foams are chemically more complex and contain a variety of thermally labile groups. The most important structures in these groups are urethanes, ureas, biurets, allophanates, isocyanurates, ethers and esters. Their thermal stability varies in the following order: [21]

biurets and allophanates < urethanes ≤ ethers < ureas < esters <isocyanurates

Biurets and allophanates are the weakest links in thermal decomposition. Dissociation of these two links normally starts at 110°C and is complete at 170°C. During pyrolysis, they are decomposed into their precursors: isocyanates and ureas from biurets,

isocyanates and urethanes from allophanates. The isocyanurate group is the most stable one of these nitrogen-containing derivatives and does not decompose until 270°C.

The TGA curve of a flexible polyurethane foam based on TDI/polyether polyol with an isocyanate index of 110, showed that this foam decomposed in nitrogen in two stages. At the temperatures of 200-300°C it lost a weight of 33.2%, and had a weight loss of 65.6% at the temperatures of 300-400°C. The studies indicated that the first stage mainly corresponded to the decomposition of the bonds with TDI, and the second stage was due to the decomposition of the polyol. [28]

Polyurethane rigid foams contain more isocyanurate structures and release polyols as major species together with some low molecular species such as CO_2. The higher the isocyanate index the more CO_2 is evolved. This was found in a study of laser pyrolysis Time-of-MS.[34] The polyol of polyethylene glycols thermally decomposed at temperatures of 300-400°C by a radical mechanism initiated by random scission of C-O and C-C bonds, producing little char.[36,37] The decomposition of urethane-modified polyisocyanurates indicated that there were two major types of decomposition occurring within the polymers at different temperatures.[38] The decomposition at about 300°C was the scission of the urethane links, whilst the decomposition at about 400°C was the scission of the isocyanurate links. The scission of the isocyanurate links becomes increasingly significant as the isocyanurate content of the polymer increases.

2.1.3.3 Charring in the condensed phase

Since the 1970's Krevelen has studied the charring behaviour of polymers in relation to combustion. [1,39] Krevelen's results show that there is a significant correlation between the char yield (CY) in pyrolysis at 850°C and the oxygen index (OI) of polymers, Equation 2.3. The polymer with a higher char yield also has a higher oxygen index.

$$OIx100=17.5+0.4CY \qquad \text{Equation 2.3}$$

Krevelen also developed the relationships between the char yield in pyrolysis and the molecular structure of the polymer, as described in Equation 2.4:

$$CY=1200\{\sum_i (CFT)_i\}/M \qquad \text{Equation 2.4}$$

where CFT is char forming tendency, which is the amount of C equivalents in the char per structural unit of the polymer and M is the molecular weight per structural unit.

Based on Equation 2.4 TDI and polyether polyol based polyurethanes have char yields of about 1%, while linear MDI and polyether polyol based polyurethanes have char yields of approximately 5%. The TGA results show that similar structured polyurethane foams with isocyanate index close to 100 form 2-3% char in an inert atmosphere. [28,29]

Generally, vinyl polymers form solid char initially by chain-stripping mechanisms and followed by cyclisation of conjugated alkene fragments, aromatisation, cross-link and condensation reactions.[18] Polyvinyl chloride and polyacrylonitrile, for example, produce about 10% char by pyrolysis via this route.[18] The char formation from polyurethanes is more complicated than vinyl polymers. It varies not only with the chemical structures of isocyanates and polyols but also with the structure of the polymer chains, i.e. side reactions' structures, isocyanate index and the extent of cross-linking. Theoretically, the chemical structures of both diisocyanate and polyol, the cross linking of the polyurethane chains and the isocyanate index determine the flammability and the char formation of polyurethanes. Aromatic/condensed aromatic or heterocyclic groups in either the diisocyanate or the polyol favour char formation. Polymeric isocyanates are excellent char formers, undergoing some decomposition at about 200°C and retaining over 40% of their original weight at 550°C.[40] In summary, high isocyanate index and cross-linking in polyurethanes tend to reduce flammability and promote char formation.[1,39,41]

Very limited work has been carried out on the char formation chemistry of polyurethanes. The only published work giving a chemical mechanism of char formation of polyurethanes is the pyrolysis of a model chemical of para-toluene isocyanate.[27] An efficient radical mechanism is postulated for the conversion of aromatic isocyanates to nitriles, scheme 1 in Figure 2.6, and a polymerisation mechanism for p-methyl/benzonitrile via a 1,7 sigmatropic shift to form a thermally stable polymeric char, scheme 2 in Figure 2.7.

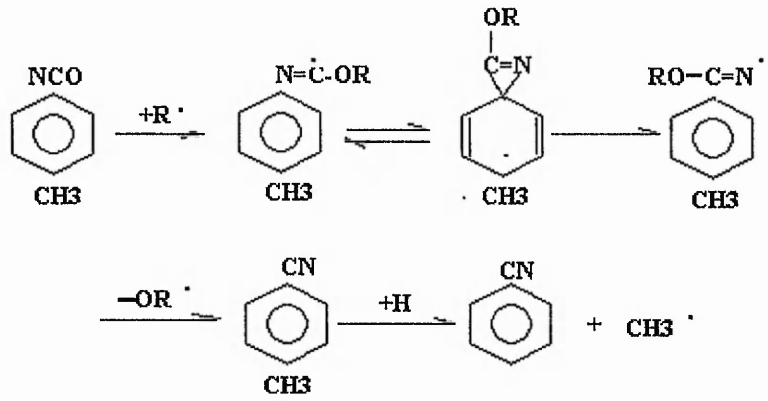

Figure 2.6 Scheme 1

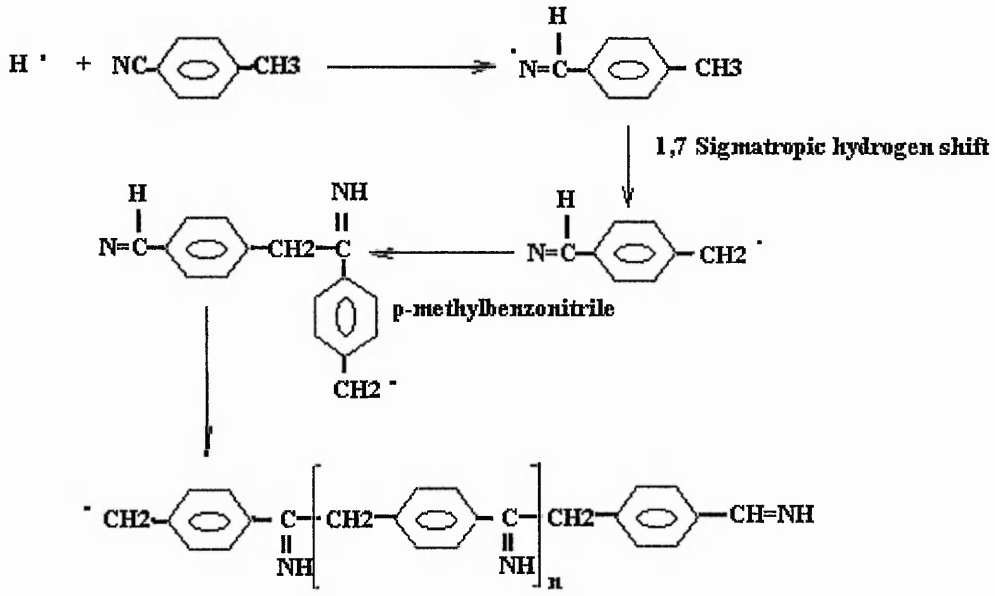

Figure 2.7 Scheme 2

2.1.3.4 Conventional fire retardancy of polyurethanes

Conventional methods for improving fire resistance of polyurethanes include the addition of phosphorus and/or halogen containing compounds either in the form of an additive or as a reactive component. [42]

The phosphorus-containing polyurethanes, either added [29,43-46] or chemically bonded phosphorus, [47-51] thermally degraded earlier and produced more char than pure polyurethanes. The higher the phosphorus content, the lower the onset temperature of

degradation and the higher the char yield. The thermal gravimetric curve of O,O-diethyl-N,N-bis(2-hydroxyethyl)aminomethyl phosphonate showed that the fire retardant began to decompose at temperatures lower than 200°C, producing volatiles such as ethylene, which contributed to the early degradation of phosphorus-containing polyurethanes. It retained 40% weight at 400°C.[40] This phosphonate itself develops a char when heated in a Muffle furnace. The oxygen index of phosphorus-containing polyurethanes is higher than the pure polyurethane and increases with the increase in P-content. [42] A phosphorus concentration of 1.5% of the total foam gave optimum fire resistance. [52]

Combinations of halogen compounds with phosphorus compounds are more effective than either halogen or phosphorus compound on their own. The haloalkyl phosphate esters, for example Tris(1,3-dichloro-2-propyl) phosphate (TDCPP), are effective for flexible polyurethane foams. The halogen components serve as a hydrogen halide or halogen radical in and immediately adjacent to the flame zone, retarding chain reactions and reducing surface flashing. The phosphates act mainly in the condensed phase by forming carbonaceous chars. The activity in the individual phases depends on the way in which the specimen is ignited. Under conditions of candle-like burning, retardation occurs mainly in the condensed phase by a mechanism apparently based on the barrier properties of the phosphorus-containing carbonaceous layer that builds up on the top of a liquid pyrolysing layer beneath the flame. By burning from the base of a sample upwards, the retardation appears to be mainly in the flame phase, which is caused by the outward flow of poor fuel and endothermic effects. The flame phase retarding is much faster than the condensed phase retarding, because the formation of a char barrier requires time. [29,43]

Grassie and Scott [53] studied the influence of phosphorous-containing fire retardants on the thermal degradation of polyurethanes made from MDI and 1,4-butanediol. The addition of ammonium polyphosphate accelerated the degradation of the polyurethane due to the formation of phosphoric acid. In addition, the phosphoric acid crosslinked with carbodiimide and formed a brown stable solid on the polymer surface, resulting in an increased char yield. The remaining polyurethane was able to avoid further degradation.

However, the effective amount of phosphorus-containing fire retardants in polyurethanes may be as high as 40%, which causes processing difficulties and a significant decrease in the physical properties of the polyurethane materials. In addition, some phosphates are water-soluble and may migrate during applications. This either shortens valid application periods of such fire retarded polyurethane materials or limits application situations.

2.1.4 The studies of intumescent fire retardancy

Intumescence can be described as fire retardant technology which cause a flammable material to foam, forming an insulating barrier when exposed to heat. A common characteristic of intumescent materials is that heat exposure initiates a chemical process that makes the material form a layer of relatively thermally stable and porous char, resulting in an insulation effect.[5]

An ideal intumescent material is able to form considerable amounts of thermally stable char. The char forms rapidly in the early stages of burning and at temperatures higher than those used for the polymer processing, but lower than those of rapid decomposition of the polymer.[54] The physical structure of the char is important for inhibiting the mass and heat transport during polymer burning. A thick and foamy char appears to be more fire resistant than a thin and brittle char.[55] The thick foamy char ideally should have closed pores of 10-60 microns.[56] The thick porous char should also have high thermal stability and sufficient strength to be able to survive in burning situations. To form intumescent chars with ideal structures, the timing of chemical reactions of the intumescent system was critical, Butler et al pointed out based on the modelling of swelling and thermal behaviour of intumescent materials.[57] If the blowing agent releases when the melt viscosity is too high, bubble growth will be limited, and the gas will tend to diffuse through the mixture without generating bubbles. If the molten polymer has too low viscosity, the bubbles will be large, resulting in a fragile and ineffective char.

However, practical intumescent fire retardant systems are not close to ideal intumescent materials. Intumescent studies also require investigation into the permeability and reactivity of chars to identify their efficiency of mass and thermal insulation and their oxidation resistance. [58]

The following aspects are essential for studying intumescent fire retardancy: intumescent formulation and char formation, gas permeability, reactivity and mechanical properties of chars. To study these properties, suitable characterisation methods need to be developed.

- **Intumescent formulation and char formation**

Char formation is the key issue in an intumescent fire retarding polymer system. Most polymers, however, cannot form sufficient chars. Phosphorus-containing fire retardants are formulated with nitrogen compounds to synergistically form effective intumescent chars when polymers burn. Typical intumescent formulations are based on a combination of ammonium polyphosphates (acid sources), melamine and its derivatives (blowing agents) as well as pentaerytritol or its derivatives (char-forming agents). These three component systems may be reduced to two if the acid source and blowing agent are combined, for example, in a melamine phosphate. In combustion, the acid source initially breaks down to yield a Lewis acid, which then acts as a catalyst in the dehydration of the polymer to form a carbonaceous char. Finally the blowing agent decomposes into volatile products. This causes the char precursors to swell and to decompose further under heat to produce an insulating thermal stable barrier, which is intumescent char. [59,60]

The research on the chemical aspects of the ammonium polyphosphate-pentaerythritol intumescent system, indicates that the char formation occurs in different stages. [61,62] At 190°C, the additives form a phosphate ester and between 280°C-350°C, an intumescent char layer develops. The intumescent char layer is formed by small aromatic molecules with branched alkyl groups, which may be bridged by phosphate species. The small aromatic molecules combine to form larger aromatic sheets between 350°C-430°C, and begin to arrange in parallel layers with anisotropy. At 560°C, the condensation process of the polyaromatic molecules develops, forming phosphocarbonaceous and polyaromatic species with anisotropy. The formation of organic phosphocarbonaceous esters limits the depolymerizaton of polymers and the evolution of volatile hydrocarbons. It also prevents the development of condensed polyaromatic structures. The condensed polyaromatic structures are bridged by polyethylenic links which provide strength to protective char shields. [63]

In intumescent formulations, char-forming polymers such as polyamide 6,[64-66] polyurethane, some inorganic chemicals such as silica[67] and graphite[68,69] can be used as charring agents. A study on a polypropylene - thermoplastic polyurethane (TPU) - Ammonium polyphosphate (APP) system [70-72] showed that polyester based polyurethanes with a higher content of hard segments in the formulation exhibited better fire retardancy. The oxygen index of the PP increased from 17 to over 26 when the additive concentration was above 40%. Correspondingly, the peak heat release rate (HRR) of the PP reduced from 1600 kw/m^2 to less than 300 kw/m^2. The viscosity of the intumescent PP was triple of that of the pure PP. The reaction between the APP and TPU changed the degradation mechanism of the polymer systems and resulted in a higher char yield and an extra weight loss step between 375-450°C which led to higher viscosity and expansion of the system at the charring stage.

Expandable graphite represents a new generation of intumescent additives which provides good fire retardancy to various materials and in particular to polyurethanes. [68,69,73-75] A polyurethane system with ammonium polyphosphate and expandable graphite as fire retardants was studied for its fire retardant mechanism. [75] The results showed that ammonium phosphate favoured char formation by interaction with the polymer, forming carbonaceous char, while the expandable graphite had no chemical reaction with the polymer. Even so, the expandable graphite has the effect of reducing the heat release rate in a polyisocyanurate polyurethane foam and a synergistic effect with phosphate compounds.[76] Expandable graphite was also added to improve the fire behaviour of water blown polyisocyanurate polyurethane foams.[77] The oxygen index (OI) of the foams increases linearly with the expandable graphite content (EG) according to: OI = 0.29EG + 23.5.

A lot of work has been carried out on the influence of formulations on char yields and heat release rates as well as oxygen indexes. However, little work has been done directly on the intumescent chars.

- **Permeability of chars**

The permeability of intumescent chars plays an important role in prohibiting the mass and heat transfer during polymer burning, as shown in Figure 2.1. Thermal transfer calculations suggest that the char barrier could be highly efficient if optimised. A char layer of 1 mm would prevent an underlying substrate from reaching ignition

temperature when the external fire atmosphere was 743°C. A 2.7mm layer would be required when the fire atmosphere was at 1500°C. [58]

In fact, the intumescent char itself is not impermeable to gases even if the pores in the char are closed and uniformly distributed. There are no reports about the pore structure or distribution in intumescent chars, nor have any other parameters been used to describe the permeability of the chars.

- **Reactivity of chars**

The reactivity of chars mainly refers to the reactions of the carbon in the solid chars with the oxygen in air and other oxidative gases such as CO_2.

$$C + 1/2O_2 \rightleftharpoons CO + 110KJ \qquad \text{Reaction 2.16}$$

$$C + O_2 \rightleftharpoons CO_2 + 390KJ \qquad \text{Reaction 2.17}$$

$$C + CO_2 \rightleftharpoons 2CO + Q \qquad \text{Reaction 2.18}$$

In intumescent chars, carbon atoms are usually in hexagonal rings, and these rings are joined together, imperfectly, to form polyaromatic lamellar molecules. These lamellae are not small perfect sheets of graphite. They contain heteroatoms such as hydrogen, oxygen, nitrogen and phosphorus.[61-63] In addition to chemical defects, crystallo-graphic defects are present and affect the carbon structures. Moreover, the impurities such as compounds containing sodium, potassium or vanadium increase the oxidation rate of the char by as much as six fold.[78] The reactivity of chars varies with intumescent formulations. So far, there has been no related work published on the reactivity of intumescent chars.

- **Mechanical properties**

The mechanical properties of intumescent chars describe the variation in the chars when external forces are exerted on them. Reshetnikov et al investigated the mechanical destruction of intumescent chars.[79,80] A compression rheometer was used to measure char strength in a cold state. A force rod examined the char destruction force during burning and a rotational table was used to investigate the destruction of tear-off and shear strength of chars. These methods were used to study intumescently formulated synthetic ethylene-propylene rubbers (intumescence ratio 1.5-2), carbamideformal-

dehyde resins (intumescence ratio 10-15) and thermoplastic polymers (intumescence ratio more than 10). The strength of these intumescent chars was approximately $10^3 N/m^2$ from the compression rheometer, $10^4 N/m^2$ from a force rod and 35-170N/m^2 tensile and shear stress from the mass centrifugal force method. All the measurements had more than 30% of error fluctuations. Other more effective and representative methods need to be developed.

- **Characterisation methods**

Intumescent chars are normally highly porous and fragile so that it is very difficult to measure their physical and mechanical properties. In fact, even simple physical properties such as bulk density and porosity are rarely reported. The physical structure of chars, however, has very significant effects on the protective efficiency of chars. The quality of the chars is more important than the char yields.

In summary, the research on intumescent chars has been carried out mainly on chemical aspects on the intumescent formulations, their ignitibility and heat release rate. No effective techniques have been developed to assess the quality of intumescent chars; and no relationship between fire retarding efficiency and the properties of intumescent chars has been established. This situation is exacerbated by the lack of understanding of intumescent char formation and the development of effective characterization techniques.

To design more effective intumescent fire retardant systems without sacrificing other properties such as mechanical performance, processability and stability in use, it is necessary to understand the intumescent char formation and assess the char quality, and then establish the relationship between the fire retarding efficiency and the quality of intumescent chars.

2.2 Carbon fibre polymer composites

Intumescent chars are the core of intumescent fire retardant polymer systems. In forming the intumescent chars, carbon atoms play the most important role. Carbon atoms can bond with themselves and other atoms principally via sp^3 (diamond-like) and sp^2 (graphite-like) hybridisation, resulting in an immense variety of structures. The intumescent char is composed of mainly polyaromatic graphene-like lamellae with

various degrees of structural order that exhibit anisotropic behaviour. The lamellae are linked together by less ordered regions and other elements, as discussed in Chapter 2.1.4. The chemical structures of intumescent chars have a direct influence on their reactivity and strength. A perfect graphite aromatic sheet would have the best oxidation resistance and mechanical properties.

Carbon fibre polymer composites are a group of well-developed reinforced polymer composites. The carbon fibres have excellent mechanical properties by making them have graphite structure in the form of fibres. The thermal stability of graphite structure of carbon fibres gives the oxidation resistance and fire retardancy to the polymer composites, so that carbon fibre polymer composites have enhanced mechanical properties and oxidation resistance. In the following section, the structure and property of graphite and carbon fibres, the reinforcement and fire retardancy of carbon fibre polymer composites will be reviewed.

2.2.1 Graphite

2.2.1.1 The structure of graphite

Graphite is one of the allotropes of carbon. It has carbons bonded by sp^2 hybridisation forming hexagonal-structured aromatic sheets that stack parallel together via delocalized π-bonding. Within each aromatic sheet, the carbon atoms are bonded to three other carbon atoms. The bonds are covalent (σ) and have a short length of 0.1415 nm and a high strength of 524 kJ/mole. The hybridized fourth valence electron is paired with another delocalized electron from the adjacent sheet by a much weaker Van der Waals bond of only 7 kJ/mole. Carbon is the only element to have this particular layered hexagonal structure. This special structure contributes to the unique properties of graphite.[78]

The interlayer spacing of graphite is relatively large, 0.3354 nm, which is more than twice the spacing between carbon atoms within the graphite sheet and approximately twice the Van der Waals radius of carbon. The stacking of these layers occurs in two slightly different ways: hexagonal and rhombohedral.

Hexagonal graphite is the thermodynamically stable form of graphite and is found in all synthetic materials. Its aromatic sheets are stacked in the most common manner of -

ABABAB-. In other words, the carbon atoms in every other layer are superimposed over each other as shown in Figure 2.8. Its crystal lattice parameters, i.e., the relative position of the carbon atoms (along the orthohexagonal axes) are: a=0.2456 nm and c=0.6708 nm. The crystal breaks along 002 with no fracture due to the weak links of the delocalized π-bonding.

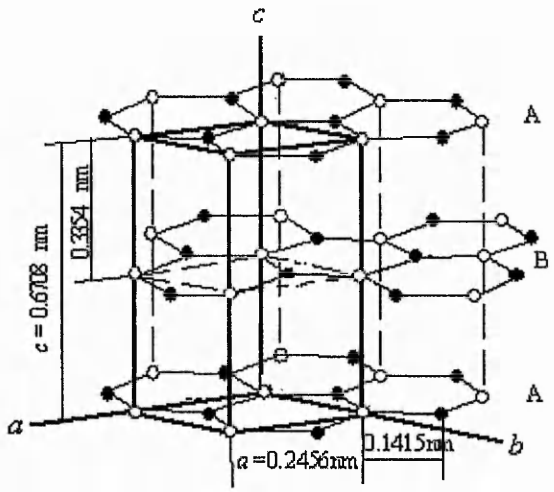

Figure 2.8 Hexagonal structure of graphite[81]

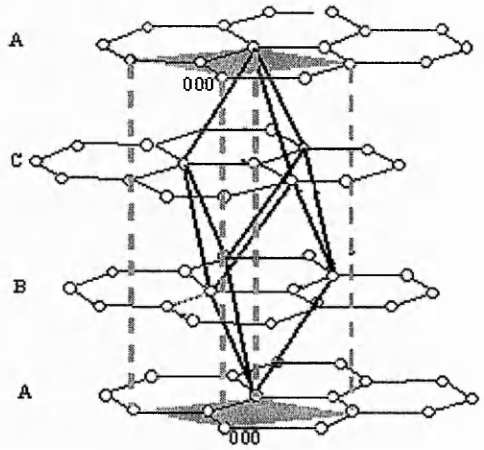

Figure 2.9 Rhombohedral stacking of graphite[81]

Rhombohedral graphite is thermodynamically unstable and can be considered as an extended stacking fault of hexagonal graphite. The graphite sheets in rhomobohedral graphite are in the stacking order of –ABCABCABC- as shown schematically in Figure 2.9. The carbon atoms in every third layer are superimposed. The crystal lattice parameters are α=0.2256 nm and c=1.0062 nm. Rhombohedral graphite is never found in its pure form but always in combination with hexagonal graphite, at times up to 40%.

The rhomobohedral graphite usually reverts to the hexagonal form during heat treatment above 1300°C.

2.2.1.2 Properties of graphite

The crystal structure of graphite results in considerable anisotropy, that is, the properties of graphite vary considerably depending on whether the properties are measured along or perpendicular to the aromatic sheet in the graphite. Such anisotropy, especially in electrical and thermal properties, can often be put to good use in applications. In polymer matrix composites, the high strength, modulus and chemical resistance of graphite are used to improve the mechanical properties and thermostability of polymers.

- **Mechanical properties of graphite**

The carbon bond within the aromatic sheet of a graphite crystal is considerably stronger than that between the sheets, with an anisotropy ratio of approximately 75. This means that the strength in the *a or b* directions (see Figure 2.8) is considerably higher than that in the *c* direction (interlamellar strength) and the graphite shears easily between aromatic sheets. The elastic modulus is 1060 GPa along *a* or *b* direction, 36.5 GPa along *c* direction and 4.5 GPa parallel to the sheets, respectively. The strength of the graphitic sheet is about 100 GPa.[82]

- **Chemical properties**

Pure graphite is one of the most chemically inert materials. It is resistant to most acids, alkalis and corrosive gases. However impurities are almost always present in both natural and artificial graphites and often have important catalytic effects on the graphite by increasing its chemical reactivity.

The anisotropy of the graphite crystals is also reflected in its chemical behaviour. Reactions with gases or vapors occur preferentially at "active sites", i.e., at the end of the aromatic sheets of the crystal, which are the zigzag or the armchair faces as shown in Figure 2.10, and at defect sites such as dislocations and vacancies. The graphite crystal exhibits large differences in surface energy in the different crystallographic directions: 5 J/m^2 in the prismatic plane but only 0.11 J/m^2 in the sheet. These differences account for the different reaction rates, i.e., slow at the sheet and fast at the

edge or prismatic surfaces found at the end of the sheets or at defects within the sheet. Consequently, graphite materials with large crystals and few defects have the best chemical resistance.[82]

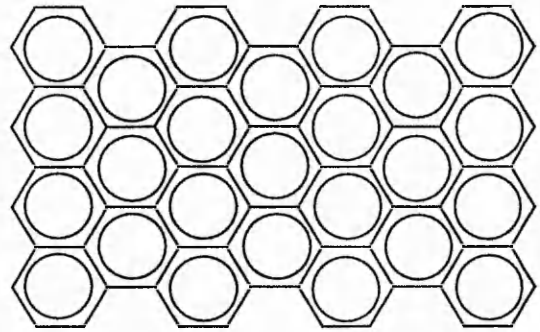

Figure 2.10 The faces of a graphite crystal

The chemical reactivity is also appreciably affected by the degree of porosity, since high porosity leads to a large surface area resulting in high chemical reactivity. Reactivity also generally increases with increasing temperatures, and at high temperatures graphite becomes far more reactive. For instance, at above 450°C it oxidizes readily with water, oxygen, some oxides and other substances.

2.2.2 Carbon fibres [83,84]

The history of carbon fibres dates back to Edison's use of carbonised rayon for the filaments of electric-light bulbs. But the carbon fibres discussed here began to be manufactured in the 1950s and 60s because of the aerospace industry's requirement for better lightweight, thermally stable materials. The low-density carbon fibres of high modulus could be used as the reinforcing elements in polymer composites.

As shown in Reaction 2.4, carbon fibre is produced by the controlled oxidation, carbonisation and graphitisation of carbon-rich organic precursors, which are already in fibre forms. The most common precursor is polyacrylonitrile (PAN), for it produces carbon fibres with the best properties, but fibres can also be made from pitch or cellulose.

To produce high axial modulus carbon fibres it is necessary to align the C-C bonds of graphite layers parallel to the fibre axis. The alignment is achieved by plastically stretching polymeric carbons either at high temperatures equivalent to the graphitisation temperatures of graphitisable carbons or by the alignment of carbon chains in the precursor prior to carbonisation. The carbon fibre from PAN is produced by the second method. Stretching of the fibres introduced during melt, spin and high temperature treatment allows graphite sheets formed to orientate in the fibre direction. The graphite sheets in carbon fibres stack parallel to each other at dimensions of approximately 3nm in width and 5nm in thickness.[84]

The heat treatment of graphitisation determines the properties of the carbon fibres. The carbon fibres increase strength and modulus together up to 1500°C of graphitisation. Above this temperature, the modulus continues to rise, whereas the strength actually decreases. Marsh-Griffith's diagram for the carbonisation process, Figure 2.11, can clearly explain this contradiction.[85]

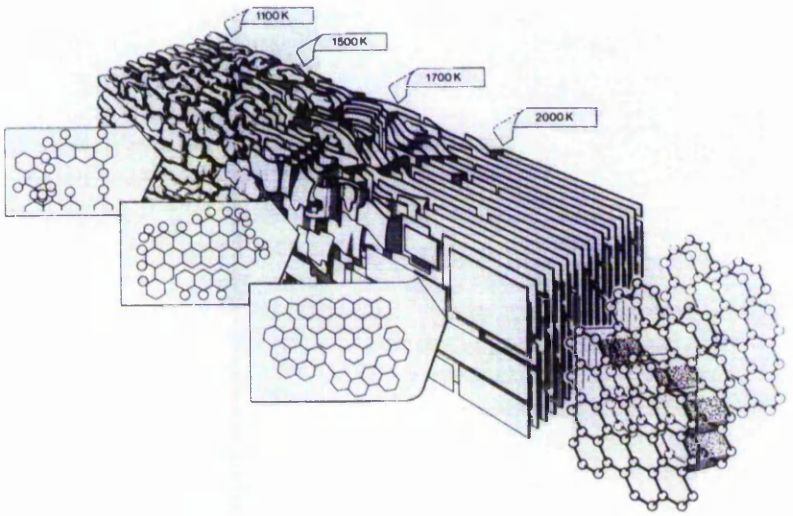

Figure 2.11 Marsh-Griffith's diagram for carbonisation/graphitisation process[78]

During the heat treatment, aromatic sheets are progressively formed as the temperatures increase. At temperatures over 1500°C, carbon fibres have better aligned aromatic sheets. The higher the temperature the more regular the structure is. The well-aligned aromatic sheets allow the fibres to have a modulus closer to the theoretical modulus of the aromatic sheets. However, the individual aromatic sheets in the fibres are not infinitely large. The lack of interconnection between the aromatic sheets leads to relatively low strength.

In order to achieve high strength, links between the aromatic sheets have to be introduced. The fibres heat-treated below 1500°C have such kind of linking structures. However, the aromatic sheets formed in this temperature range are underdeveloped and cannot be well aligned in the fibre direction. This structure cannot have a high modulus close to the theoretical value of the aromatic sheets.

There are, therefore, two main groups of carbon fibres. High modulus fibres, which are heat-treated at a temperature above 2500°C, have higher axial stiffness but inferior strength. High strength fibres, heat-treated up to only 1500°C, have a higher strength but rather inferior stiffness. Table 2.1 shows strength and modulus figures of commercial PAN-based carbon fibres. The strength of high strength fibres may be up to 5.9 GPa with a Young's modulus of less than 265 GPa. High modulus fibres may have a modulus up to 440 GPa with a maximum strength of up to 4.5 GPa.

Table 2.1 Strength and modulus figures for commercial PAN-based carbon fibres [84]

Grade	Tensile Modulus (GPa)	Tensile Strength (GPa)
High Strength	<265	3.6~5.9
Intermediate Modulus	265~320	4.1~5.3
High Modulus	320~440	2.7~4.8
Ultra High Modulus	~440	3.4~4.5

The structural contradiction of carbon fibres makes it impossible to produce carbon fibres having both high strength and high modulus close to the theoretical values of graphite aromatic sheets. The strength of carbon fibres is far lower than the theoretical value of graphite aromatic sheets. Actually, the tensile strength of high strength carbon fibres is only about 5% of the theoretical value, which is the link strength between the graphite sheets rather than that of a graphite sheet itself.

The most widely used carbon fibres are the family of high strength fibres, with modulus of 230 GPa and strength of 3.6 GPa. Typical dimensions of such kind of high strength carbon fibres are in Table 2.2. The diameter of the fibres is approximate 7.1 μm and the d-spacing of the aromatic sheets in the fibres is approximately 0.35 nm, which is larger than those in graphite, 0.3354 nm. The above discussion shows that carbon fibres are two dimensional micro-scale materials. They show the advanced properties of graphite, but do not fulfil the potential of graphite-structured materials in mechanical properties.

Table 2.2 Typical dimensions of high strength carbon fibres[84]

Parameters	Dimensions
Fibre diameter	~7.1 μm
Graphite layer spacing	0.35 nm

2.2.3 Reinforcement of carbon fibre polymer composites

Carbon fibre polymer composites are materials consisting of fibres embedded in or bonded to a polymer matrix with distinct interfaces between the two constituent phases. The carbon fibres are of high strength and modulus and serve as the principal load-carrying members. The polymer matrix must keep the fibres in a desired location and orientation, separating the fibres from each other to avoid mutual abrasion during periodic straining of the composites. The matrix acts as a load transfer medium between the fibres, and in less ideal cases where loads are complex, the matrix may even have to bear loads in the transverse direction to the fibre axis. The matrix is the source of composite toughness since it is generally more ductile than the fibres. In a composite, both the fibres and the matrix largely retain their identities and yet the resulting material has many properties that cannot be achieved with either of the constituents acting alone. [86]

The fibres can be incorporated into a matrix either in continuous lengths or in discontinuous lengths such as chopped fibres or whiskers. In general, continuous fibres are usually arranged parallel in one or more directions. The high modulus fibres entirely carry the stress if the fibres are subjected to a tensile stress parallel to the fibre direction. In this case, the unidirectional reinforced composites can be weak and crack in the matrix along the fibres when loaded in the transverse direction. If the composites is designed for more than one directional loads, the fibres have to arranged along all the loading directions. Continuous fibre-reinforced composites have high strength and modulus. They are utilised in primary structural applications and are considered high-performance structural materials.

In the case of the chopped fibre dispersed randomly in the matrix, the composite formed has improved mechanical strength in all directions. The improvement depends upon the aspect ratio of the fibre and the interaction of the polymer matrix and the fibre at the

interface. Short-fibre composites have low strength and modulus and are used in lightly loaded or secondary structural applications.

The microstructure and properties of the interface between the fibre and the matrix play a critical role. A better interfacial bond will impart to a composite better properties such as interlaminar shear strength, delamination resistance, fatigue and corrosion resistance. Therefore, carbon fibres have surface treatments after they are formed, to improve the bonding with the matrix, and chemical sizing which serves to protect them during handling. However, the aspect ratio of short fibres and the interaction area between the fibres and the matrix cannot be altered significantly because of the form and dimension of carbon fibres (see Table 2.2). These limit the improvement of the short carbon fibre polymer composites.

The above discussions indicate that both carbon fibre and carbon fibre composite approaches to make materials stronger are not perfect. The parallel continuous fibre composite can only reinforce in the fibre's directions. It cannot avoid low strain fracture and matrix cracking. Short fibre-reinforced composites are restricted by the aspect ratio of short fibres and the limited interface interactions so that the reinforcement is much lower than the potential of carbon materials. Nanocomposites have shown potential to overcome these limitations to fully utilise the potential of carbon materials in reinforcing polymers.

2.2.4 Fire retardancy of carbon fibre polymer composites

Carbon fibres not only mechanically reinforce the composites, but also impart their oxidation resistance to the composites, although they play a role of inert filler in polymer systems during combustion. [87] Carbon fibres do not affect the decomposition of polymers or the reactions of polymer systems, but these inert fillers alter the heat transfer and distribution of burning systems and affect the ignitibility of the polymer. [87]

Research into thermal behaviour and combustion performance of carbon fibre-epoxy resin composites indicates that the orientation of the fibres strongly affects the ignitibility of the composites. In composites where the fibres are perpendicular to the flame front, the Oxygen Index is high, whereas where the fibres parallel to the flame front, the Oxygen Index is low. [87] In the composites with a crossed orientation of

carbon fibres the OI linearly increases from that of pure epoxy matrices to OI = 100 when fibres loading increases from 0 to 65%.

No published documents have reported on the influence of short carbon fibres on the flammability of the polymer composites or on the fire behaviour of the composites with low fibre contents. Clay/nylon 6 nanocomposites have shown much improved thermal stability and much decreased peak heat release rate due to the formation of a layer of char at the burning surface. In light of this evidence and the effect of the particle size of inert fillers on the ignitibility of polymers, that is, the finer the inert filler, the more difficult the polymer system to be ignited,[88] it can be proposed that graphite/polymer nanocomposites offer a promising approach to design a new generation fire retardant and reinforced polymer products.

2.3 Graphite polymer nanocomposites

As discussed above, carbon fibre polymer composites not only improve the mechanical properties, but also influence the ignitability and burning behaviour of polymers. Carbon fibres are structurally micro-scale fillers, as shown in Table 2.2, which only partially fulfils the potential of carbon materials in polymer reinforcement. After the success of clay/nylon 6 nanocomposites in enhancing the mechanical properties and thermo-stability of the nylon 6, the idea of dispersing graphite sheets into polymers in single layers to produce graphite/ polymer nanocomposites is very attractive particularly as the nanocomposites may have both improved mechanical properties and fire retardance compared to their base polymers.

This part of literature review concentrates on clay/nylon 6 nanocomposites, the first clay/polymer nanocomposites that have attracted wide attention and been intensively studied, to show how far this field has been explored and the research progress in graphite/polymer nanocomposites. Finally, the research on fire retardancy of polymer nanocomposites is reviewed.

2.3.1 Nanocomposites and nano-structures

Polymer nanocomposites are defined as materials in which fillers are dispersed in the polymer matrix with at least one dimension in nanoscale. [89] In terms of how many dimensions of the dispersed fillers are in nanoscale, nanocomposites can be identified as

three-dimensional, two-dimensional and one-dimensional nanocomposites. The clay/ nylon 6 nanocomposites mentioned above belong to the one-dimensional nano-composites, because the clay layers have a thickness of a few nanometers, while the other two dimensions are in hundreds or thousands of nanometers. In this thesis, polymer nanocomposites refer to the one-dimensional nanocomposites, because both clay and graphite have 2D layered structures.

Nano-structures of layered mineral polymer nanocomposites are determined by the interaction of mineral layers with polymer chains. The dispersion of mineral layers in a polymer matrix can result in traditional microcomposites, intercalated nanocomposites and exfoliated nanocomposites. As an example, these three types of clay polymer composites are shown in Figure 2.12. Traditional microcomposites (Figure 2.12a) contain aggregated clay layers without polymer chains between them. Intercalated composites (Figure 2.12b) have extended polymer chains between the clay layers resulting in a well-ordered multilayer morphology and increased interlayer spacing between the clay layers. The exfoliated or delaminated nanocomposites are characterised by random dispersion of every single clay layers in a polymer matrix, as shown in Figure 2.12c.

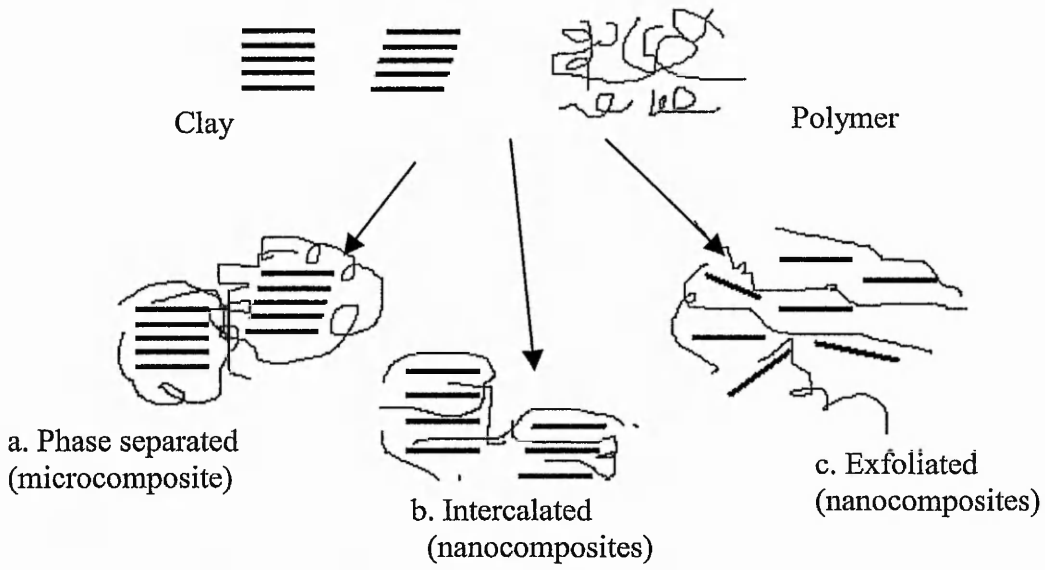

Figure 2.12 Three types of clay polymer nanocomposites (a) phase-separated microcomposite, (b) intercalated nanocomposite, (c) exfoliated nanocomposite.

To produce graphite/polymer nanocomposites means either to insert the polymer chains into the galleries of the graphite sheets or to disperse graphite sheets uniformly into a continuous polymer matrix.

2.3.2 Principles of enhancement of polymer nanocomposites

Polymer nanocomposites are reinforced by the nano-filler in a similar mechanism to the reinforcement of randomly dispersed chopped fibre composites. Theories by Cox[90] and Kelly[91] are commonly used to estimate the reinforcing effect of fibre fillers. According to these theories, the degree of reinforcement depends on the rigidity and aspect ratio of the filler, and the interaction strength between the filler and the polymer matrix. All these three factors are not optimised in conventional composites. But the complete dispersion of nano fillers in a polymer matrix may optimise the composite system in following aspects. [84,89,92]

- The mechanical properties of nanofillers are those of single sheet of fillers, which are much higher than those of aggregates, because single sheets rarely exhibit defects in their structures.

- The high aspect ratios of nanolayers are conducive to reinforcement, which is not possible in conventional composites.

- The coupling between the tremendous surface area of the nano-filler (~760m^2/g for clay) and the polymer matrix may optimise the wetting of the filler by the polymer, the chemical bonding, if there is any, mechanical interlocking and crystalline interactions at the interface between the filler and the polymer.

- The number increase in reinforcing elements and the improved interface interaction facilitate stress transfer to the reinforcement phase and deflecting cracks, resulting in tensile and toughening improvements of the composites.

Furthermore, relatively impermeable mineral layers in polymer nanocomposites provide a tortuous pathway for any permeant to traverse through the nanocomposite, as shown in Figure 2.13. This results in enhanced barrier characteristics, chemical resistance, reduced solvent uptake and flame retardancy of polymer nanocomposites. [92]

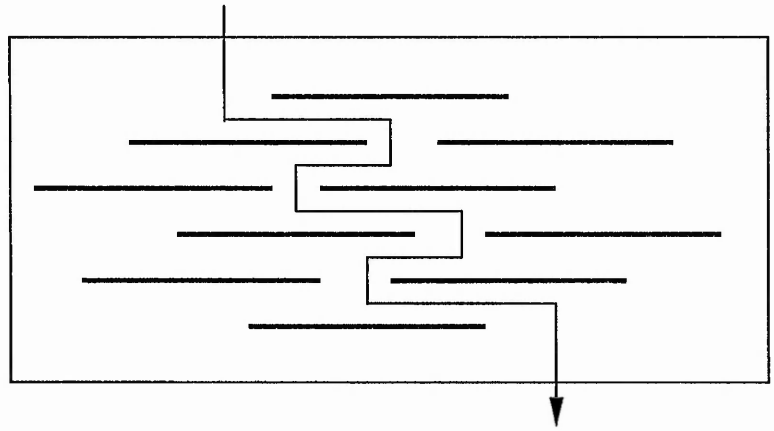

Figure 2.13 A model for the torturous zigzag diffusion path in polymer/clay nanocomposites

2.3.3 Synthesis of nanocomposites

Complete dispersion or exfoliation of filler layers in a monomer or polymer matrix may involve three steps similar to the dispersion of powders in liquids.[93] The first step is wetting the surface of the fillers by the monomer or polymer molecules. The second step is intercalation of the monomer or polymer molecules into the galleries of the filler layers, and the third step is exfoliation of the layers. The first and second steps are determined by thermodynamics, while the third step is controlled by external mechanical forces such as shear forces and reaction driving forces.[94] The thermodynamic rule for wetting and intercalation is:

$$\Delta G = \Delta H - T\Delta S < 0$$

where ΔG is the Gibbs free energy change, ΔH is the enthalpic change and ΔS is the entropic change.

Only when the Gibbs free energy change is negative, can the wetting and intercalation occur. In this case, the polymer nanocomposites have to have a lower energy content than the sum of that of the polymer and the filler.

The interplay of the enthalpic and entropic factors of a filler polymer system determines whether the filler disperses, intercalates or exfoliates in the polymer.[95-97] The dispersion of a filler in a polymer requires sufficiently favourable enthalpic contributions to overcome any entropic penalties. Only when the filler surface is

compatible with the polymer system, polymer nanocomposites can be synthesized using appropriate methods. [98]

Compared to graphite, clay/polymer nanocomposites have been much more extensively studied. The following five strategies have been developed to synthesize polymer clay nanocomposites.[89]

- **Solution intercalation**

The clay is exfoliated into single layers using a solvent in which the polymer or a prepolymer is soluble. Clay, owing to the weak forces between the layers, can be easily dispersed in a suitable solvent. The polymer then adsorbs onto the swollen or delaminated clay layers. When the solvent is evaporated or the mixture is precipitated, the layers reassemble, sandwiching the polymer to form, in the best case, an ordered multilayer structure.

- ***In situ* intercalative polymerisation**

In this technique, the clay is swollen in a liquid monomer or a monomer solution so that the polymerization can occur in the galleries of the clay layers.

- **Melt intercalation**

In melt intercalation, the clay is mixed with the polymer matrix in the molten state. Under these conditions and if the layer surfaces are sufficiently compatible with the chosen polymer, the molten polymer can insert itself into the interlayer spaces of the clay and form either an intercalated or an exfoliated nanocomposite.

- **Template synthesis**

In this technique, the silicates are formed *in situ* in an aqueous solution containing the polymer. The polymer aids the nucleation and growth of the silicates and gets trapped within the layers as they grow.

- **Solid intercalation** [99]

The clay is directly blended with polymers in the solid state. The solid mixture is then simply compressed forming nanocomposites with well-intercalated structures.

Forming nanocomposites by melt processing and solid intercalation have advantages over the others. Firstly, these two methods are environmentally friendly since no solvents are required. Secondly, conventional polymer processing equipments can be used to produce nanocomposites, reducing capital costs. Moreover, manufacturers are able to select the final product specifications by alteration of polymer grade, choice of filler and level of reinforcement.

These five methods represent all the methods developed to produce different types of polymer nanocomposites. It is important to use a suitable method to match the characteristics of the chosen nanofiller and polymer system.

2.3.4 The progress in clay/nylon 6 nanocomposites

The first clay/nylon 6 nanocomposites synthesized and commercialised were montmorillonite/nylon 6 nanocomposites. The montmorillonite was modified with alkylammonium surfactants which made the clay compatible to the nylon. The nanocomposites have been produced by both *in situ* polymerisation and melt processing. [100-109]

The research team of Usuki and Kojima et al in Tokyo [100-102] modified a natural Na-montmorillonite with alkylammonium surfactants. The cation-exchanged montmorillonites, called organoclay, were swollen by ε-caprolactam monomer producing the interlayer spacing increased montmorillonites. The ε-caprolactam in the interlayer galleries of the montmorillonites was polymerised, yielding clay/nylon 6 nanocomposites.

Such synthesized clay/nylon 6 nanocomposites were studied by X-ray diffraction and transmission electron microscopy. [103-105] The studies revealed that the layers of the montmorillonites were uniformly dispersed in the nylon 6 and formed either delaminated or intercalated structures. The clay layers and the nylon 6 crystallites had a planar orientation. The clay/nylon 6 nanocomposites had significantly improved mechanical and physical properties compared to the pure nylon 6, as shown in Table 2.3.

Table 2.3 Mechanical and thermal properties of the clay/nylon 6 nanocomposite with 4.2 wt% of clay [103]

Property	Nanocomposite	Nylon-6
Tensile Strength, MPa	107	69
Tensile Modulus, GPa	2.1	1.1
Heat distortion temperature, °C	145	65
Impact strength, kJ/m^2	2.8	2.3
Water adsorption, %	0.51	0.87
Coefficient of thermal expansion	$6.3x10^{-5}$	$13x10^{-5}$

The nanocomposites exhibit large increases in tensile strength, modulus and heat distortion temperature as compared with the original nylon. The composites also have lower water sensitivity, reduced permeability to gases and a smaller thermal coefficient of expansion. All of these improvements can be realized without a loss of clarity in the polymer. Moreover, different from conventional composites, nanocomposites have similar processability to the neat polymer and can be produced in films and fibres.

Melt intercalation has also been applied to synthesize clay/nylon 6 nanocomposites. [106-109] Early work by Giannelis et al [106] revealed that the intercalation of nylon 6 chains into the galleries of an organoclay occured spontaneously by heating a mixture of the polymer and clay powder above the glass transition or melt temperature of the polymer. Once the polymer has achieved sufficient mobility, its chains can diffuse into the host clay galleries, thereby producing an intercalated polymer-clay structure. Intercalation is greatly enhanced by maximizing the number of polymer host intercalations through appropriate selection of organically modified clay. Detailed studies have been carried out on the effects of organoclay structures on the morphology and properties of nylon 6 nanocomposites. [110-111]

Melt-processing techniques and parameters have obvious effects on composite properties. Vaia et al[107,108] have stated that intercalation can be improved through the use of conventional processing techniques such as extrusion, mixing and ultra-sonication, which all produce shear forces. Of these melt-processing techniques, twin-screw extrusion has been proven to be the most effective for the exfoliation and dispersion of clay layers.

Usuki et al [111] studied a nylon 6 intercalated with different clays (montmorillonite, saponite, hectrite and synthetic mica) using ^{15}N-CP/MAS NMR. The study indicates that montmorillonite interacts strongly with the nylon 6 by ionic intercalation, and the resulting nanocomposite has the best mechanical properties. This is one of the reasons why these nanocomposites are superior in strength and modulus and have comparable impact strength to the nylon 6.

A clay-induced crystal transformation from the α-form to the γ-form of nylon 6 has been reported[103,106,112-114]. X-ray diffraction and DSC data show that the exfoliated structures are strongly influenced by the crystallisation nature of nylon 6, favouring the formation of γ-crystals rather than α-form which is observed in the pure nylon 6. Cooling scans of DSC showed that the exfoliated clay layers increased the crystallization rate of the polymer as it had a strong heterophase nucleation effect. The observed improvement in properties of the nanocomposites, especially the toughness, may be associated with this increase in the γ-phase crystallisation. [115]

The fundamental mechanisms for property enhancement and alteration of equilibrium chain conformation near the polymer-clay interface have been investigated. [112-116] The heterogeneity of the nanostructure, the orientational distribution of the clay layers, the strength of the polymer-clay interface interactions and the influence of clay arrangement on polymer morphology and conformation all affect the final nanocomposite properties.

Although the research on the fundamental mechanisms for property enhancement has gone into morphological details, it has not yet reached the stage of establishing the correlation between the structure and mechanical and physical properties.

2.3.5 The progress in graphite/polymer nanocomposites

There are two factors that hinder graphite directly intercalating with polymers: One is the small interlayer distance of graphite sheets, only 0.3354nm; the other is that graphite sheets are highly hydrophobic and organophobic so that graphite is not compatible with polymers. In order to synthesize graphite/polymer nanocomposites, it is necessary to functionalise and expand the graphite sheets.

A number of researchers have used expanded graphite, graphite intercalation compound and graphite oxide to produce graphite/polymer nanocomposites.

- **Expanded graphite/polymer "nanocomposites"**

Expanded graphite can be produced by the following method. Graphite flakes are firstly intercalated by a mixture of concentrated sulphuric and nitric acids. After the acids are washed away by water, a small amount of the acids remain in the defects of the graphite crystal structure. Such treated graphite, called expandable graphite, is then heated at temperatures above 600°C producing expanded graphite. During heating, the chemical residue in the expandable graphite is released in the form of gases, causing the graphite sheets to separate. This graphite product has a much higher volume than the original graphite, and is called expanded graphite.

Expanded graphite has been used to produce electronically conducting composites with nylon 6[117], PMMA[118-120], PS[121,122] and PVC[123]. The composites are generally synthesized either by *in situ* polymerisation or solution intercalation methods in order to retain the expanded structure of expanded graphites. Chen et al. [122] powdered expanded graphite by sonicating it in a 70% aqueous alcohol solution, obtaining graphite powders with a thickness ranging 30-80 nm and a diameter ranging 0.5-20 μm. This improved the dispersion of the expanded graphite in the polymer matrix and reduced the aggregation of the graphite sheets. As the thickness of graphite sheets in polymer matrix is in nano-scale, the composites are called nanocomposites. These kinds of nanocomposites exhibit markedly lower percolation threshold of conductivity compared to conventional graphite/polymer composites. However, the nano-scale aggregates of graphite sheets result in poor mechanical properties.

None of the reported expanded graphite/polymer nanocomposites have single graphite sheets in a polymer matrix similar to that of clay/polymer nanocomposites.

- **Graphite intercalation compound/polymer nanocomposites**

Graphite intercalation compounds are the graphite compounds which have chemicals intercalated in the interlayer galleries of the graphite. The graphite sheets are very strong and stable due to the very strong C-C covalent bonds. The interlayer bonding of the sheets is weak. Both the strong sheet and the weak interlayer bonding of graphite make it possible to insert chemicals into the interlayer space of graphite forming new layer expanded crystal structures.

Potassium intercalated graphite has an interlayer spacing of 0.54 nm when the intercalation stage is 1, that is, potassium atoms have inserted themselves into every gallery between the graphite sheets. This potassium-intercalated graphite, normally formulated as KC_8, still has a narrow interlayer spacing, and its graphite sheets virtually keep intact having a similar surface compatibility with polymers to graphite itself. Uhl and Wilkie[124] synthesized graphite/PS nanocomposites using KC_8 as graphite source. They adopted both bulk and solution *in situ* polymerisation methods and produced composites that had structures where the graphene layers were partly intercalated by the PS and partly unchanged. The produced composites had a slightly increased thermal stability and decreased mechanical properties compared to the pure PS.

Xiao et al.[125] synthesised graphite/PS nanocomposites by the *in situ* polymerisation of styrene in a tetrahydrofuran solution system. The system contained potassium and tetrahydrofuran graphite intercalation compound. The TEM micrographs showed that the graphite sheets were dispersed in the polystyrene matrix with a thickness less than 100 nm. The composites exhibited a higher glass transition temperature and a higher thermal stability compared to the pure PS.

- **Graphite oxide/polymer nanocomposites**

Graphite oxide is namely a type of oxidized graphite and is one of the earliest lamellar compounds to be investigated. Graphite oxide has a two dimensional lamellar structure. The interlayer distance varies between 0.6 and 1.1nm, depending on the amount of water absorbed.[126]

Graphite oxide has been intercalated with PEO[127,128], PVA[129,130], polyaniline[131], polyacrylamide [132] and poly(acrylic acid). [133] These polar polymers were intercalated either by an exfoliation/absorption process[127-130] or by *in situ* polymerisation. [131-133] These intercalated compounds are different from the other composites discussed here as they are potential conductive materials rather than commodity engineering materials. In the reported graphite oxide/polymer intercalated materials, the polymers existed mainly in the galleries of the graphite oxide. The polymers intercalated with graphite oxide are polar polymers with either oxygen-containing groups or nitrogen-containing groups. The layer expansion caused by the intercalation process depends on the intercalation conditions. [127]

In summary, expanded graphite or graphite intercalation compound-based polymer nanocomposites have not been synthesized with single graphite sheets in the polymer matrix. A few polar polymers have intercalated with graphite oxide, but all the composites studied are potential electrical conductive materials rather than engineering materials.

2.3.6 Fire retardancy of polymer nanocomposites

The clay/nylon 6 nanocomposites have been found not only having improved mechanical properties but also enhanced thermal stability and char formation. A cone calorimeter study of the nanocomposites showed [134] that the peak heat-releasing rate (HRR) of the delaminated clay/nylon-6 nanocomposites decreased from 1010 kw/m^2 to 378 kw/m^2 when the clay content was 5%. This was accomplished with the formation of a thin layer of integrated char.

The polymers that have been examined for fire retarding properties of their nanocomposites are nylon 6, nylon 12, PS, PMMA and polypropylene-graft-maleic anhydride. Two mechanisms have been proposed to account for the reduction in the heat release rate. **A barrier mechanism** recognises that the clay has a barrier function to insulate the polymer from the fire and to hinder the decomposed gases releasing from the polymer. [135] This mechanism is consistent with the TGA results of several different polymer/clay nanocomposites, that is, intercalated nanocomposites are more thermally stable than exfoliated nanocomposites. [136-138] **A radical trapping mechanism** occurs due to the presence of iron, or other paramagnetic impurities which are structural components in the clay. [139]

The surface structures of PS, PMMA and PVC/clay nanocomposites were examined using X-ray photoelectron spectra during thermal degradation.[140-142] The results from non-char formation polymers show that carbon is lost and oxygen accumulates at the surface of the degrading polymers. This indicates that the clay accumulation at the degrading surface forms a barrier hindering the heat and mass transfer, resulting in decreased peak heat release rates of the nanocomposites. For char-formation polymers, for example PVC, the degrading surface at high temperatures is dominated by carbon rather than oxygen. The presence of the clay does retard the chain-stripping degradation of the PVC. Both the PVC and clay contribute to the char formation.

The combustion chars of clay/nylon 6 and clay/thermoset epoxy nanocomposites were examined by TEM.[143] The TEM images of the char cross-sections show a multi layered clay structure, with 1nm thick clay sheets forming a large array of fairly even layers. The XRD analysis of these chars shows that the interlayer spacing of the char is the same, 1.3 nm, and is independent of the chemical structure of the polymer system and nanostructure type.

When the char yields of nanocomposites are compared to that of their corresponding pure polymers, whether they are thermoplastics or thermosets, little improvement in the carbonaceous char yields is observed, once the presence of the clay in the residue is accounted for.[143] This result indicates that, although the flame retardancy mechanism may be very similar for each of the systems studied, it is not via retention of a large fraction of carbonaceous char in the condensed phase.

So far, no publications have reported the fire retarding properties of graphite/polymer nanocomposites.

2.4 Summary remarks

The literature review has discussed the fundamentals of polymer combustion and fire retardancy, carbon fibre polymer composites and graphite/polymer nanocomposites.

Inflammable polymers are normally added fire retardants to allow them to be used in practical applications. Among current fire retarding mechanisms, intumescent fire retardancy has advantages over others in terms of fire retarding efficiency and environmental concerns. However, research into intumescent fire retardancy has not examined the structure and quality of intumescent chars or the relationship between the fire retarding efficiency and char quality. This has inhibited the design of better intumescent fire retarding polymer systems.

The quality of intumescent chars determines the intumescent fire retarding efficiency of polymer systems. Their permeability and reactivity are the most important properties for assessing the char quality. The permeability is mostly determined by the char structure and morphology, while the reactivity of intumescent chars is closely related to the chemical bonding of carbon in the intumescent chars. The ideal carbon bonding to make thermally stable chars is probably that found in graphite. There has been little research into the quality of intumescent chars.

In addition to the lack of understanding of intumescent chars themselves, the amount of conventional intumescent fire retardants used in commercial applications is normally approximately up to 40%, which results in a decrease of approximately 20% in the mechanical properties of the polymer materials. Carbon fibres, composed of graphite sheets, have been successful in reinforcing polymers as reinforcement fillers. They are excellent not only in improving mechanical properties, but also in thermal stability and oxidation resistance. Their polymer composites have been well studied for reinforcement, but both carbon fibres and carbon fibre polymer composite approaches did not fulfil the potential of graphite sheets. The fire retarding and the char formation behaviour of carbon fibre/ polymer composites have not yet been well studied.

Graphite/polymer nanocomposites would have graphite sheets in their composites and in their chars when they are burnt. The graphite sheets would be dispersed in single layers in graphite/polymer nanocomposites. Well-dispersed graphite sheets would improve the mechanical properties and fire retardancy of the nanocomposites towards to fulfil the potential of graphite sheets in mechanical performance and thermal stability. Graphite/polymer nanocomposites have a great promise to be a new generation of fire retarding and reinforcing polymer materials.

Chapter 3
Experimental Methods

3.1 Introduction

The experimental methods introduced all the methods used in the investigations of intumescent mechanisms and graphite/polyurethane nanocomposites. The investigation of intumescent mechanisms was based on developing a number of char characterisation techniques, which involved a series of rigid polyurethane foams, and was carried out on three commercial polyurethane fire-stopping products. The work on graphite/polyurethane nanocomposites included the modification of graphites and the synthesis and characterisation of graphite/polyurethane nanocomposites.

3.2 Materials studied

The materials used for the development of char characterisation techniques were a series of well-known rigid polyurethane foams produced from ICI precursors. The use of well-known foams allows the burning assessment techniques to be developed and validated, also the relationship between the intumescent fire retarding effectiveness and the properties of the intumescent chars to be established.

The ICI precursors were a polymeric diphenylmethane diisocyanate, with an average functionality of 2.7, and a polypropylene glycol with a number average molecular weight of 425 (VIZ PPG-425). The foams produced were coded as PU173, PU328, PU594, PU856 and PU1476, respectively, where the numbers indicated the isocyanate index of the foams. These foams were light yellow in colour.

Three existing commercial polyurethane fire-stopping products produced by Hilti AG were investigated by the developed characterisation techniques to investigate their intumescent mechanisms and evaluate the quality of the intumescent chars formed. The three Hilti products included one commercial rigid polyurethane foam, one newly developed flexible polyurethane foam and one polyurethane-based sheet. Details of the properties of these materials were not available.

Five types of graphite from different suppliers were screened and modified for the synthesis of graphite polyurethane nanocomposites. One of them was graphite flake from Aldrich, coded as Aldrich-F, and the other four were powders from Aldrich, BDH, LUH and NGS, coded as Aldrich-P, BDH-P, LUH-P and NGS-P, respectively. Of these, Aldrich-P is synthetic graphite, and the others are natural graphites. Aldrich and BDH are laboratory-scale suppliers and NGS and LUH are industrial suppliers. The properties of the graphites provided by suppliers are listed in Table 3.1.

Table 3.1 Properties of the graphite samples

	Type	**Flake Size**	**Grade**
Aldrich-F	Flake	75% 150μm	-
Aldrich-P	Synthetic	1-2μm average 1.4μm	-
BDH-P	Natural	99.5%<50μm	-
LUH-P	Micronised crystalline	---	GHL 1701
NGS-P	Micronised flake	50%<2μm	MF2/99.5-99.9E

3.3 Burning tests

Three burning methods were developed to study the intumescent mechanisms and charring ability of the samples at different burning conditions. They are natural burning, Muffle furnace burning with and without load.

Natural burning is a single direction burning method, which aims to simulate a real fire situation and to display the whole of the intumescent char forming process and protection of its underlying polymer. Natural burning was carried out in a fume cupboard in a well-ventilated environment. A Bunsen burner was used to ignite the samples. The flame of the Bunsen burner was adjusted with the air vents until the bright blue inner cone was observed. The hottest part of the flame, just above the blue inner cone, was used to ignite and burn the samples. After burning the whole burned black part was defined as intumescent char. This method was used to produce intumescent chars for mechanism studies.

The Muffle furnace experiments were used to establish the total char yield of the samples. Samples of a given mass were burnt in a Muffle furnace at 600°C for a known length of time. Furnace burning without load was carried out in a quartz crucible. The

quartz crucible has a diameter of 50 mm and a height of 10 mm and had been heated to constant weight at 600°C in the Muffle furnace before being used to burn the samples.

The burning under load in a Muffle furnace test is designed for burning samples under pressure in a badly ventilated burning atmosphere to simulate some real burning conditions for fire stopping products. It is also suitable for the samples that produce light and loose chars to examine the total char yield. A steel mould, as shown in Figure 3.1, was used to burn samples under load in a Muffle furnace. The load used was a steel cylinder of 400g, which was placed on the top of the sample during burning. The mould has an internal diameter of 50 mm. A sample cutter was used to prepare the samples also shown in Figure 3.1. The char yield after being burned at 600°C for 30 minutes can represent the total char yield.

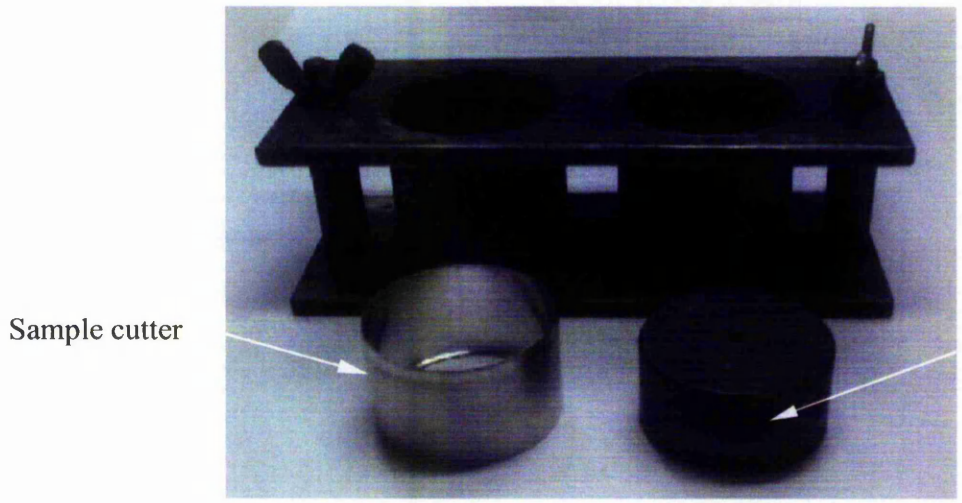

Figure 3.1 The mould for the burning under load in a Muffle furnace

Burning tests of the PU 173 - PU1476: The foams of the PU173 – PU1476 used for developing characterisation techniques were ground into powders. The powders were prepared by pressing a 0.25g of sample in a steel mould with a diameter of 13 mm at 8 MPa for 10 minutes. The pressed discs were used for both the natural burning test and furnace burning without load.

Burning tests of the Hilti products: The commercial fire stopping products used for studying intumescent mechanisms were cut into bars with a cross section of 20x20 mm for the natural burning test. The length of the samples was sufficient in each case for a

saturated thickness of char to be developed. The saturated thickness of char refers to the thickness of char that does not increase obviously when the sample was burnt for a longer time.

The commercial fire stopping products were also cut into discs with a diameter of 50 mm for burning under load. The sample mass used was approximately 3 g.

Burning tests of graphite/polyurethane nanocomposites: Graphite/polymer nanocomposites synthesised were burnt by both natural burning and furnace burning without load. When the nanocomposites were in the form of films, the samples prepared were a quarter of round films with a diameter of approximately 50 mm. While the nanocomposites in the form of foams, the samples prepared were a part of a cylinder of Ø50x5 mm.

All the samples were dried in a vacuum oven at 80°C for two hours before burning tests were carried out.

3.4 Char yield

The intumescent char produced from natural burning was not completely burned. Its yield was defined as residue yield and measured by the following method. Samples were weighed W_0 g before being burnt. The whole of the burnt sample was weighed W_1 g. The unburned part was separated from the char and weighed as W_2 g. The residue yield was then calculated using Equation 3.1:

$$\mathrm{Re}\,sidueYield(Natural) = \frac{W_1 - W_2}{W_0 - W_2} \times 100\% \qquad \text{Equation 3.1}$$

The char yield by burning in a Muffle furnace both with and without load was calculated by dividing the burnt sample weight W_3 after burning by the weight W_0 before burning.

$$CharYield(Muffle) = \frac{W_3}{W_0} \times 100\% \qquad \text{Equation 3.2}$$

3.5 Measurement of open porosity of the chars

The permeability of the char may be characterized by open porosity. The measurement of open porosity is based on the Archimedean principle and has been developed into standard methods such as ASTM C-20. The bulk density, the weight per unit bulk volume of the material, can be also obtained. The measurement involves weighing the dried char in air, W_d, the water saturated char in air, W_{sa}, and the water saturated char suspended in water, W_{su}. The open porosity, P_o, and bulk density, D_b, can be calculated by the following equations:

$$Po = \frac{W_{sa} - W_d}{W_{sa} - W_{su}} \times 100,\% \qquad \text{Equation 3.3}$$

$$D_b = \frac{W_d}{W_{sa} - W_{su}} \times 1000,\ kg/m^3 \qquad \text{Equation 3.4}$$

The dried weight of char was measured after drying the sample at 105°C for 2 hours. The char was boiled in distilled water for 30 minutes and left in the water 24 hours to ensure water saturation of the open pores.

An analytical balance, August Sauter KG. D-7470 Ebingen 1, was used to measure all the weights. A metal mesh bucket and metal wire were used to hang the sample, which was suspended in water, on the balance. If the sample floated in the water, a metal disc was placed on the sample to sink it to the bottom of the bucket. The wire, bucket and disc as a system were suspended in distilled water and weighed with and without sample. The results were recorded G g and G_0 g respectively. The suspended weight is the difference between G and G_0.

$$W_{su} = G - G_0,\ g \qquad \text{Equation 3.5}$$

The water boiling method applied in this study may cause some damage of the pore structure of the char. However repeating experiments showed that the experimental deviation was less than 5%. Compared to other methods such as mercury intrusion, the change of the pore structure due to damage is less significant.

3.6 Morphological studies

Stereo-microscopy, polarized reflected optical microscopy and scanning electron microscopy (SEM) were applied to study the morphology of the chars. Stereomicroscopy and SEM used naturally fractured specimens. The specimens for SEM observation were coated with gold to obtain a good conductivity. The specimens for examination by polarized reflected optical microscopy were polished.

Preparation of polished specimens: The chars produced by the natural burning test were highly porous and were reinforced with a low viscosity adhesive such as Scotch-weldTM 3M cyanoacrylate adhesive to avoid deformation of the samples in the following preparation. The reinforced char blocks were cut vertically to expose the cross-section which showed the char structure at different burning depths. The samples were then mounted in a cold set resin such as Struers Acryfix Kit. The mounted specimens were ground with SiC paper gritsizes 200, 400, 800 and 1200 successively. After grinding the specimens were polished using polishing cloth with Alpha 1μm Metprep Polishing alumina in an aqueous slurry. Grinding and polishing were carried out using a Buehler Motopol ^{TM} 2000 grinder/polisher.

Microscopy: An Olympus stereomicroscope with magnification between 7 to 40 times was applied to investigate the 3-D morphology of the samples and their chars. A Leitz Orthoplan Metalurgical microscope was used to investigate the char textures at high magnifications. An ISI-DS130 Dual Stage Scanning Electron Microscope was also used to investigate the intumescent chars. The acceleration voltage applied was 25kV.

3.7 Mechanical characterisation of the chars

The hardness of the chars was examined to determine their strength to resist external forces. The indentation methods applied to assess the strength of intumescent chars were the mini load Vicker hardness to determine the Vicker hardness of the char walls and a durometry technique to characterise the bulk strength of chars.

A *Leitz* mini load Vicker hardness tester was used to measure the hardness of a material in micro-scale. The indenter is a square-based pyramid whose opposite sides meet at the apex at an angle of 136°, as shown in Figure 3.2. The indent was measured by a digital

camera image analysis system (Archive4Images version 3.20b). The Vickers hardness (H_v) was calculated using following equation:

$$H_v = 1.854(F/d^2) \qquad \text{Equation 3.6}$$

where F is the applied load and d the diagonal length of the indent.

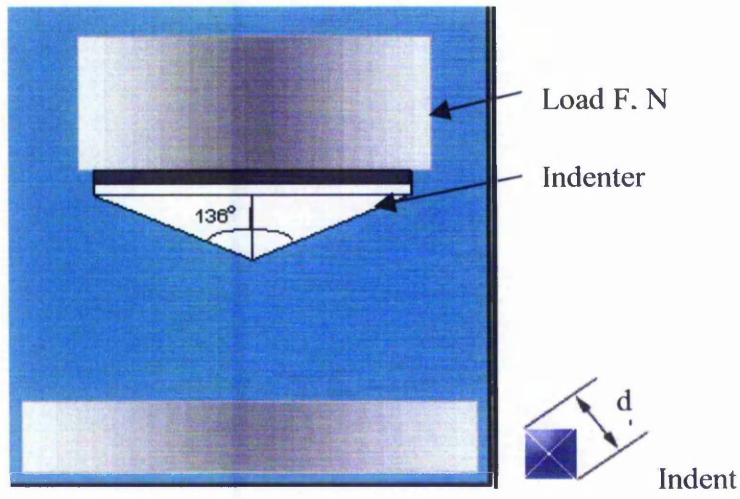

Figure 3.2 Indentation of Vicker hardness

The samples used for the mini load Vicker hardness measurement were those reinforced, mounted and polished specimens. The valid indents were made only on the char wall but the reinforcing or mounting resin.

A Rex Durometer, Model1600 designed for Type 00 Shore hardness tests was applied to measure durometer hardness. The durometer exerts a static pressure on a semi-sphere tipped indenter, which has a diameter of 2.4 mm and length of 2.7 mm. The durometer hardness is determined by the extent of penetration of the indenter into samples, ranging from 0 to 100. The reading is 0 when the indenter totally goes into the sample and 100 when the penetration depth of the indenter is zero. The reading is a comprehensive response of elastic and plastic deformation.

The samples used for durometer hardness measurement were the chars produced by natural burning. The measurement was carried out either at the top surface of the chars or on the transverse section.

3.8 Thermogravimetric analysis

A Thermal Science STA 1500 thermogravimetric analyser (TGA) was used for thermogravimetric analysis of graphite oxide and its polymer nanocomposites. Approximately 7 mg of samples were placed in a sample bucket and heated from ambient temperature to 600°C at a heating rate of 15°C/min under either flowing argon (50 ml/min).

3.9 Characterisation of the nanostructures

A X-ray diffraction spectrometer was used to characterise nano-structures of graphite in the samples studied. X-ray diffraction patterns were measured by a Philip's X-ray diffractometer with CuKα_1 or Cr incident X-ray source. The measurements were carried out under conditions of 30 mA current, 40 kV voltage and a scanning rate of 1°/min at a step of 0.02°.

In graphite, its aromatic sheets are principally stacked in a manner of ABAB. The crystal unit cell is hexagonal and has a size of a=b=0.2456 nm and c= 0.6708 nm. Its most characteristic peaks at 002 2θ= 26.56°, 100 2θ= 42.46° and 101 2θ= 44.65° can be calculated by the following formula[144]:

$$Sin^2\theta_{hkl} = \frac{\lambda^2}{3a^2}(h^2 + hk + k^2) + \frac{\lambda^2}{4c^2}l^2 \qquad \text{Equation 3.7}$$

where θ is the diffraction angle; a and c are side length of the hexagon and unit cell height respectively; h, k and l are lattice positions; λ is the wavelength of the incident x-ray, for CuKα_1 λ=0.1540 nm, for Cr λ=0.2290 nm.

The spacing (distance) of crystal planes was calculated by Bragg's law, Equation 3.8.

$$d = \frac{n\lambda}{2}\sin^{-1}\theta \qquad \text{Equation 3.8}$$

where d is the crystal plane distance, λ incident radiation wavelength, θ the diffraction angle and n is the order of diffraction.

Sherrer Equations[78] (Equations 3.9 and 3.10) were applied to calculate the stacking width and height of graphite crystallites:

$$\text{Stack width: } La = 1.84\,\lambda/\beta\cos(\theta) \qquad \text{Equation 3.9}$$

$$\text{Stack height: } Lc = 0.9\,\lambda/\beta\cos(\theta) \qquad \text{Equation 3.10}$$

where λ is the wavelength of the incident X-ray, θ is the diffraction angle and $\beta^2 = B^2 - b^2$. B and b are the half widths of the sample peak and a highly crystalline standard respectively. Here b=0.3°.

3.10 Synthesis of expandable and expanded graphite

Expandable graphite was prepared by acid treatment of graphite flakes with a mixture of concentrated H_2SO_4 (Prolabo, 98%) and HNO_3 (Prolabo, 68%) (90:10 vol). Three grams of the Aldrich-F was stirred in 20ml of the acid mixture at room temperatures for two hours. After filtration, the treated graphite flakes were washed with distilled water until sulphate ions free and then dried in a vacuum oven at 50°C for 5 hours to obtain expandable graphite.

The expandable graphite was heated in a preheated crucible at 800°C for 1 minute to produce expanded graphite whose volume was a few hundred times higher than the original graphite flakes.

3.11 Synthesis of graphite oxide

A modified Hummers and Offeman method [145] was applied to produce graphite oxide. Graphite powder (10g) was added to 230ml of cold concentrated H_2SO_4 (0°C) (Prolabo, 98%). Potassium permanganate (30g) (Aldrich, 97%) was then added gradually with stirring. An ice bath was used to keep the temperature below 20°C. The mixture was then stirred at 35°C for 30 minutes. Distilled water (460 ml) was then slowly added. This resulted in an increase of temperature to 98°C. The reactant was held at 98°C for 15 minutes. Afterwards, the reaction was terminated by the addition of a large amount of distilled water (1.4L). Hydrogen peroxide aqueous solution (100ml) (Aldrich, 35%) was added to convert impurities into water-soluble salts. The mixture was filtered, and then washed successively with 5%HCl aqueous solution until sulphate ions could not be

detected with $BaCl_2$ aqueous solution. The mixture was further washed using distilled water.

3.12 The intercalation of graphite oxide with hydrophilic polymers

Graphite oxides synthesised were intercalated with hydrophilic polymers such as polyethylene oxide (Aldrich, Mn600,000), polyethylene glycol (Aldrich, Mn1500) or polyvinyl pyrrolidone (Aldrich, Mn55,000). Graphite oxide (1g) was dispersed in 300 ml of distilled water and sonicated for 30 minutes to improve the dispersion. The slurry was then stirred at room temperature for 24 hours. A hydrophilic polymer (1g) dissolved in 200 ml distilled water was added to the graphite oxide suspension. The mixture was sonicated for 30 minutes and then stirred for 24 hours. The aqueous suspension was dried in a fanned oven at room temperatures. After drying, the intercalated products were cast into films. The films were ground for further synthesis studies. The sonication was carried out in a Kerry ultrasonication bath with a model No. PUL55.

3.13 Synthesis of graphite/polyurethane nanocomposites

A polyurethane foam formulation was applied to synthesise graphite/polyurethane nanocomposite foams and to examine the nanostructure and the char formation of the nanocomposites produced. The diisocyanate and polyol components were a tolylene diisocyanate (TDI) (Aldrich, 98%, 80/20) and a polyethylene glycol with a number average molecular weight of 300 (Aldrich, Mn300), respectively. The polyol was dried over 4Å molecular sieve, which was baked at 250°C for 4 hours in advance. Water (3% based on the polyol weight) was used the as blowing agent and 1,4-Diadabicylo[2,2,2]octane (0.1% based on the polyol weight) as the catalyst. The isocyanate index of the foams was 105. The graphite source, water and catalyst were dispersed in the polyol by grinding and sonication. The mixture was then polymerised with the TDI to produce the graphite/polyurethane nanocomposites.

3.14 Ash content of graphites

All the graphites used in this project had their ash content examined. One gram of graphite was burned in a Muffle furnace at 850°C until it had a constant weight. The ash content was measured by dividing the mass of the sample after burning (M g) by the original mass of the sample before burning (M_0 g):

$$AshContent = \frac{M}{M_0} \times 100\% \qquad \text{Equation 3.11}$$

Chapter 4

The Development of Methodologies for Characterisation of Intumescent Chars

4.1 Introduction

The development of commercial intumescent fire retardant systems has been going on for a few decades. Further development has been hindered by the lack of understanding of the swollen condensed phase formed during burning and the relationship between intumescent fire retarding efficiency and the quality of intumescent chars. To develop better fire retarding systems, it is essential to study the intumescent mechanisms of existing intumescent fire-retarding products, to determine their weaknesses and to establish the relationship between intumescent fire retarding efficiency and the properties of intumescent chars. Based on these studies, the nano-technology approach can be applied to design a new generation of intumescent fire retarding polymer systems.

In the literature, there are few valid techniques developed for the characterisation of intumescent chars. Thus, techniques need to be developed to characterise the protection, the structure, permeability, reactivity and strength of intumescent chars.

This Chapter gives details of the techniques developed for the characterisation of intumescent chars. The techniques were applied to a series of well-known rigid polyurethane foams for the characterisation validation of the chars.

4.2 Production of intumescent chars

The characteristics of intumescent fire retardancy are that a layer of swollen carbonaceous char forms on the top of burning polymer and the char layer protects its underlying polymer from further burning. Char yields and intumescent ratios are used to evaluate how much of the polymer being converted into more thermally stable carbonaceous char and how much the char expanded.

Values of char yields depend not only on the chemical structure of polymers, but also on the way chars are produced and what additives have been added in polymer systems. On laboratory-scale, char yields are normally measured by heating samples in an inert atmosphere or in air such as in thermal gravimetric experiments or in a Muffle furnace or in a cone calorimeter. These methods completely burn or decompose polymer samples. They cannot exhibit that the char formed protects the underlying polymers from further burning.

In this project, the intumescent chars studied were produced by a single direction heated, well-ventilated natural burning method. The samples prepared for burning had sufficient thickness to produce a thickly saturated char, namely, where there was unburned polymer at the base of the burnt samples. The transverse cross-section of the intumescent char presents the whole burning process. It maps the charring history. The yield of the thickly saturated char was then calculated as residue yield (Equation3.1). The char formed by natural burning was not completely burnt due to the protection of the top part. The protection was evaluated by calculating the difference between the natural burning residue yield and the char yield burnt in a Muffle furnace, marked as char yield (furnace). The calculation of char yield difference is described in Equation 4.1.

Char Yield Difference = Residue Yield (natural) – Char Yield (furnace), wt.%

Equation 4.1

Intumescent ratios of the char are usually measured by expansion ratio of the sample thickness or volume. In terms of intumescent barrier functions, the absolute char thickness is more important than the expansion ratio. Thus, the designed natural burning method burns a sample until a saturated layer of char forms on the top of samples, to show how thick a layer of char is needed to protect its underneath for a given polymer system. For fire-stopping intumescent polymer products, volume expansion is more important. The volume expansion ratio is defined as the ratio of the volume of intumescent char to the volume of the sample before burning. Fire stopping products would burn under volume-constrained conditions in which the char was formed under pressure and a badly ventilated combustion environment. A burning under load method

was designed to simulate these conditions. Application details of this method will be discussed further in Chapter 5.

The samples of the PU173, PU328, PU856 and PU1476 were burnt by the natural burning method to produce intumescent chars for characterization studies. The residue/char yields of both natural burning and furnace burning were examined, and their relation to isocyanate indexes are shown in Figure 4.1. By natural burning, the PU173 produced 29.2% of residue. With the increase in isocyanate index, the natural burning residue yields increased to 37.8% for the PU328 and 54.5% for the PU856 and then remained constant as the isocyanate index of the PU foams increased further.

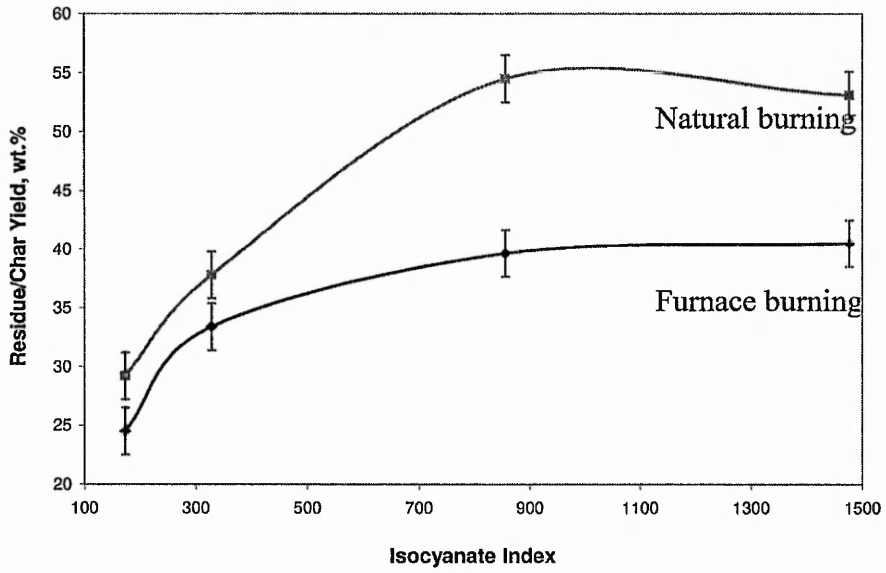

Figure 4.1 The variation of char yields with isocyanate index of the PU samples

The char yields obtained by burning in the Muffle furnace varied with the isocyanate index of the PU samples in a similar manner to that by the natural burning method except the Muffle char yields were lower than those of natural burning. The natural burning test heated the samples unidirectionally, and the combustion of the sample was incomplete as the char layer produced in burning protected the underneath polymer. In the case of the samples tested in the Muffle furnace, the samples were heated from all directions and were more completely burnt. The difference in the char yields between these two burning methods increased with the increase in isocyanate index of the samples until the isocyanate index was 856. This will be discussed further in Chapter 4.3.

The chars produced from natural burning expanded and had saturated thicknesses. As examples, the chars of the PU 173 and PU1476 samples are shown in Figure 4.2. The top surfaces of the chars, which had the Bunsen flame directed on them, were black and had smaller diameters than the rest of the chars. The burnt samples had the bottoms which were yellow in colour, indicating they had been protected from burning by the char formed above. These are typical intumescent fire retarding phenomenon. The variations in the dimensions of the chars are presented in Table 4.1.

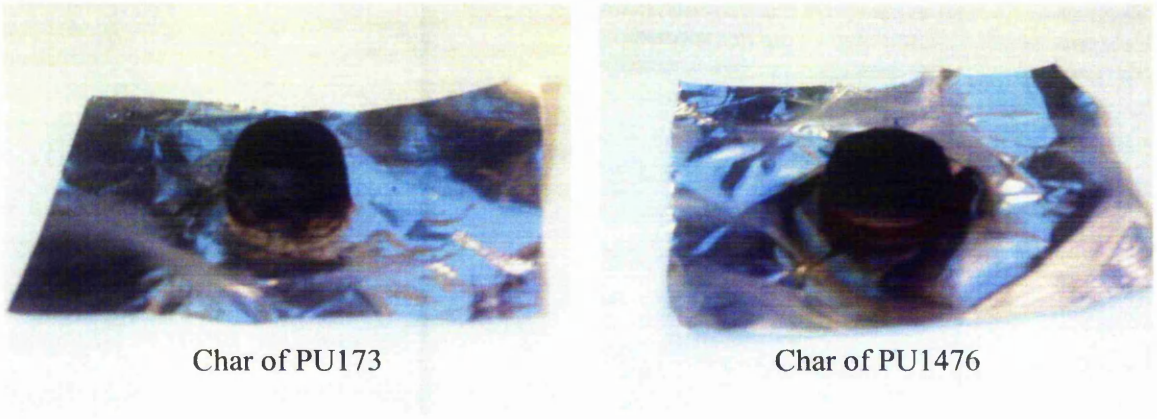

Char of PU173 Char of PU1476

Figure 4.2 Chars of the PU 173 and PU1476 samples, by natural burning

Table 4.1 Variations in dimension of the PU foams after natural burning

Samples	Original Size	Residue Size
PU173	Ø13.00x3.00mm	Ø12.0x9.34mm
PU328	Ø13.00x3.38mm	Ø13.20x6.46mm
PU856	Ø13.00x3.60mm	Ø13.70x5.52mm
PU1476	Ø13.00x3.66mm	Ø13.90x4.88mm

The volume expansion ratios of the samples were calculated by taking the chars as cylinders. The variations of the volume expansion ratios and char thickness with the isocyanate index are shown in Figures 4.3 a & b. As the isocyanate index increased from 173 to 1476, the volume expansion ratios of the chars decreased from 2.65 to 1.52, the char thickness decreased from 9.34 mm to 4.88 mm.

This series of samples contain isocynurate structures. [34] Isocynurate structures are more thermally stable than urethane structures due to their hexagonal cyclostructures, which converts easily into condensed aromatic compounds as char in the condensed phase.

The sample with a higher isocyanate index has more isocynurate structures and can produce more char and less decomposed volatiles resulting in a smaller expansion of the char. This is also consistent with the variation in the char yields with the isocyanate index, as shown in Figure 4.1.

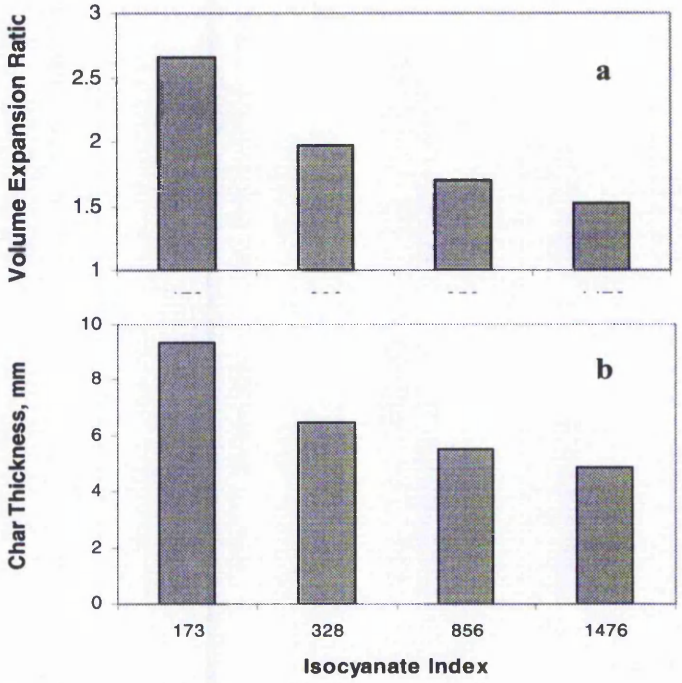

Figure 4.3 The variation in volume expansion ratio (a) and char thickness (b) with the isocyanate index of the PU samples after natural burning

4.3 Characterization of gas permeability of chars

Intumescent chars have two roles in protecting the underlying polymer. They act as a barrier that prevents decomposed inflammable gases, which are released during burning and act as fuel, from reaching the burning zone. The char also insulates the underlying polymer from the combustion heat. The heat transfer between the burning zone and the underlying polymer of the intumescent char involves radiation, thermal conductivity and convection three forms. Among them the convection correlates with the gas permeability of the chars, while the radiation is related to the integrity of chars rather than the gas permeability of chars. The conductivity of the combustion heat is determined by the char structure and thickness. Thus, the efficiency of char barrier is determined mainly by the integrity, thickness and gas permeability of the intumescent

chars with a given chemical structure. The gas permeability of chars is correlated with the porosity of the chars, especially, the open porosity and open pore distribution. The open porosity is the volume fraction of the open pores in a porous material, which can be penetrated by a liquid or a gas. However, no published work has studied the open porosity or permeability of intumescent chars so far, because of the difficulty in handling the brittle and fragile intumescent chars that have random geometry.

Open porosity can be examined by volumetric saturation of the pores with a gas or a liquid. Well-developed methods include gas adsorption and mercury intrusion. Nitrogen and carbon dioxide are commonly used gas adsorbents. Nitrogen adsorption measures the pore volume and the distribution of pores ranging in size from 2 nm to 200 nm. Carbon dioxide adsorption is only able to measure micropores. In terms of IUPAC classification, a micropore is less than 2 nm in diameter. The pores at the range of 2-50 nm are mesopore and those larger than 50 nm are macropore. Gas adsorption methods are suitable for the measurement of pores in nano-scale.

Mercury intrusion uses non-wetting mercury to fill the pores of a porous material and gain information on pore volume and distribution. As a consequence of this non-wetting medium, a high pressure is needed to force mercury into small pores. This method may measure pores ranging in size from 4 nm to 120 μm by adjusting the intrusion pressure from vacuum to 400MPa.

Intumescent chars have a large volume of pores and fissures. The pores and fissures have a wide distribution in size, commonly, up to a few millimetres. The chars must be treated in their entirety. Due to the wide distribution in pore sizes and the brittleness of the intumescent chars, the well-developed gas adsorption and mercury intrusion methods are not suitable for the porosity study of intumescent chars. In this project, water was used as an adsorbent to saturate the pores in the intumescent chars.

A study of open porosity was carried out on the naturally burnt chars of the PU173, PU328, PU856 and PU1476 samples using the water saturation method. The variation in open porosities with the isocyanate index is shown in Figure 4.4. The open porosity of the char decreases as the isocyanate index of the foams increases. The percentage change in open porosity is from 93.6% for the char of the PU173 to 86.0% for the char

of the PU 1476. This agrees with the larger expansion of the char with lower isocyanate index.

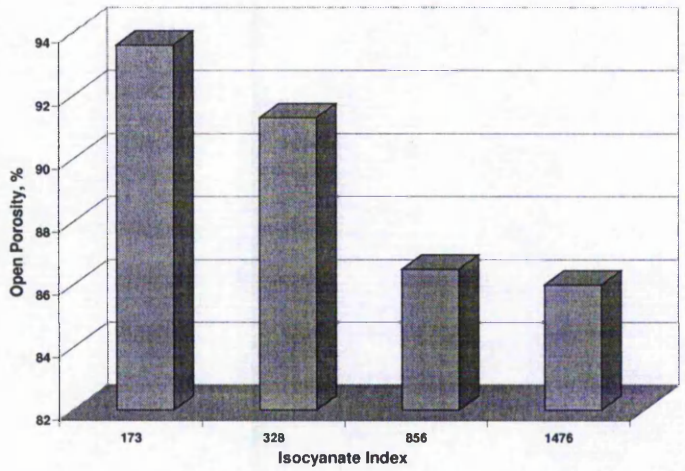

Figure 4.4 Open porosities of the natural burnt chars *vs* isocyanate index

The differences in the char yields between natural burning and burning in the Muffle furnace are plotted against the open porosities measured from the naturally burnt chars in Figure 4.5.

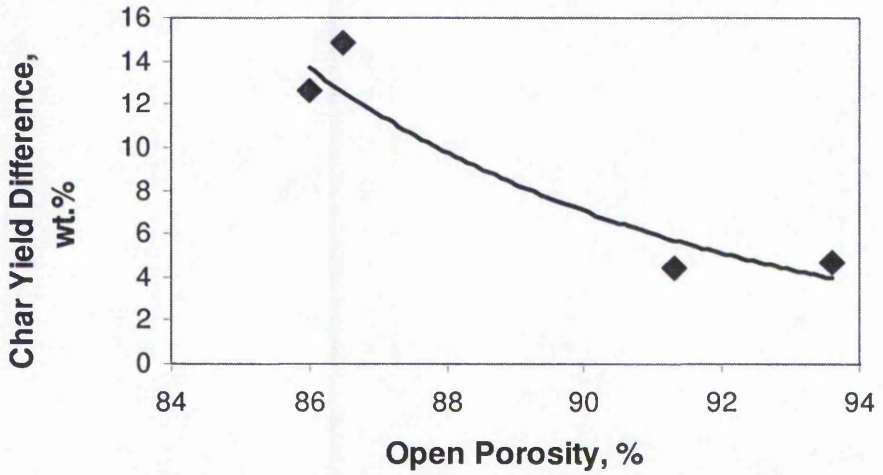

Figure 4.5 Variation of char yield difference between natural burning and burning in the Muffle furnace with the open porosities of the naturally burnt chars

This figure shows that when the naturally burnt char has more than 90% of open porosity the natural burning method produces about 4% more char compared to burning in a Muffle furnace. The char yield difference is 12-14% when the naturally burnt chars with open porosity of about 86%. The lower the open porosity, the higher the difference

in the char yields. As the char yield difference is a measure of the protection of the intumescent char barrier, the chars with lower open porosity have better barrier effects in protecting the polymer underneath from further burning.

4.4 Char structures

The open porosity determines the gas permeability of chars, but it cannot give information on closed pores and interconnectivity between pores. These are important factors in permeability, reactivity and strength of intumescent chars.

Stereo-microscopy, reflected optical microscopy and scanning electron microscopy (SEM) were applied to study the morphology of chars. Stereo-microscopy at magnification from 7 to 40 times is a powerful technique for the study of integrity of chars and interconnectivity of large pores. A polarized reflected optical microscope with a magnification of 500 times is used for the observation of closed pores in micro scale and interactions between phases especially for samples where inert additives are involved. The reflectivity of the chars formed from polymers may also distinguish the reactivity of the chars. Scanning electron microscopy can clearly show char morphology at a large range of magnifications. The combination of these three microscopies allows the char morphology and structure from macro to micro scale to be examined. Table 4.2 lists the features of these three microscopies.

Table 4.2 Features of three microscopies

Microscopy	Sample preparation	Study range	Key features
Stereo	Very easy	Macro	3D, integrity, open pores, interconnectivity
Polarised reflected	Complicated Time consumed	Micro	2D, closed pores, interaction of phases, reactivity
Scanning Electron	Easy	Macro-Micro	3D, interconnectivity, open pores, interaction of phases

The naturally burnt chars of the PU173 and PU856 samples were studied by means of a polarized reflected optical microscope. The micrographs are shown in Figures 4.6. The chars were vertically cut to expose the char at different burning depths. The

micrographs labelled top are from close to burning surface, the micrographs labelled middle are from the middle of the chars and bottom micrographs are from close to the unburned bases. The chars are composed of char wall (the bright structures in the micrographs) and a large number of fissures (the darker part), which are occupied by the mounting material.

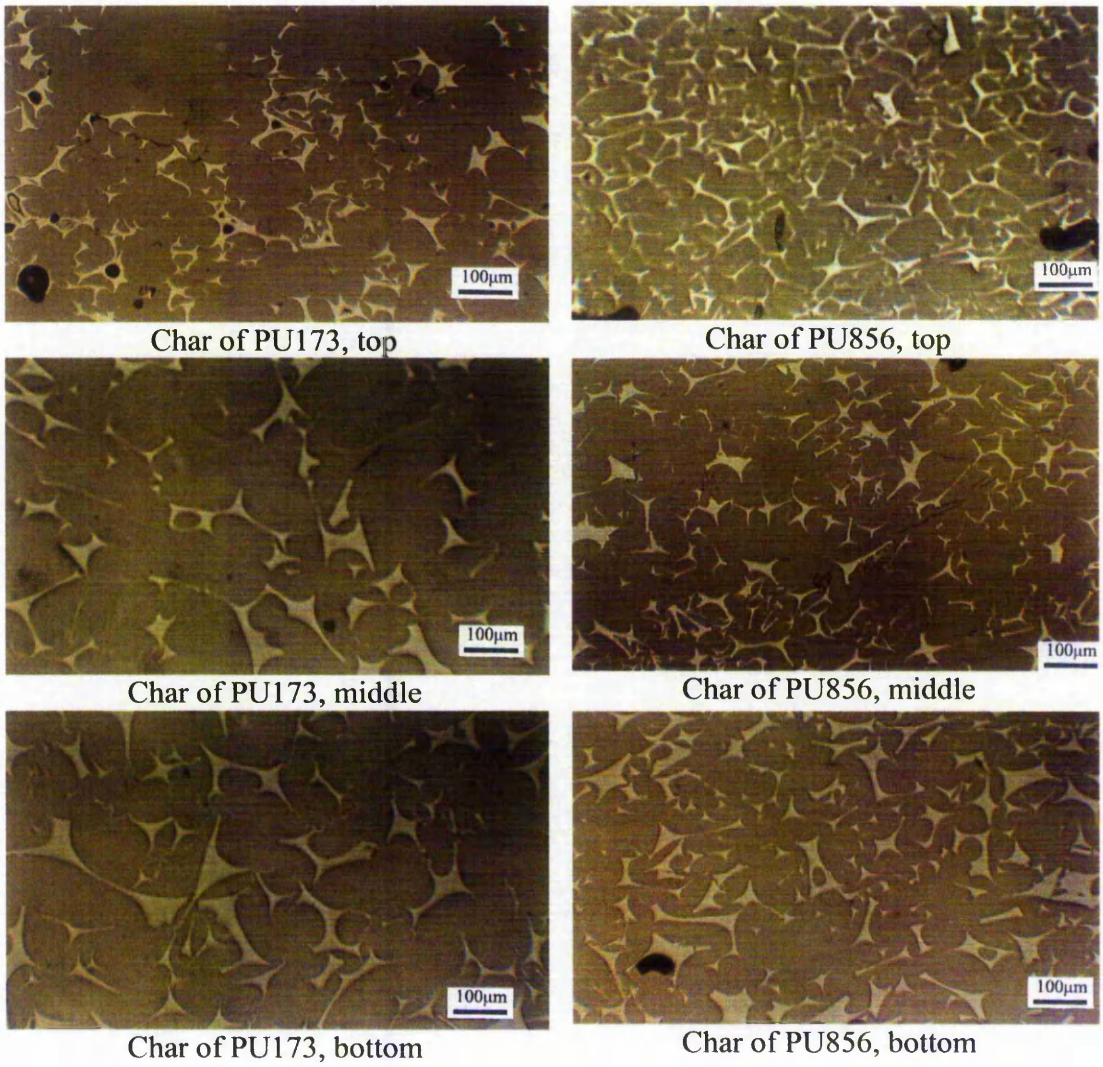

Figure 4.6 The char structures of the naturally burnt chars of the PU173 and PU856 samples. The bright structures are char walls; the darker parts are fissures occupied by resin. (Polarized reflected micrographs)

The char walls from the burning surface to the unburned interface have clear edges and corners, indicating that the foam walls did not melt during the burning process. There are very few closed pores in the chars. All the fissures are virtually open. The

micrographs from the top sections of the chars show that the charred foam walls are smaller in size and agglomerate closer together than those in the middle and bottom of the chars. The char walls are thicker and more widely dispersed when they are further away from the burning surface. Comparing the micrographs of the chars of the PU173 and PU856, the char of the PU173 has larger fissures. The fissures contribute to the high open porosity of the char. The information from these micrographs is consistent with both the open porosity measurements and volume expansion ratios.

The colour of the char wall becomes darker towards the bottom of the chars. Studies of coal and coke have shown that polymeric organic materials have a higher reflectivity when they have denser aromatic structures.[78] The variation in colour of the char wall indicates that the chemical structures of the char walls at the top of the char have higher aromaticity than those at the bottom. The aromaticity of the chars increases with the isocyanate index of the original foams. The higher the aromaticity of the char, the char has a higher oxidation resistance and a lower reactivity.

4.5 Mechanical properties of chars

The mechanical properties of a solid material refer to the response of the material when it is subjected to an external force. The core mechanical property of materials is strength. In light of how materials behave and how failures occur in a variety of loading conditions, materials can be used more effectively and safely.

When a load is applied, a material has one of two possible responses: deformation or fracture. The deformation, either elastic or plastic, can be clearly demonstrated by either a tensile or an indentation test, respectively. In both tests, materials at first resist the external force applied by elastic deformation. When the tensile or shear stress is increased beyond the elastic limit of the material the basic structures of the material becomes distorted by dislocation mechanisms and then plastic deformation occurs. If the stress increases further beyond the plastic limit of the material fractures occur. [78]

A fracture is the separation of a material into two or more parts. The nature of the fracture depends upon the material, and is affected by the type of applied stress, geometrical features of the sample and environmental conditions. In high porosity materials, the pore characteristics are the most significant factors that influence the

strength. With increasing porosity, the strength of a material decreases. In addition to total porosity, the pore size and shape are also important.[78]

Indentation tests can measure the plastic and/or elastic deformations of a material at the same time. Durometer hardness and nano-indentation test measure both plastic and elastic deformation while the Vicker hardness test only measures the plastic deformation. In this study, miniload Vicker hardness and durometer hardness methods were applied to measure the char wall hardness and the bulk strength of the intumescent char, respectively.

The indents of a mini load Vicker hardness indentor made on the char wall are shown in Figure 4.7. Due to the non-continuity and small dimensions of the char wall, the indents are more difficult to make than on a continuous material. The indents are clear if the whole indent is on the char wall.

Figure 4.7 Indents of the mini load Vicker hardness on the char wall of the PU173 sample

The hardness of the naturally burnt chars of the PU173, PU328, PU856 and PU1476 samples were investigated by means of the Vicker mini load hardness test. The Vicker hardness of the char walls in the middle and at the bottom of the chars are plotted against the isocyanate index in Figure 4.8. The hardness of the char wall at the bottom increases from 84.2MPa to 324.4MPa as the isocyanate index rises from 173 to 856, and then tends to be constant. This indicates that the increase in isocyanate index makes the polyurethane harder until the isocyanate index reaches approximately 850. Increasing the isocyanate index further does not affect the hardness of these polyurethanes. Similarly, the char wall in the middle of the char has a maximum hardness of 540.2MPa when the isocyanate index is approximately 850. The char wall in the middle of the PU1476 sample was very brittle, and cracks occurred when the material was indented, making it difficult to obtain accurate hardness values. The char wall at the top of the chars was brittle. When the char wall was indented, they cracked, and the results were considered to be invalid.

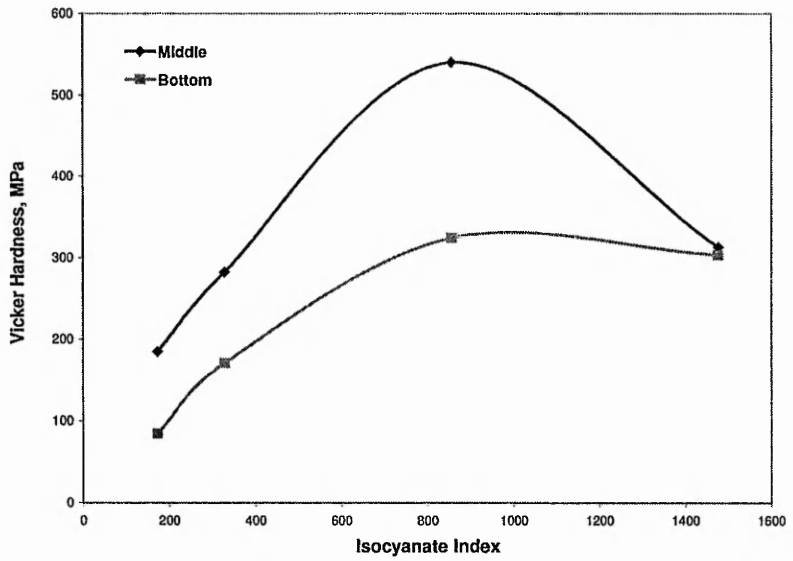

Figure 4.8 Vicker hardness of the charred PU walls vs isocyanate index

The Vicker indentation methods can only measure the hardness of the char wall. It is not able to measure the strength of the whole chars to show the strength of integrity of the char walls. A durometry technique was developed to characterise the bulk strength of the intumescent chars of the PUs. The measurements were carried out only on the top of the chars instead of on the cross section of the chars because the chars were small. The results are shown in Figure 4.9.

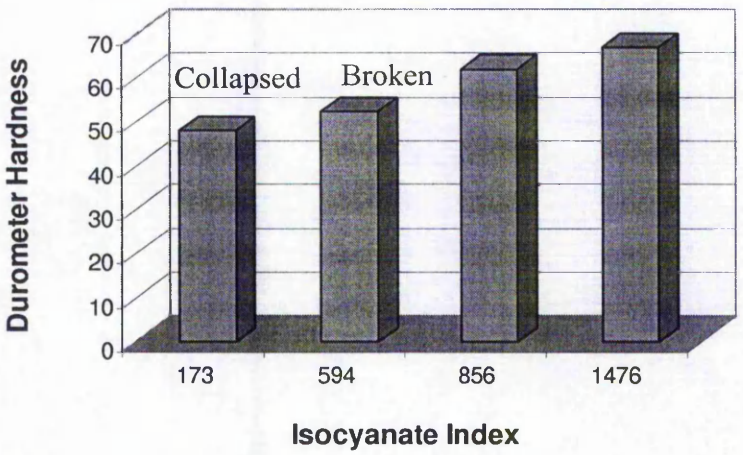

Figure 4.9 Durometer hardness of the PU foam chars *vs* isocyanate index

The four chars behaved differently when the measurements were carried out. The char of PU173 sample had an initial durometer reading of 48 which decreased gradually to 0. The char structure collapsed under the load of the test. The char of the PU594 had a durometer hardness of 52.5, however, the test left cracks originating from the indented point on the sample. The chars of PU856 and PU1476 samples had durometer hardnesses of 62 and 67, respectively. No collapsing of the structure or cracks appeared during these measurements. The indents of these three types are shown in Figure 4.10.

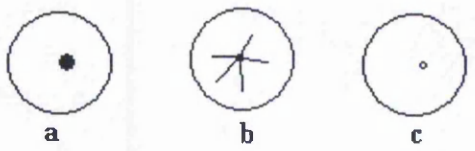

Figure 4.10 Three types of indents: (a) collapsing, (b) cracking, (c) shallow indent

In the case of the PU173 char, the char wall cannot support the load applied by the durometer, because of the large size of the fissures underneath it, so the indenter sinks into the char (Figure 4.10a). When this happens, the durometer reading decreases gradually to zero. The cracking shown by the PU594 char (Figure 4.10b) may be a random phenomenon due to the lack of interconnection between the char walls. With the increase in isocyanate index, the chars of the PU856 and PU1476 have a lower open porosity so that the small char wall pieces support each other. The indentations did not

damage the chars. These chars have integrity and strength (Figure 4.10c). Overall, the char having lower open porosity has higher strength.

4.6 Summary remarks

A number of characterisation techniques for intumescent chars have been developed and tested on a series of well-known rigid polyurethane foams, whose isocyanate indexes are ranged from 173 to 1476.

The single direction well-ventilated natural burning method shows that the thickly saturated intumescent chars formed protect its underneath from further burning. The intumescent chars were used for characterisation studies.

The gas permeability of intumescent chars is measured by open porosity. Open porosity is measured by water saturation of the intumescent chars.

Microscopy is used to study the morphology and structure of intumescent chars to show the char formation, closed pores and integrity of the chars.

The Vicker Hardness is applied as a measure of the mechanical property of the char wall and the durometer hardness as a measure of the bulk strength of the intumescent chars.

The protection efficiency of intumescent chars is evaluated by the difference in the char yields between natural burning and Muffle furnace burning. The larger the difference, the better is the protection.

The protective efficiency of the intumescent chars is related to their open porosities: the lower the open porosity, the better is the protection.

Chapter 5

Investigation of the Mechanisms of Intumescent Chars

5.1 Introduction

Three commercial polyurethane fire-retarding products from Hilti AG were studied using the characterization techniques developed in Chapter 4. The information on these samples, provided by the company, was that they were polyurethane-based products: a rigid foam, a flexible foam and a sheet. The composition and microstructure of the products, therefore, were investigated as a part of the mechanistic study. Studies on the intumescent behaviour of the products, char yields and gas permeability, morphology, mechanical properties and reactivity of the chars were carried out. The results obtained led to the intumescent mechanisms of these fire retarding polyurethane products.

5.2 The composition and microstructure of the products

The Hilti rigid foam studied contained two phases, continuous red-coloured polyurethane and dispersed black graphite flakes as shown in the stereo-micrographs in Figures 5.1 a & b. The red-coloured polyurethane was transparent under the microscope and formed the pore walls of the foam. The foam was highly porous and most of the pores were closed. The diameter of the pores ranged from 150 to 500 μm. The average thickness of the pore walls was approximately 50 μm. The graphite flakes ranged from 100 to 700 μm in length and were randomly orientated in the foam as shown in Figure 5.1a.

The pore distribution in the foam was not uniform, which is shown in Figure 5.1b. The area at bottom right hand side of the image is denser than the rest of the sample. The open porosity and bulk density of the foam were 39% and 246 kg/m^3, respectively. The closed pore structure gives the foam a low coefficient of thermal conductivity, which allows it to be used as a thermal insulant.

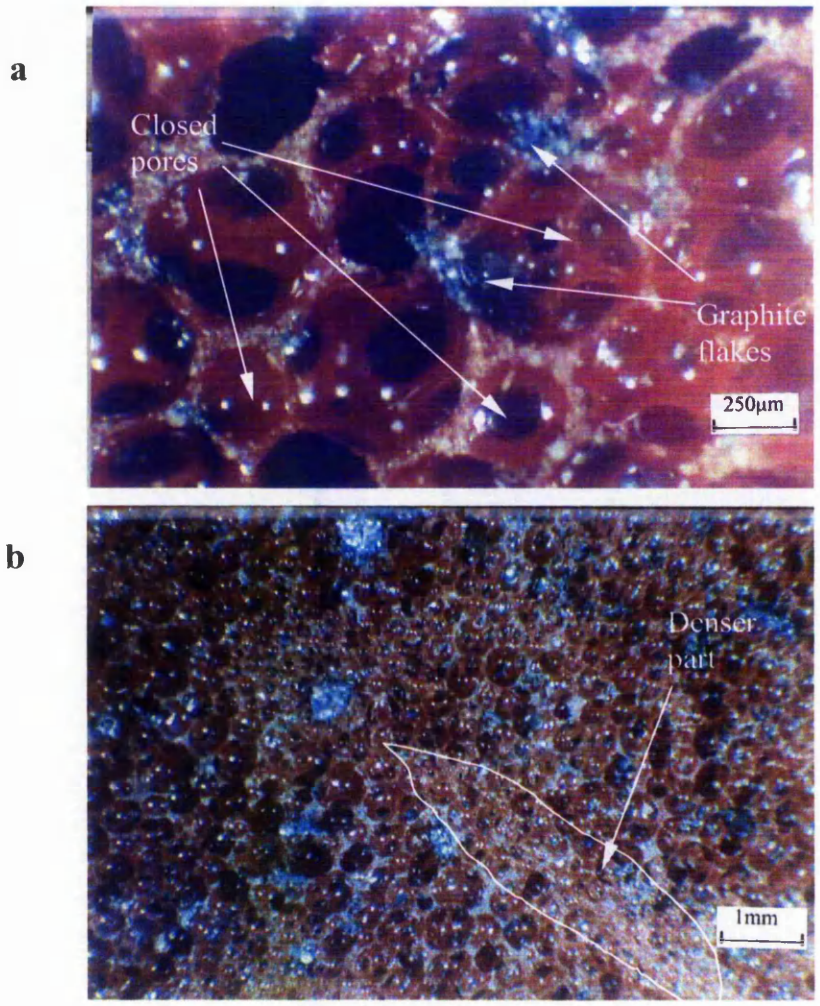

Figure 5.1 A typical structure of the Hilti rigid foam. (Stereomicroscope)

The Hilti flexible foam was red in colour and had an open pore structure with irregular-shaped voids, as shown in Figure 5.2. The pore dimensions varied in size from about 50 to 500 μm. Some voids reached up to 2 mm in length. The pores and voids resulted in a high open porosity of 90.3% and low bulk density of 84 kg/m^3.

Under the stereomicroscope, small white dots in the walls of the flexible foam were observed. In order to examine them the foam was completely burnt in a Muffle furnace at 850°C for 2 hours. After being exposed to such extensive oxidation conditions, all the carbon was burnt out so that other species in the material could be identified. The stereo-micrographs of the flexible foam residue are shown in Figures 5.3 a & b.

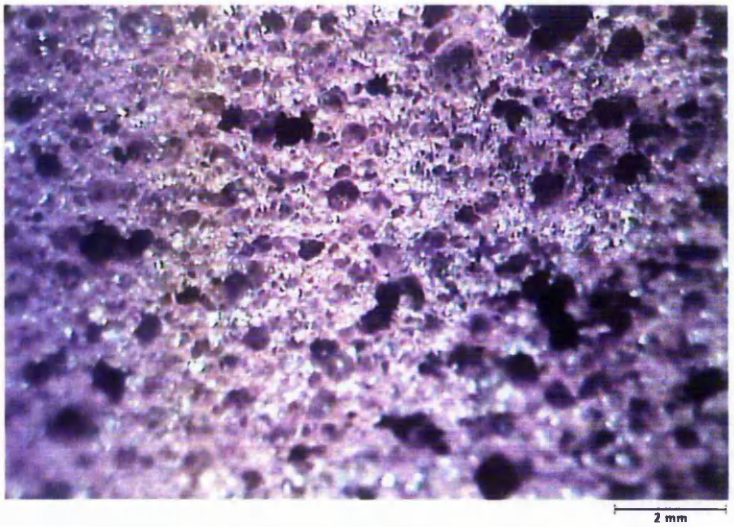

Figure 5.2 A typical stereo micrograph of the Hilti flexible foam

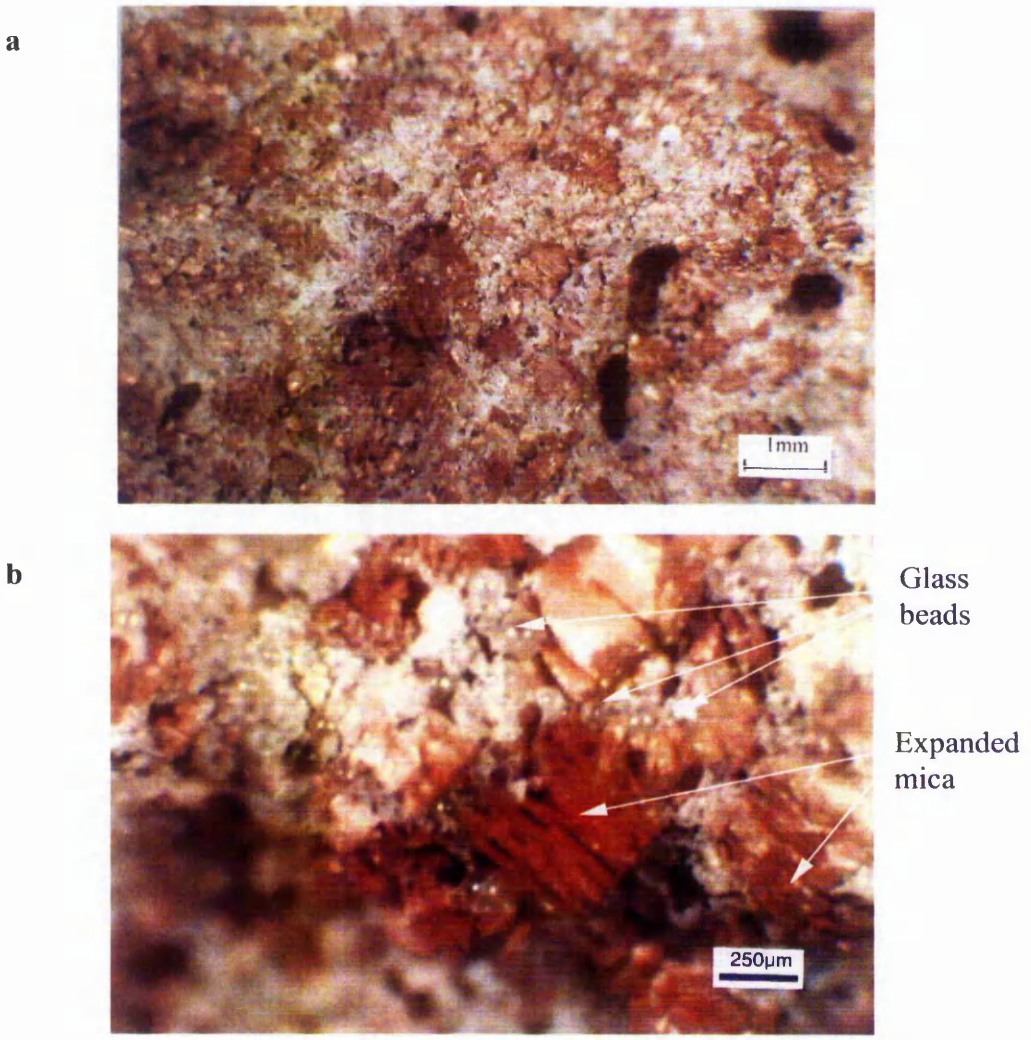

Figure 5.3 Stereo micrographs of the residue of the Hilti flexible foam being burnt in a Muffle furnace at 850°C for 2 hours

Three different inorganic additives are identified from the residue. The scattered white ash is from inorganic salt additives (Figure 5.3a). The ball-shaped particles in the residue are glass beads while the yellow accordion-like structures are expanded mica (Figure 5.3b). The ash yield was 42.2%, suggesting that the foam was half filled with inorganic additives, mainly glass beads and mica. The glass beads had diameters ranging from 50 to 150 μm, average 90 μm. The accordion-like structures of the expanded mica had a width of 200-600 μm, with an average value of 395 μm. These data were measured from the micrographs of the polished residue specimens.

The Hilti PU sheet was black and rubbery. A stereo micrograph taken from a vertically naturally fractured cross-section is shown in Figure 5.4. White fibres were observed in the sheet. There were also some white particles which might be inorganic additives. These particles exist in aggregates rather than being well-dispersed in the sheet. Other components in the sheet were very difficult to identify without further analysis. The sheet was cut vertically, mounted in acrylic resin and polished to examine the components further. A stereo micrograph of the specimen is shown in Figure 5.5.

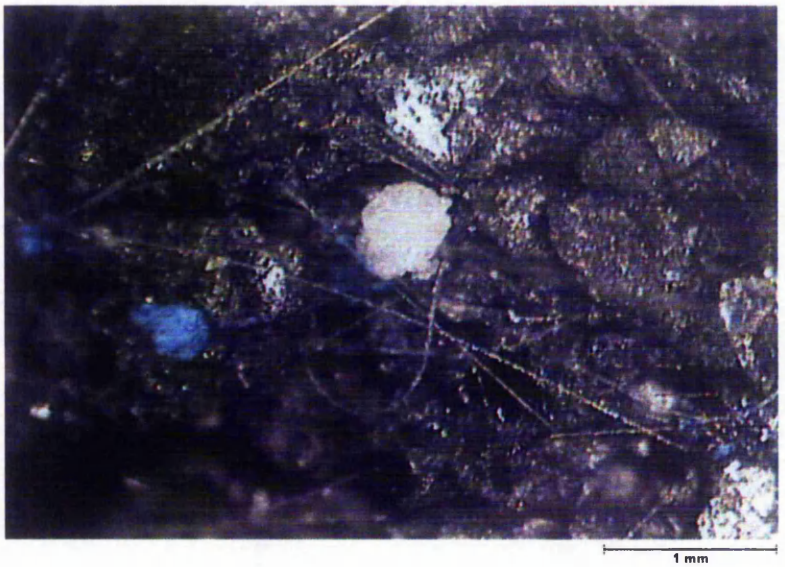

Figure 5.4 A stereo micrograph of the Hilti sheet from a vertically naturally fractured cross-section

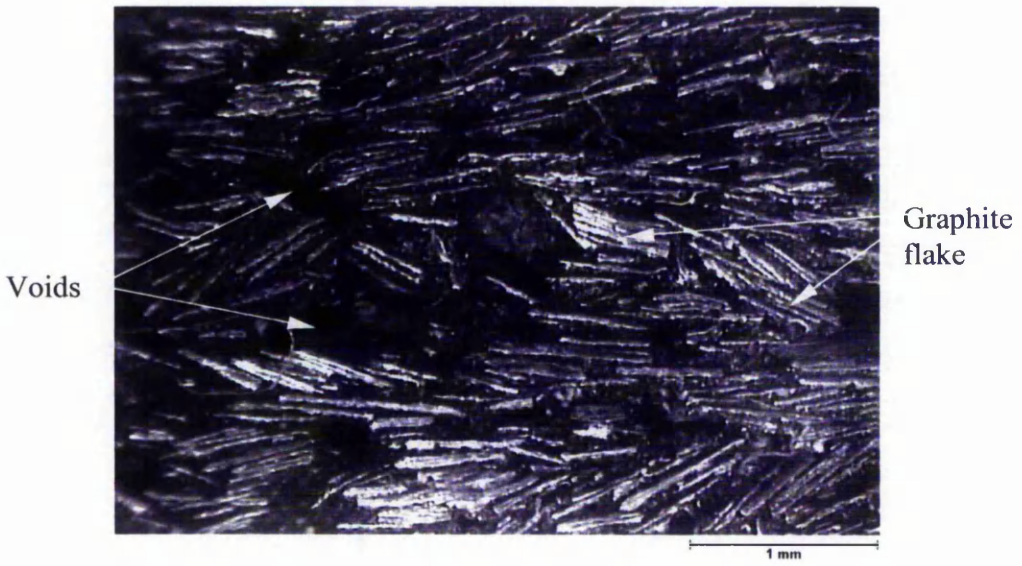

Figure 5.5 A stereo micrograph of the Hilti sheet from a polished cross-section

Graphite flakes are clearly visible and are a major component in the sheet. These graphite flakes range from 0.5 mm to 1 mm in length with a thickness of approximately 30 μm. The graphite flakes aggregate together parallel to each other while the aggregates are randomly orientated in the sheet. Among the aggregates of the graphite flakes are large voids.

The Hilti PU sheet had an open porosity of 45.3%, and a bulk density of 729 kg/m^3. The Durometer hardness reading was 85, which decreased to 84 after 15 seconds, indicating the sheet exhibiting viscoelastic behaviour.

The compositions and physical properties of the three PU products are summarised in Table 5.1. These three Hilti PU products appear to be composed of different polyurethanes, and contained large amounts of inorganic additives. The rigid foam and the sheet had graphite flakes, especially the sheet was composed of a very large amount of graphite flakes, and it also had white fibres. The flexible PU foam had mica and glass beads as additives.

The physical properties of these products depended on both the physical form of the polymer products and the amount of additives. The flexible foam had very low density because of the high porosity. The rigid foam had a large amount of closed pores so that its open porosity was only 39%. The sheet had 45.3% of open pores. It was more than that of the rigid foam, because the polyurethane did not fill the gaps among the aggregated graphite flakes of the sheet.

Table 5.1 The compositions and physical properties of the three Hilti PU products

Samples	Composition		Properties		
	Polyurethane	**Main additives**	**Db, kg/m^3**	**Po, %**	**Hd**
Rigid PU foam	Polyurethane 1	Expandable graphite	246	39.0	89
Flexible PU foam	Polyurethane 2	Mica, glass bead, inorganic salts	84	90.3	-
PU sheet	Polyurethane 3	Expandable graphite, fibre, inorganic salt	729	45.3	85

5.3 The intumescent behaviour

The intumescent behaviour of the Hilti PU products was studied by the natural burning test. The samples studied were cut into bars with a cross-sectional area of 20x20mm and a length of 20 mm for the rigid foam, 50 mm for the flexible foam and 6 mm for the sheet, to ensure a saturated char layer to be produced. These samples only burned when a Bunsen flame was directed on them. They extinguished immediately when the flame was removed. This behaviour suggests that these products have been very well fire retarded in gas phase, for example, by adding significant amount of gas phase fire retardants such as halogen-contained fire retardants or melamine-based fire retardants and graphite flakes. The samples were constantly and compulsively burned with a Bunsen flame for specified periods of time. The details of the intumescent behaviour of the samples will be discussed as follows.

The samples of the Hilti rigid foam formed worm-like black strands immediately when the Bunsen flame was directed onto their top surfaces, indicating that the graphite flakes in the foam were expandable graphite. After a few seconds, an orange flame of combustible decomposed gases appeared, whose base was close to the interface between the unburnt foam and the strands. The number of strands increased as the burning process continued, forming a thick expanded black layer above the foam, as shown in Figure 5.6. After approximately 2.5 minutes, the flame could be no longer observed. Smoke and dripping of the polymer were not observed during burning. The burnt foam had swelled vertically, whereas its cross section retained a similar shape and dimensions to that of the original sample (Figure 5.6). The burnt residue of the Hilti rigid foam was

composed of two parts: a black part of the burnt residue which was defined as char and a red part which was the unburnt foam. The char thickness refers to the average height of the char measured from the char/polymer interface to the upper burnt surface of the char.

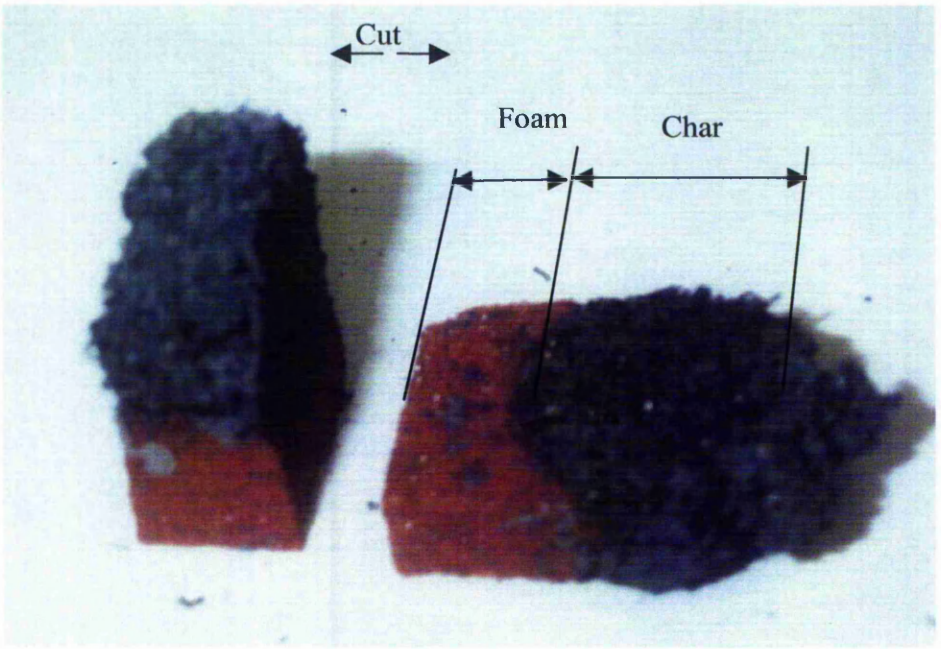

Figure 5.6 The appearance of the Hilti rigid foam after being burnt

The thickness of char and unburnt foam are plotted against burning time in Figure 5.7. As the foam was burnt a layer of char formed. The char thickness increased rapidly in the first 3 minutes and then gradually levelled off at 23 mm. This thickness is called the saturated char thickness of the Hilti rigid foam. Correspondingly, the thickness of the unburnt foam decreases steadily in the first three minutes and then levelled off at 9 mm. The thickness expansion ratio of the foam decreases from 5 at 0.5 minute to 2.2 when the saturated char layer formed, indicating that a few millimetre of the foam at the top produces a layer of thicker but low-density char.

The weight losses of the samples with burning time are plotted in Figure 5.8. The weight loss of the sample increased steadily during the first 2.5 minutes of burning and then levelled off. These results agree with the changes in the thickness of the char and unburnt foam with burning time (Figure 5.7), indicating that neither the underlying foam nor the char were obviously burnt further after three minutes. The char formed on the top of the foam protected the underlying polymer from further burning.

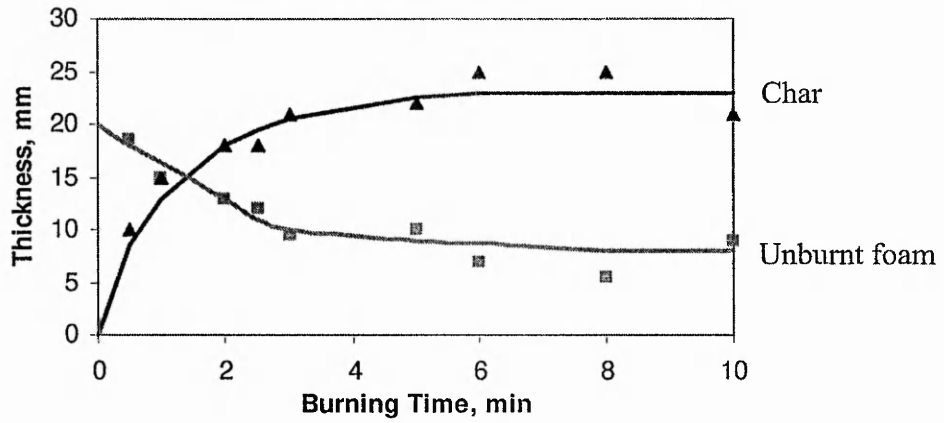

Figure 5.7 The thicknesses of the char and unburnt foam of the Hilti rigid foam *vs* burning time.

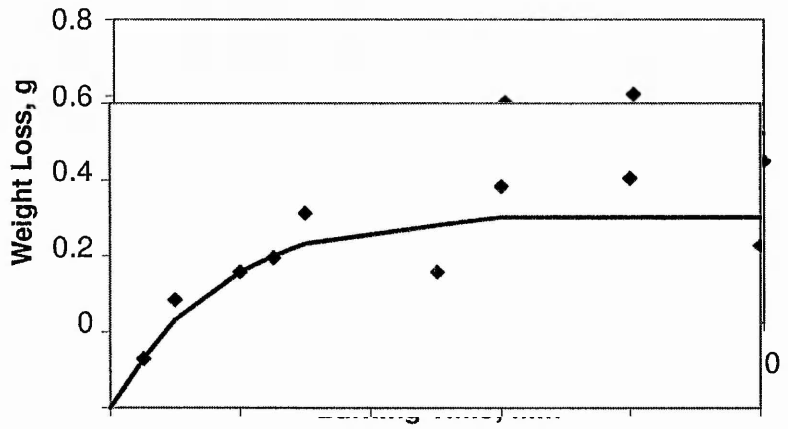

Figure 5.8 The weight loss of the Hilti rigid foam *vs* burning time

Similar investigations were carried out for the Hilti flexible foam. During the natural burning test, a flame of decomposed gases could be observed when the Bunsen flame was incident on the top surface of the flexible foam sample and gradually died away in the first 2.5 minutes of burning. No visible smoke was observed while burning. The burnt foam shrank, but a layer of char formed on the top of the unburnt foam. The char had a similar cross sectional area to the original foam sample. A burnt sample of the Hilti flexible foam is shown in Figure 5.9.

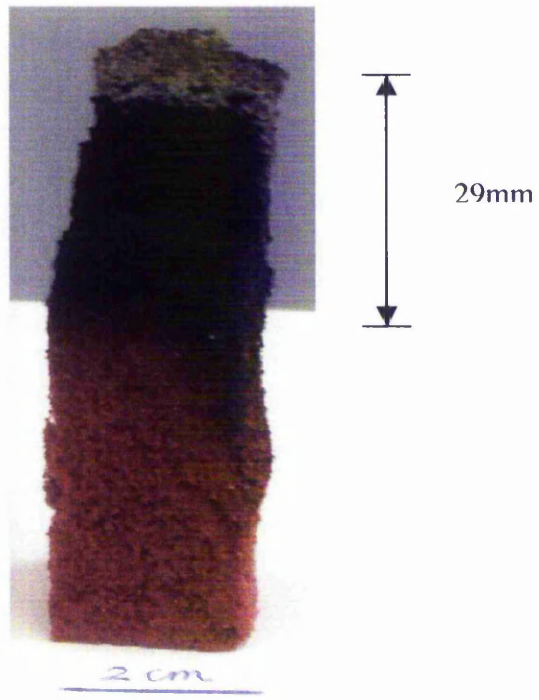

Figure 5.9 A burnt sample of the Hilti flexible foam after the natural burning test for 5minutes

The thicknesses of the char and unburnt sample and the weight loss of the samples after being burnt for specified periods of time are shown in Figures 5.10 a & b, respectively. The curves show that the char layer increases rapidly in the first 2-3 minutes of burning and then levels off at 29 mm, although the char layer formed is shorter that its precursor. The expansion ratio of the char in the whole burning period is approximately 0.7 (Figure 5.10 a). These results indicate that the char formed from the flexible foam does not vary considerably with burning time in terms of the char thickness. The samples lost weight dramatically in the first two minutes of burning and rapidly formed a char (Figure 5.10 b). The weight loss and char thickness changed little when the burning time exceeded 3 minutes. The saturated char thickness of the flexible foam was 29 mm, which protected the underneath foam.

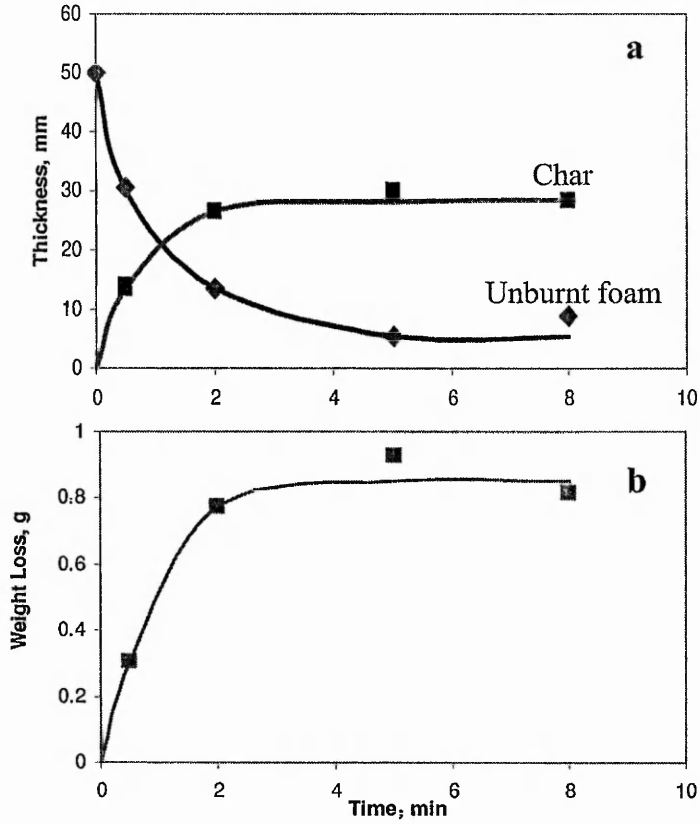

Figure 5.10 The char and unburnt foam thicknesses (a) and the weight loss history (b) of the Hilti flexible foam by natural burning

During the natural burning test, the Hilti sheet could not be ignited when the flame of a Bunsen burner was directed onto it. No visible flame of decomposed gases could be observed. During the burning process, graphite flakes expanded into worm-like strands and produced a well-expanded char as shown in Figure 5.11. The very high loading of the expandable graphite flakes and their orientation perpendicular to the flame might be the most important cause of the non-ignitable. This agrees with the results of Modesti et al that the oxygen index of polyurethane foams containing expandable graphite increases linearly with the loading of the expandable graphite.[77] After 5 minutes burning, a 30 mm thick char was produced from an approximately 1 mm thick sample.

Figure 5.11 The appearance of a char produced from the Hilti PU sheet after natural burning for 5 minutes

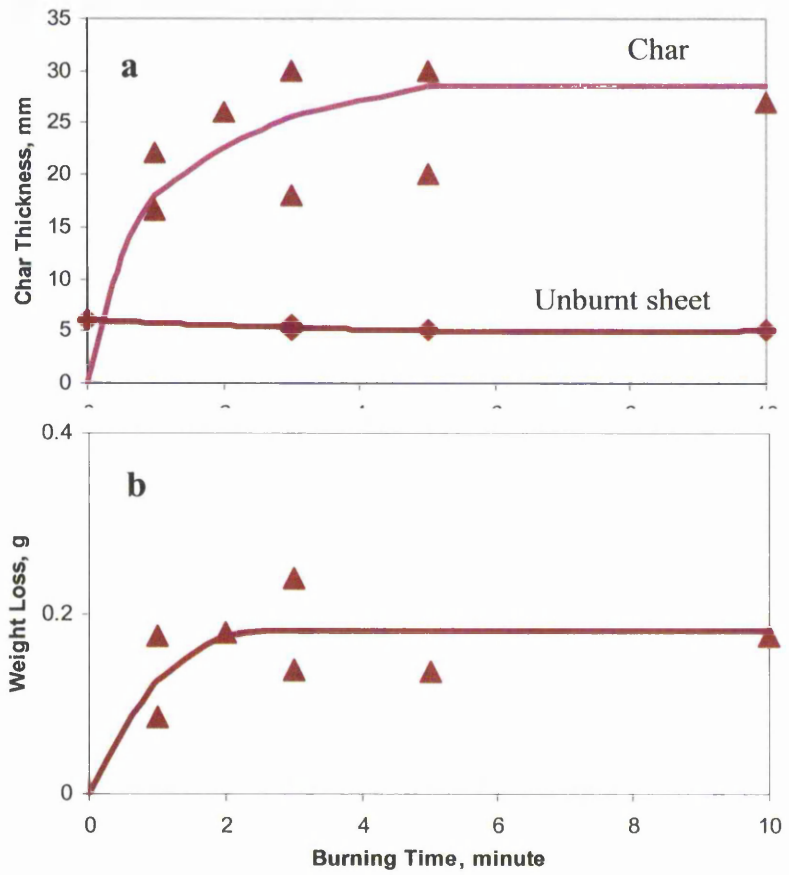

Figure 5.12 The char thickness and weight loss history of the Hilti sheet by natural burning

The char and unburnt foam thickness and weight loss *vs* burning time are presented in Figures 5.12 a & b. The scattered points may be caused by either the non-uniformity of the structure of the sample or/and the geometric irregularity of the sheet, for example the sheet was initially uneven and winkled. During burning, the char layer sometimes disintegrated which exposed the polymer layer underneath to further burning. This decreased the char thickness and increased the weight loss of the sample. Overall, the Hilti sheet produced a thick layer of char in the first 2 minutes of burning, and most of the weight loss occurred during this period of time. After 2 minutes, both the char thickness and the weight loss tended to level off. The Hilti sheet produced 30 mm thick of saturated char when approximately 1 mm of the sample was burnt.

The Hilti rigid foam, flexible foam and sheet could not sustain burning after ignition with a Bunsen flame. During the natural burning test, they did not produce smoke, nor did they drip. They all formed integrated chars on the top of the burnt samples. After being burnt for 2-3 minutes, the chars all reached their saturated thicknesses respectively, as shown in Figure 5.13a. The saturated char thicknesses are 23 mm for the rigid foam, 29 mm for the flexible foam and approximately 30 mm for the PU sheet.

However, not all of the chars were formed by expansion. The Hilti rigid foam and sheet, which contained expandable graphite flakes, expanded to form their chars. The expansion ratios were 2.2 and 30 respectively. In contrast, the expansion ratio of the flexible foam was 0.7, indicating the foam shrank by 32% when forming the char layer. The products containing expandable graphite flakes increase their volumes when burnt and can fill cavities in the case of fire. In contrast, the flexible foam containing mica and glass beads decreases its volume when burnt. The limited expansion of the mica cannot compensate the contraction of the polymer foam. It cannot fill any cavity or gaps by expansion in the case of fire.

During char formation, the samples lost the weight at different rates as shown in Figure 5.13b. The sheet lost least weight in ten minutes burning, which was about 0.2 g. The flexible foam lost the most weight, about 0.8 g, whereas the rigid foam lost approximately 0.5 g of weight. This data shows that the weight loss of the samples is ordered as: the flexible foam > the rigid foam > the sheet.

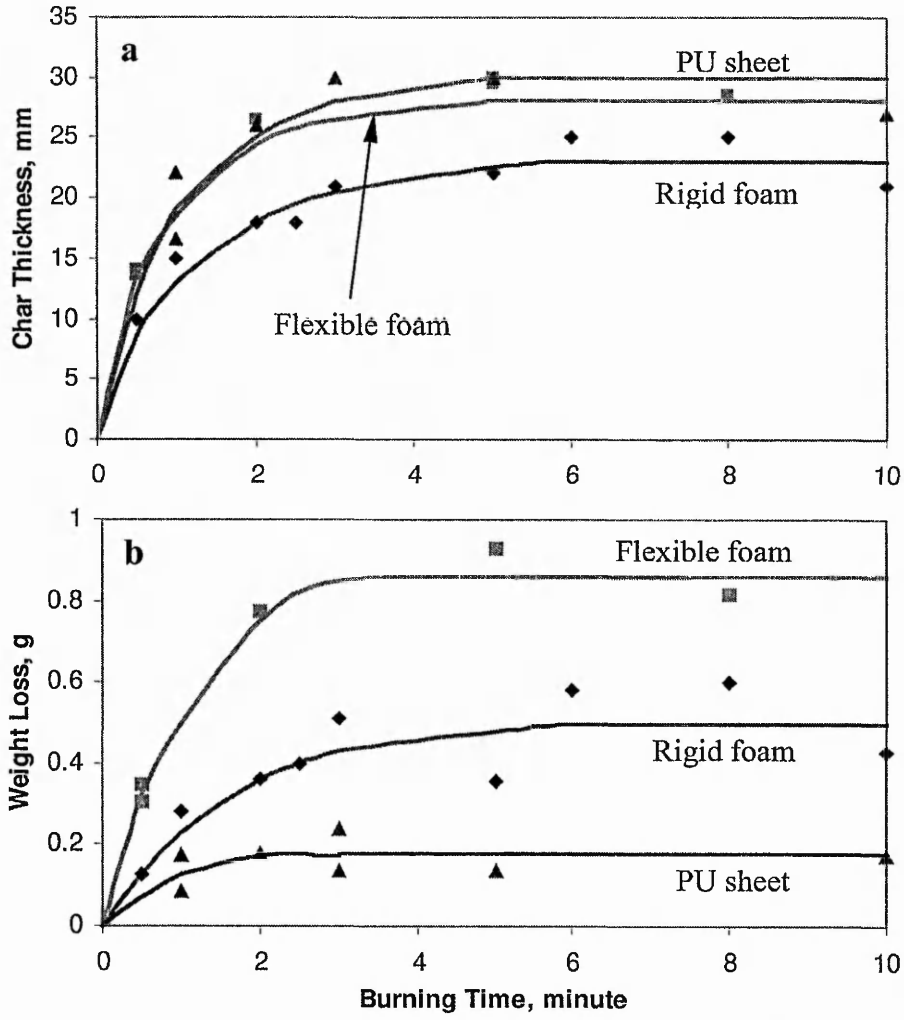

Figure 5.13 The char thickness curves (a) and weight loss curves (b) of the three Hilti products

5.4 The residue yield and permeability

The char yields and open porosities (permeability) of the naturally burnt chars are given in Table 5.2.

Table 5.2 Residue yields and the properties of the naturally burnt chars

Sample	Bulk Density of Sample, kg/m^3	Residue Yield, %	Bulk Density of Char, kg/m^3	Open porosity of Char	Saturated Char Thickness, mm	Expan -sion Ratio
Rigid foam	246	52.6	46.8	83.3	23	2.2
Flexible foam	84	57.3	116	89.7	29	0.7
Sheet	729	44.5	~11*	>95*	30	30

*Calculated value

The residue yield of the Hilti rigid foam was 52.6 wt.%. The bulk density of the char was 46.8 kg/m^3 that was only one fifth of that of the original foam, 246 kg/m^3. The open porosity of the char increased from 39% for the original foam to 83.3%. This indicates that most of the closed pores in the original foam had been destroyed during burning.

The Hilti flexible foam produced 57.3% of residue. The char formed had a bulk density of 116 kg/m^3, which is significantly higher than that of the original foam (84 kg/m^3), and the open porosity of the char was 89.7%, which is close to that of the original foam (90.3%).

The Hilti sheet had a residue yield of 44.5%, although the weight loss of the sample was approximately only 0.2 g. The char had only a very low bulk density of around 11 kg/m^3. This is calculated from its weight and measured dimensions due to the fragility of the char.

The saturated char thickness expresses the effective barrier thickness for a given intumescent char. The intumescent characteristics and char properties of these three products show that both the char yield and the expansion ratio have no direct correlation with the saturated char thickness. The bulk density, also the char yield, is influenced by additives. It is not quantitatively related to the saturated char thickness. Among all measured parameters, the open porosity of the chars has a consistent variation with the saturated char thickness. The intumescent char with a lower open porosity of 83.3%, that is the rigid foam, needed a thinner char (23 mm) to stop burning, while the chars with a open porosity of approximately 90% and above needed approximately 30 mm thick of char to stop burning. The open porosity as a parameter of gas permeability of intumescent chars plays a more important role than char yield and expansion ratio in intumescent fire retardancy. This is the first work that has characterized the gas permeability of intumescent chars and showed the importance of the char permeability in intumescent fire retarding polymer systems.

5.5 Char morphology

The three fire retarding products studied contain inorganic additives. Microscopic techniques were used to investigate not only the char structure, pore structures and distribution, and the progressive char formation of the polymers but also the different inorganic additives and their interaction with charred polymers.

Stereo micrographs of the burnt surface of the Hilti rigid foam are shown in Figure 5.14. Figure 5.14a shows that the expanded graphite strands are confined in the char. The confinement of the graphite strands within the char is due to the strands entanglement with each other and adhesion of the charred PU (Figure 5.14b). These micrographs indicate that the PU has molten and flowed downwards through the sample during burning, either coating the graphite strands or forming film bridges between the graphite strands. As the burning process continued, the PU charred and formed an integrated char with the expanded graphite strands.

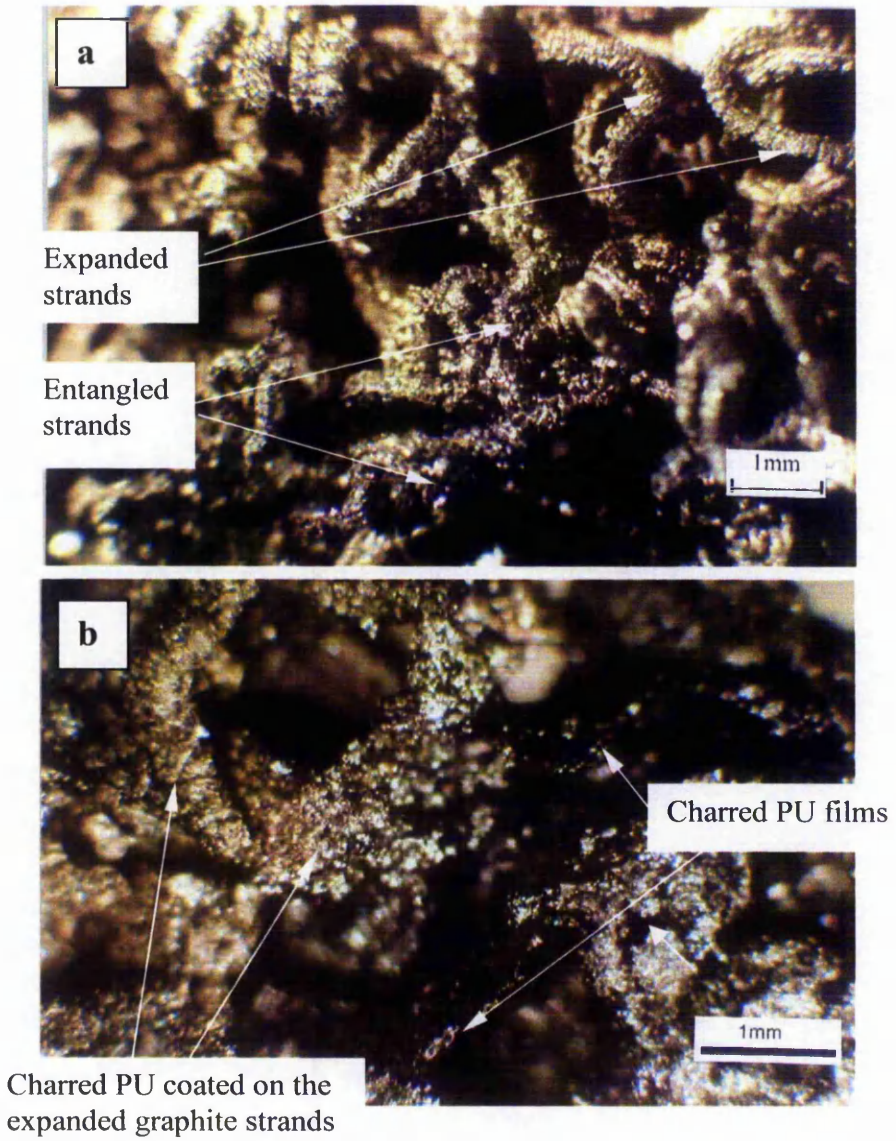

Figure 5.14 Stereo micrographs from the burned surface of the Hilti rigid foam

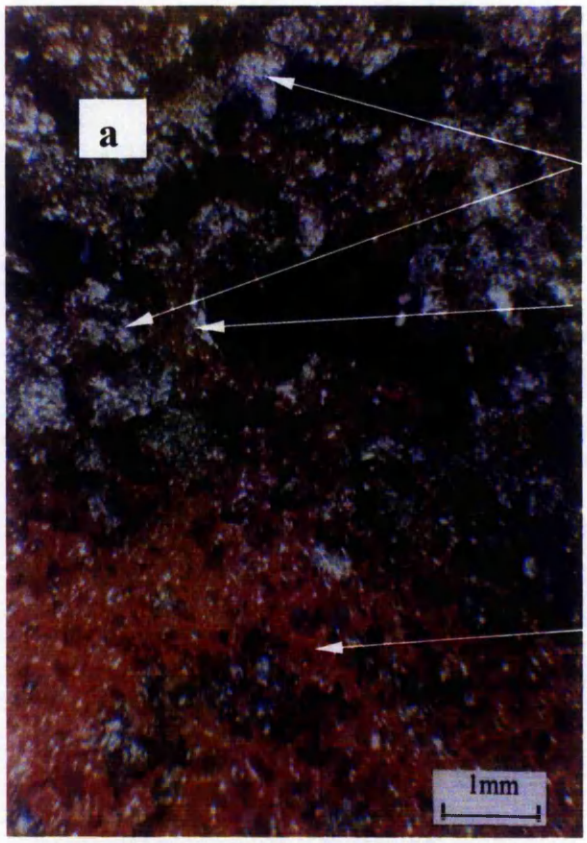

Expanded graphite covered by melted PU

Melted PU coated around expanded Graphite

Red PU foam

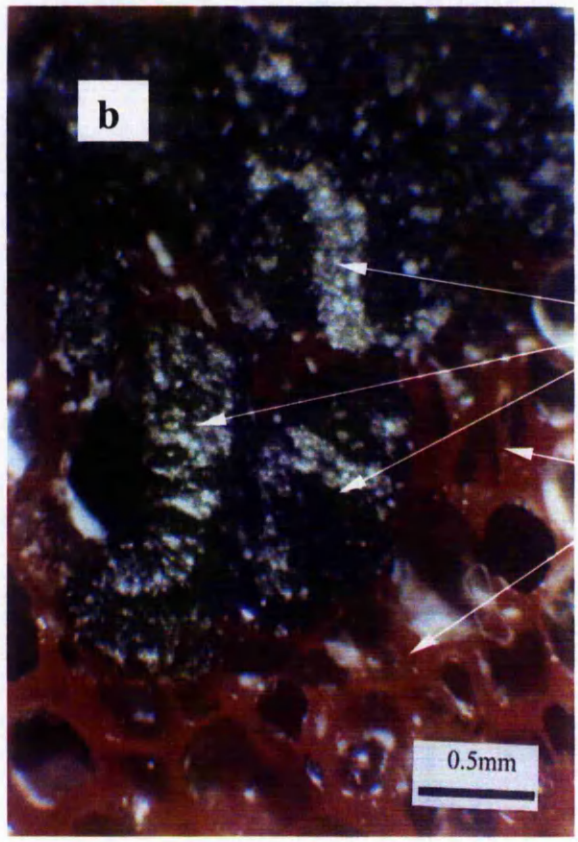

Expanded graphite strands

Red PU foam

Figure 5.15 Stereo micrographs of the burnt residue of the Hilti rigid PU foam in the region of the char-foam interface: a. from a simply cut cross-section, b. from a polished cross-section.

The char structure in the region close to the char-polymer interface is shown in Figures 5.15 a & b. The molten PU appears as a reddish shining phase which coats the expanded graphite strands. The expanded graphite strands form the skeleton of the char. Further away from the interface in the char, the PU phase becomes darker and darker. This indicates the increase in the degradation extent of the PU and the increased carbon content in the condensed char phase.

By comparing Figures 5.14 and 5.15, it can be seen that the char located close to the burning surface has larger voids than that close to the interface. This is due to the relatively free expansion of the graphite flakes at the burning surface, which is consistent with the variation in expansion ratio with the burning time.

A schematic illustration of the intumescent charring mechanism of the rigid PU foam is depicted in Figure 5.16. The char is mainly composed of expanded graphite strands and charred PU. The expanded graphite strands are entangled and bound by the charred PU forming an integrated char. The expanded graphite strands are coated by the charred PU. The extent of coating and binding of the strands by the charred PU decreases gradually from the char-polymer interface towards the external char surface due to the more complete decomposition of the polyurethane and relatively free expansion of the expandable graphite flakes at the surface. This results in larger pore structures close to the burning surface.

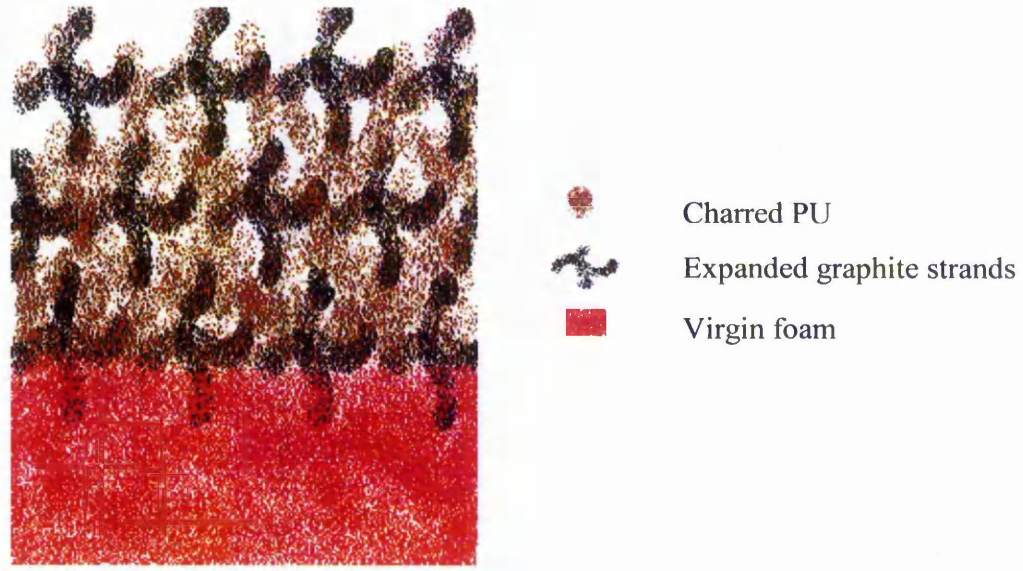

Figure 5.16 A schematic illustration of the intumescent mechanism of the Hilti rigid foam

Stereo micrographs of the naturally burnt char of the Hilti flexible foam at the burning surface are shown in Figures 5.17 a & b.

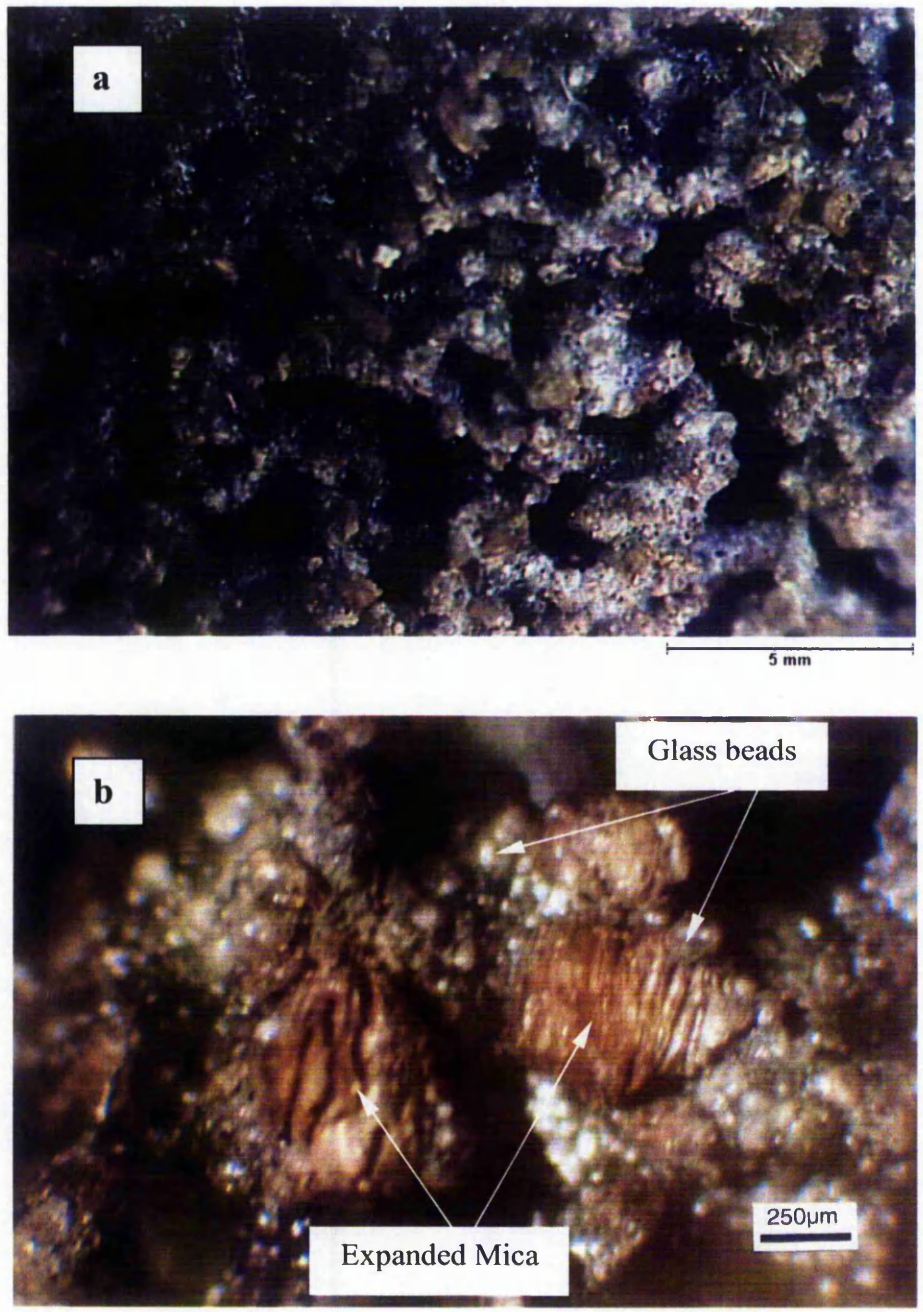

Figure 5.17 Stereo micrographs of the naturally burnt char of the Hilti flexible foam at the burning surface

Inorganic additives, that is, expanded mica and glass beads are the major components of the char. The black areas are carbonaceous residues from the polyurethane. Mica flakes expanded slightly and did not cause expansion of the char like the expandable

graphite flakes did in the rigid foam. The pore size in the char was larger than the voids found in the original foam. The fissures were up to 10 mm in length.

In the char-polymer interface region, as shown in Figure 5.18, the thin walls of the flexible foam rapidly melted forming a char with large pores and thicker walls than observed in the original foam. The char, apart from the burning surface, was black and had more than 15.4% of carbonaceous residue from the PU. These black carbonaceous residues of the PU coated the glass beads and expanded mica and integrated the char into a cohesive structure.

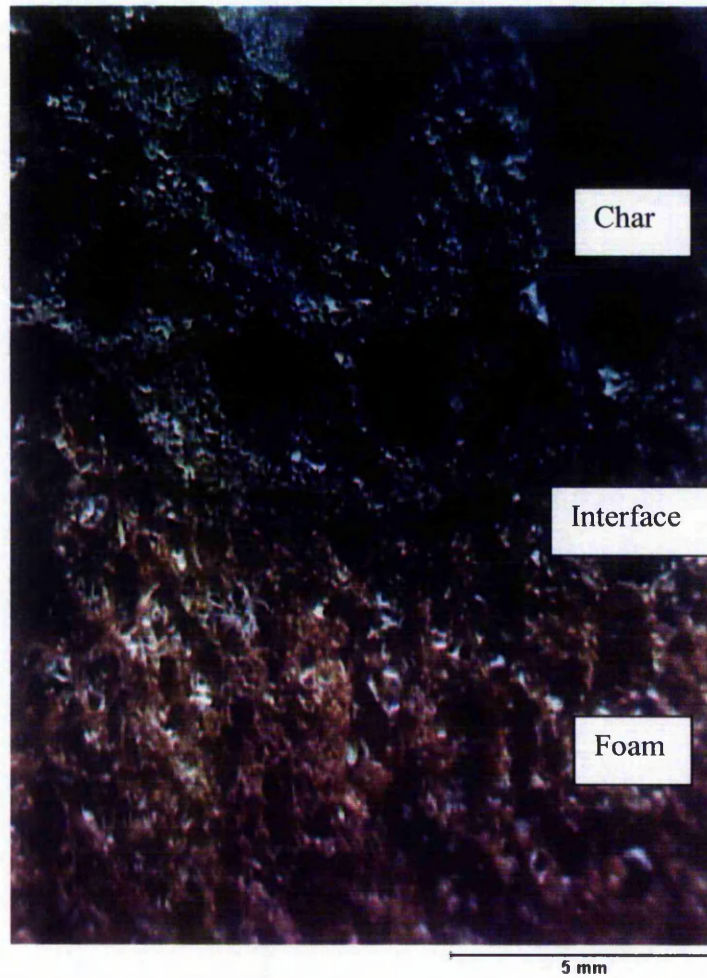

Figure 5.18 A stereo-micrograph of the naturally burnt char of the Hilti flexible foam at the char-polymer interface.

A schematic illustration of the char structure of the Hilti flexible foam is shown in Figure 5.19. The char is made up of randomly orientated expanded mica and glass beads and linked together by the charred PU, to form a 3D porous structure. The large pores have internal smooth surface. This is possibly due to the action of decomposed gases

during burning. The charred PU coats and binds the glass beads and expanded mica into an integrated char. When the charred PU is burnt out completely, the residues are yellowish inorganic powders.

Figure 5.19 A schematic illustration of intumescent mechanism of the Hilti flexible foam

Similar characterisation techniques were applied to investigate the Hilti sheet. A stereo micrograph in the char/polymer interface region of a naturally burnt sample is shown in Figure 5.20. The char is composed mostly of expanded graphite strands. The fibres distributed in the char are of similar dimensions to those in the unburnt sheet, Figures 5.4 and 5.20. The overall char structure was very fragile and easily disintegrated into the expanded graphite strands. There were 3-5 mm gaps between the solid components of the char. The charred PU could be observed only in the region close to the char-polymer interface due to the fact that there was only a small amount of the PU in the sheet and even less in the char. Also the large amount of the graphite flakes expanded dramatically. In the regions over 4 mm from the interface, the charred PU could not be observed by the stereomicroscope. Therefore, SEM was applied to investigate the char morphology at higher magnifications.

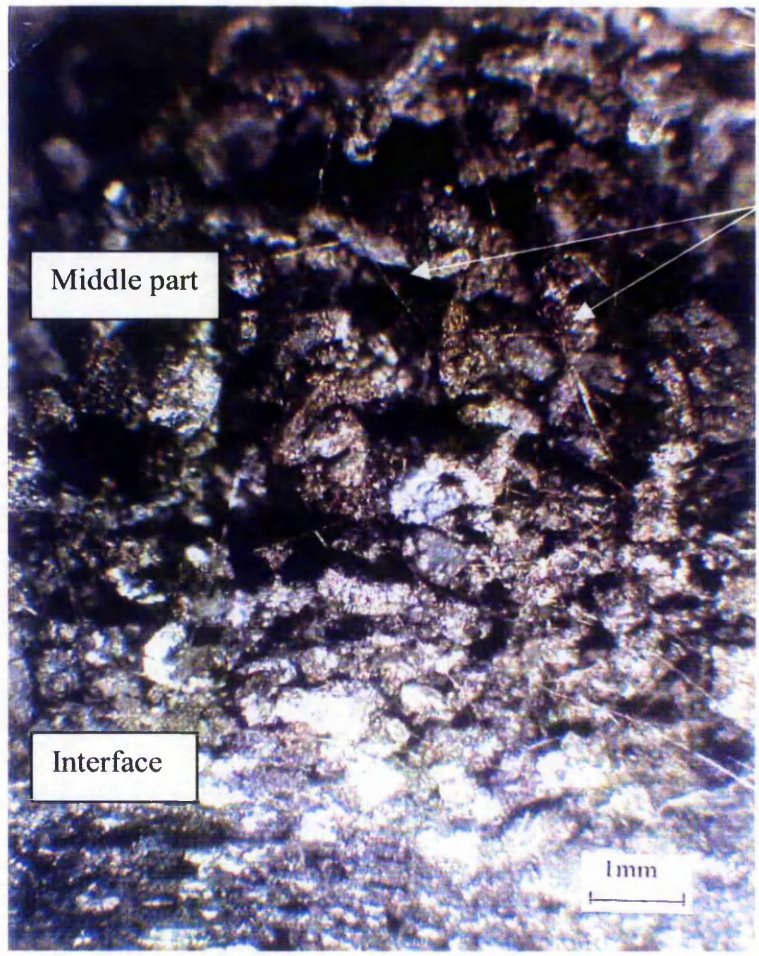

Figure 5.20 A stereo-micrograph of the naturally burnt char of the Hilti sheet at the char/ polymer interface

The SEM study examined samples from the interface, middle and external surface of the char. The corresponding micrographs are shown in Figures 5.21 to 5.23, respectively.

In the region of the interface, the graphite flakes have slightly expanded (Figure 5.21 a). The softened / molten PU has unevenly coated the fibres and smoothly coated the external surfaces of the graphite flakes, as shown in Figure 5.21 b. There are a significant number of other particles in the PU which remain in the polymer when it melts and coats the graphite flakes.

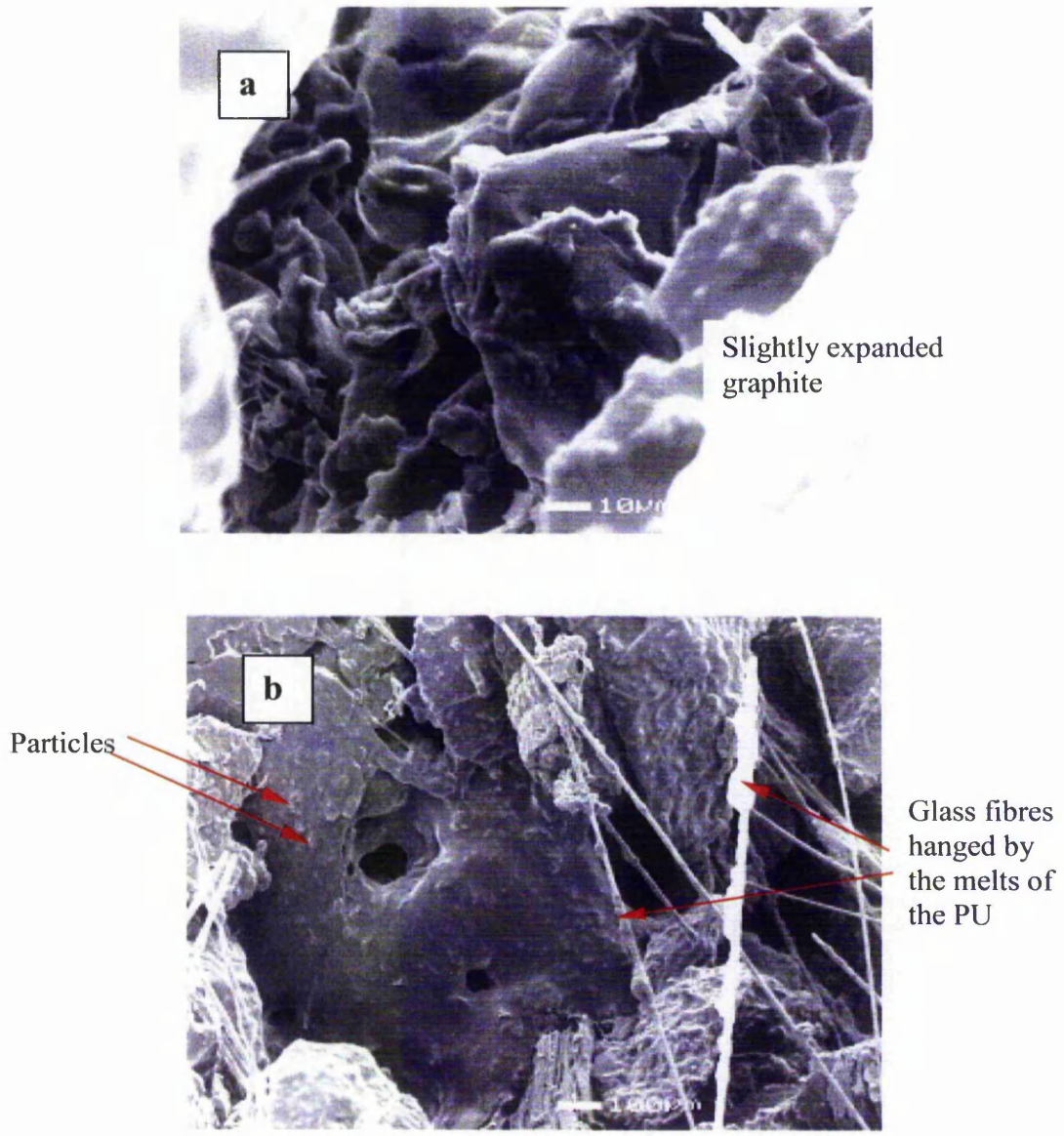

Figure 5.21 SEM micrographs of the naturally burnt char of the Hilti PU sheet close to the interface

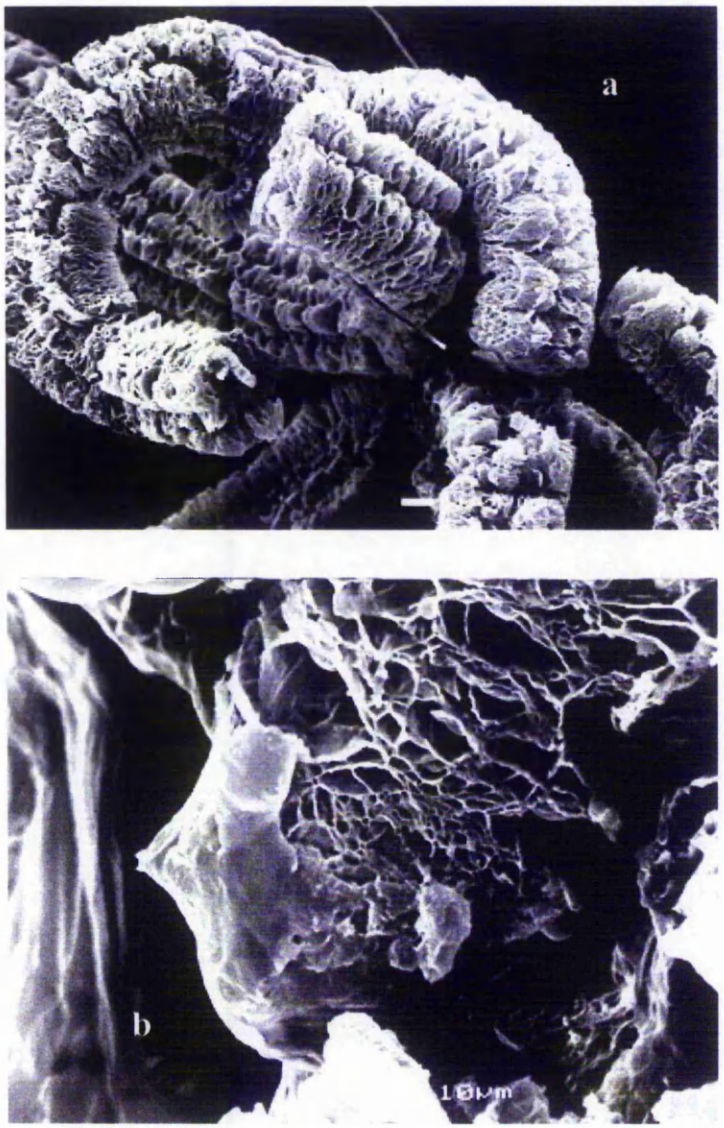

Figure 5.22 SEM micrographs of the PU sheet char in the middle of the char

In the middle part of the char, the graphite flakes were well expanded (Figures 5.22 a). The expanded graphite strands entangled and were also bound by the fibres. The polymer did not entirely coat the expanded graphite strands (Figure 5.22 b), it only covered small areas. The charred PU could reinforce neither the expanded graphite strands nor the char.

The charred PU was not present in the top part of the char, which had been close to the flame. Some ash-like residue remained in the gaps of the expanded graphite strands, as shown in Figure 5.23. This ash-like residue was most probably the particles which were observed in the PU.

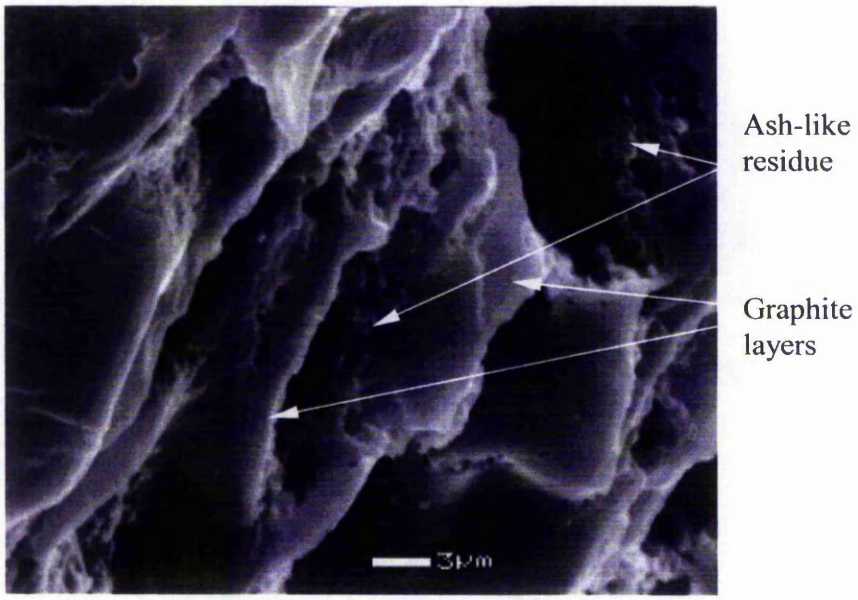

Figure 5.23 A SEM micrograph of the naturally burnt char of the Hilti sheet close to the burning surface

A schematic illustration of the intumescent charring mechanism of the polyurethane sheet is depicted in Figure 5.24.

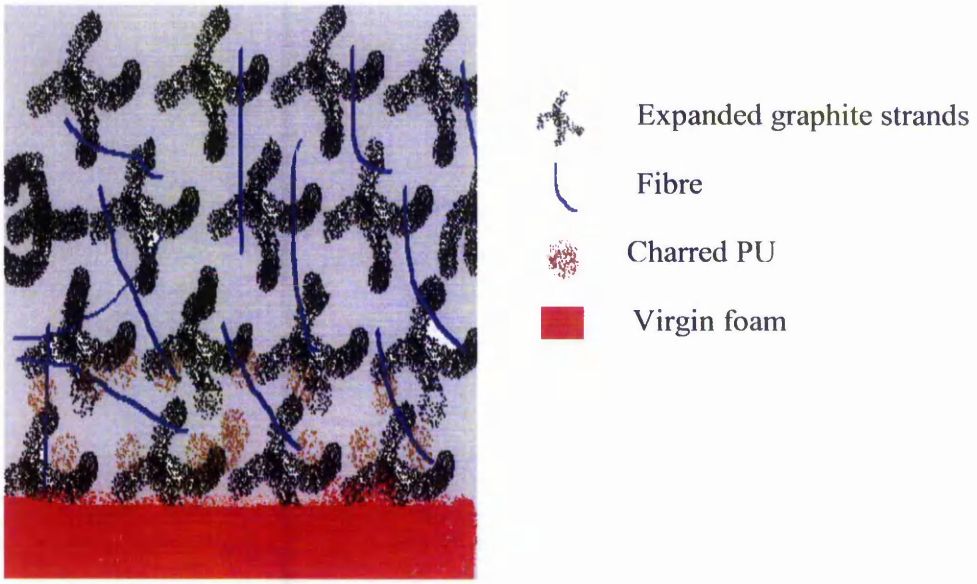

Figure 5.24 A schematic illustration of intumescent mechanism of the Hilti sheet

The PU sheet is composed mostly of expandable graphite flakes. There are also significant amounts of fibres, PU and unknown inorganic powder salts. During burning, the graphite flakes expand dramatically into accordion-like strands, which are

entangled. The char is held together by the entanglement and the fibres. There is insufficient PU in the sheet to coat and bind the expanded graphite strands. The PU softens and decomposes into gases and charred PU. The charred PU has low resistance to oxidation and gradually burns out leaving only inorganic additives. The resulting char is integrated, but has large voids and is very fragile.

5.6 Mechanical properties of chars

Intumescent chars should not only have low gas permeability and good integrity, but also have strength to resist the thermal stresses, air currents and water impact of fire hoses. To resist these forces, the bulk strength of the chars is more important than the char wall strength.

This study has shown that the intumescent chars are composed of charred polyurethane and inorganic additives. The inorganic additives include very soft expanded graphite strands, fibers, expanded mica, glass beads and powdery additives. The chars are highly porous with high open porosities and do not have uniform structures from the burning surface to the char/polymer interface. Therefore, the vertically cut cross-sections of the chars were investigated using a durometer hardness test to measure the bulk strength of the intumescent chars.

The chars used for the durometer hardness measurements were samples burned by the natural burning method for 3 minutes. The durometer hardnesses of the three chars are plotted against the distance to the char/polymer interface in Figures 5.25 a to c. The hardness readings scattered significantly due to irregular voids in the chars. It should be noted that the original products also had irregular structures and pores.

The three chars have different patterns of the durometer hardness *vs* distance to the interface. The chars of the rigid foam and the sheet have decreased durometer hardness away from char-polymer interface towards the top of the char, while the flexible foam char has relatively constant durometer hardness from the interface to the burning surface.

The rigid foam char had hardness varying from 62 to 82 at the interface, which was close to that of the original foam (89). The hardness then decreased away from the interface and down to zero when the distance from the interface reached to 16 mm.

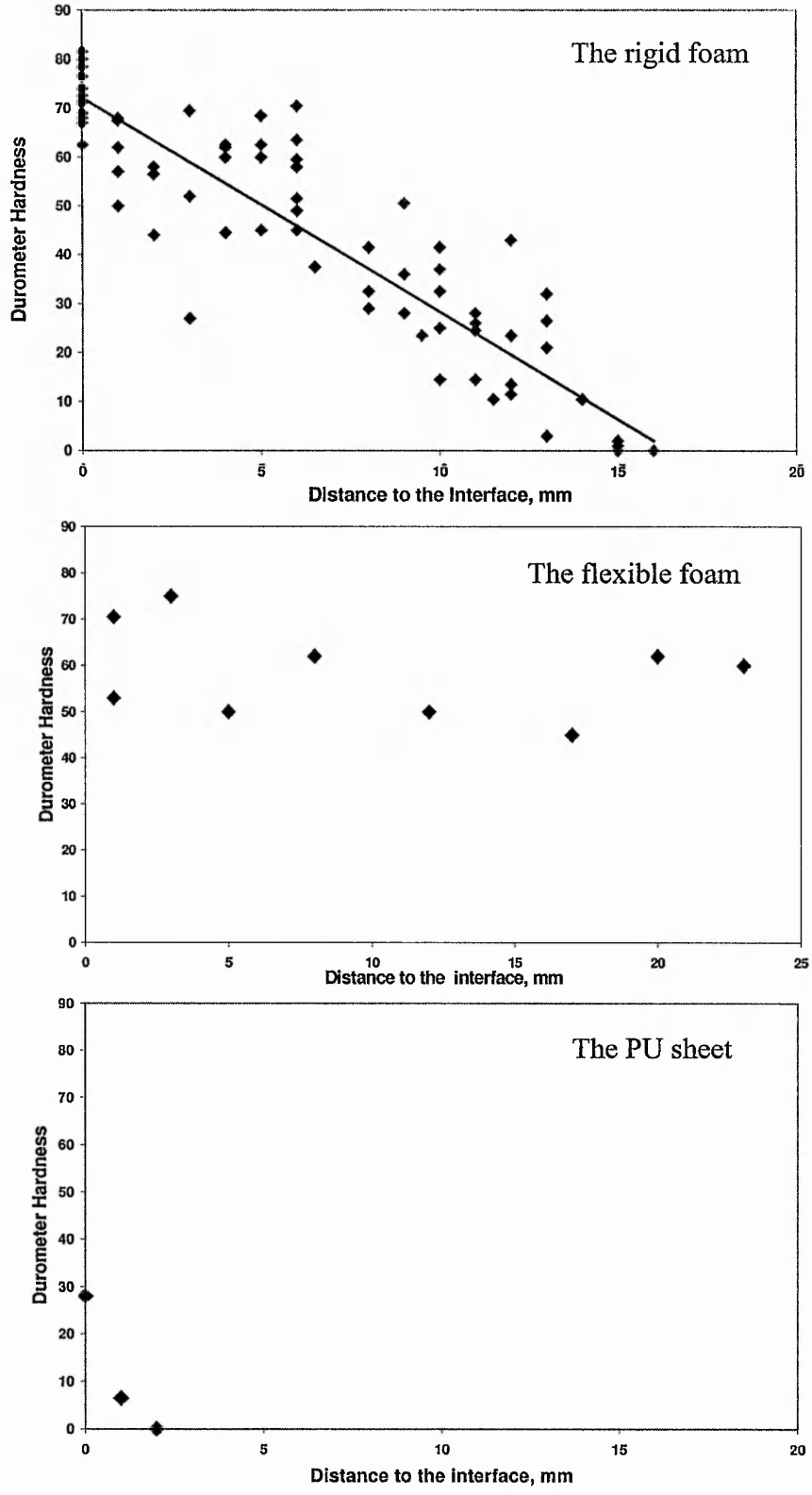

Figure 5.25 Durometer hardnesses of the chars *vs* the distance to the char/ polymer interface.

As a bulk strength parameter, the durometer hardness varies not only with the strength of the char wall but also with the void distribution within the char. As discussed in Chapter 5.4, from the char/polymer interface to the burning surface, the rigid foam char contained less and less charred PU and increased number of voids which were larger in size. Because of the increased number of voids and the decreased entanglement of the graphite strands close to burning surface, the top layer (c.a.10 mm) of the char had no bulk strength. The char had higher bulk strength as the void sizes decreased and the charred PU content increased. The char was stronger close to the char-polymer interface.

The PU sheet char was not as strong as that of the rigid foam, although both had expanded graphite strands. Its durometer hardness at the interface was only 28, which was lower than that of the original sheet (84-85), and decreased rapidly to 6.5 at 1 mm above the interface and to 0 at 2 mm above the interface (Figure 5.25 c). The slight expansion of the graphite flakes in the interface region made the char there soft. The large amount of the expanded graphite strands in the PU sheet char were poorly bound by the glass fibres and entanglement of the expanded graphite strands, as discussed in Chapter 5.4. The very large voids in the char and the lack of coating by the charred polymer on the expanded graphite strands led to the char having no bulk strength.

The char of the naturally burnt flexible foam was rigid. The hardness of the char was approximately 60 at all the distances to the interface (Figure 5.25 b), indicating that the hardness mainly came from the expanded mica strands and glass beads in the char, because this char was mainly composed of the expanded mica and glass beads, as discussed in Chapter 5.4. The expanded mica and glass beads were bound together by the charred PU, which was approximately 26.4% in the char. The fluctuation of the readings comes from the structure of the measuring surfaces. If the indenter was over a void in the wall, the reading was lower.

In terms of the three products studied, the intumescent chars are composed of more than two components. All the components contribute to the strength of the chars. The charred polymer plays different roles in the different chars. In the char of the flexible foam, the expanded mica and glass beads have individual strength. The charred polyurethane is needed to bind the mica and glass beads together to form an integrated char. The longer the charred polyurethane resists oxidation and remains in the char, the

longer the char retains its strength. Once the charred polymer is burnt out, the char no longer has any strength and it disintegrates into particles, because these particles rarely have effective interaction on themselves.

Loose expanded graphite strands do not have any bulk strength. In the Hilti rigid foam and sheet samples, the charred PU is needed to keep the expanded graphite strands together and reinforce the char giving the char strength. In the case of the rigid foam, the charred polyurethane coats the expanded graphite strands better and resists oxidation during burning, resulting in an integrated and firm char. The polyurethane in the sheet does not effectively coat the expanded graphite strands and does not resist oxidation during burning. The resulting char is not cohesive and is very weak and porous.

5.7 Burning under load

The three Hilti products studied are either fire stopping products or potential fire stopping products. Fire stopping products are used in constrained spaces. When exposed to external heat they may burn but form expanded chars which occupy the constrained space and stop the propagation of fire. The three products were examined for the fire stopping properties by burning samples under load in order to simulate the real fire stopping conditions, that is constrained expansion in a badly ventilated burning environment.

The char yields from burning under load are plotted against burning time in Figure 5.26. During the burning, the char yields reduce in the first 24 minutes for the rigid foam, 20 minutes for the flexible foam and 15 minutes for the sheet, and then tend to level off at 31.8%, 53.1% and 43.7%, respectively. Besides the differences in the PU contents in the products, how long the PU takes to melt and coat the additives influences the char formation and the mechanical properties of the char. The PU types are different in the three Hilti products, and this affects how they behave in the fire situation. The PU in the rigid foam takes significantly longer time to form a solid char, so that the charring polymer has time to coat the expanded graphite strands before solidification, resulting in better coating and reinforcement.

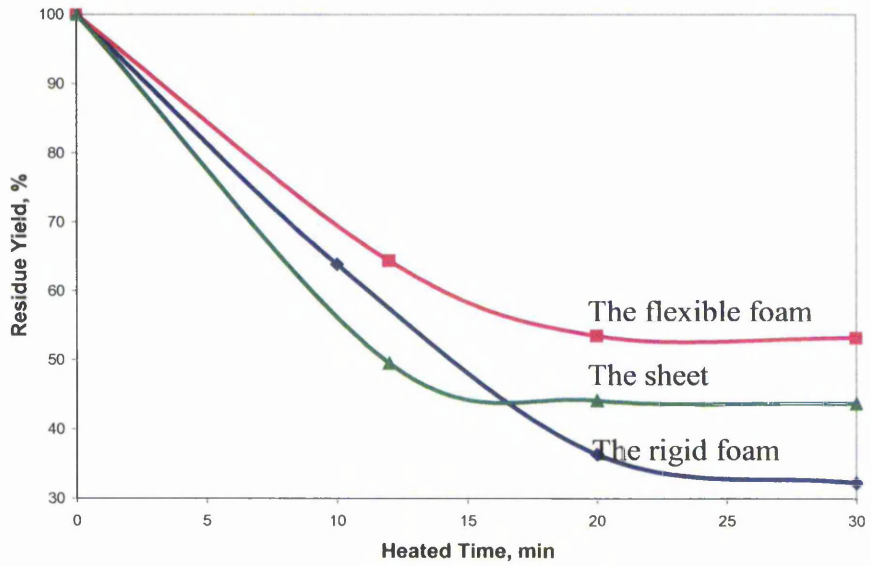

Figure 5.26 The variations of char yield of the three Hilti products with heating time (by under load burning)

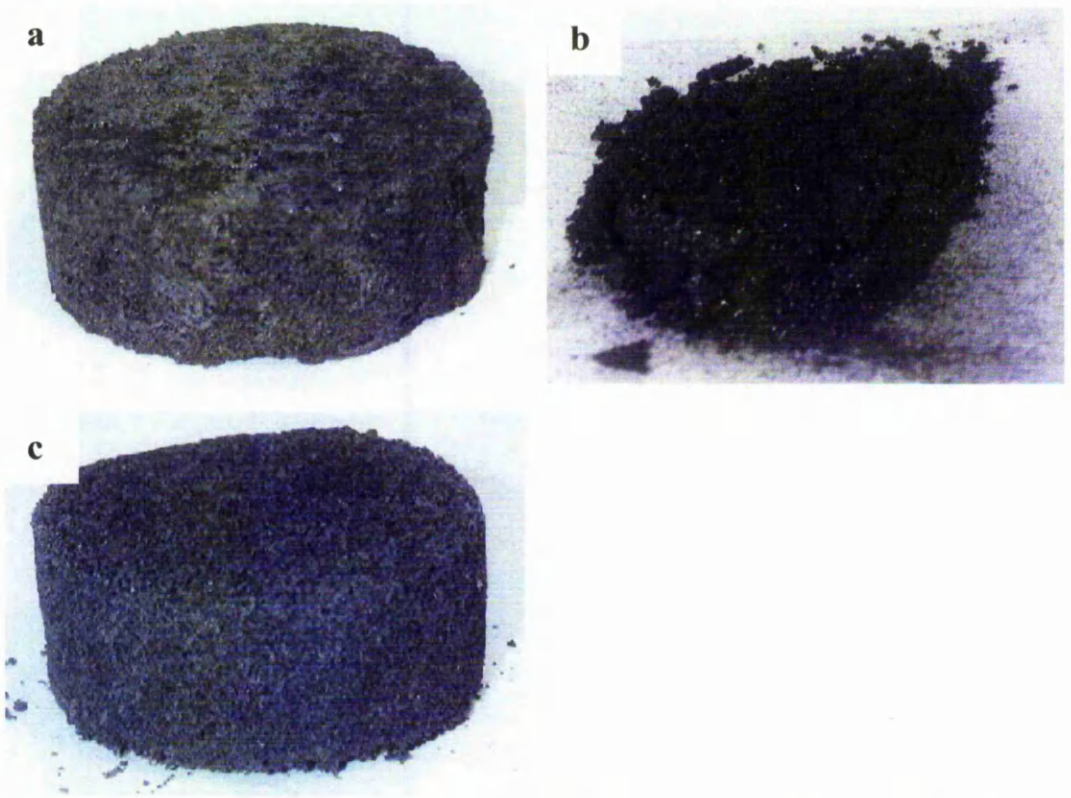

Figure 5.27 Chars of the rigid polyurethane foam(a), the flexible foam (b) and the PU sheet (c) by burning under load after 30 minutes

The chars burnt under load for 30 minutes were studied. The chars of the three products are shown in Figures 5.27 a to c. The Hilti rigid foam and sheet produced char cylinders (Figures 5.27 a & b), while the Hilti flexible foam formed a powdery residue (Figure 5.27 c).

The char of the flexible foam totally collapsed. The examination of the char showed that the total char yield was 53.1%, of which 20.5% was charred PU. The charred PU did not give sufficient strength to the char to withstand the external force. The reduction in volume of the sample during burning and the lack of interaction between the glass beads and mica are the major reasons for the collapse. The char powder had a bulk density of 277 kg/m^3, contributed by the mica and glass beads.

The chars of the rigid foam and the PU sheet were investigated by means of SEM. The images are shown in Figures 5.28 a to d. The graphite strands in the rigid foam char are coated entirely by the charred polyurethane (Figure 5.28 a). During the burning process, the polyurethane melted, bubbled and flowed to coat the expanded graphite strands (Figure 5.28 b). The bubbles were caused, during burning, by the decomposed gases of the polymer. These results indicate further that the polyurethane of this rigid foam can form a significant amount of char during both natural burning and isothermal burning in a Muffle furnace at 600°C even after 30 minutes. The melting and bubbling indicate that the charring of the PU is not mainly from polyisocynurate as in the PU173-PU1476 samples studied in Chapter 4 nor from high functionality of the polyol, [42] but appears to be caused by the intumescent fire retardants such as phosphorus compounds.

The images of the PU sheet char (Figure 5.28 c & d) show no charred polyurethane on the expanded graphite strands, indicating that the polyurethane has been burned out after 30 minutes at 600°C. The expanded graphite strands are closely entangled together (Figure 5.28 c).

The under load charring results of the Hilti samples are summarised in Table 5.3. The two graphite-containing products expanded during burning. The expansion ratio was 1.3 times for the rigid foam and 11.7 times for the PU sheet. The chars had a bulk density of 58.3 kg/m^3 for the rigid foam and 28.0 kg/m^3 for the PU sheet. The durometer hardnesses of the chars were 64.7 for the rigid foam and 25.5 for the PU sheet. The bulk strength of the chars varies consistently with their bulk density. The rigid foam char, which had higher density, also had a higher strength.

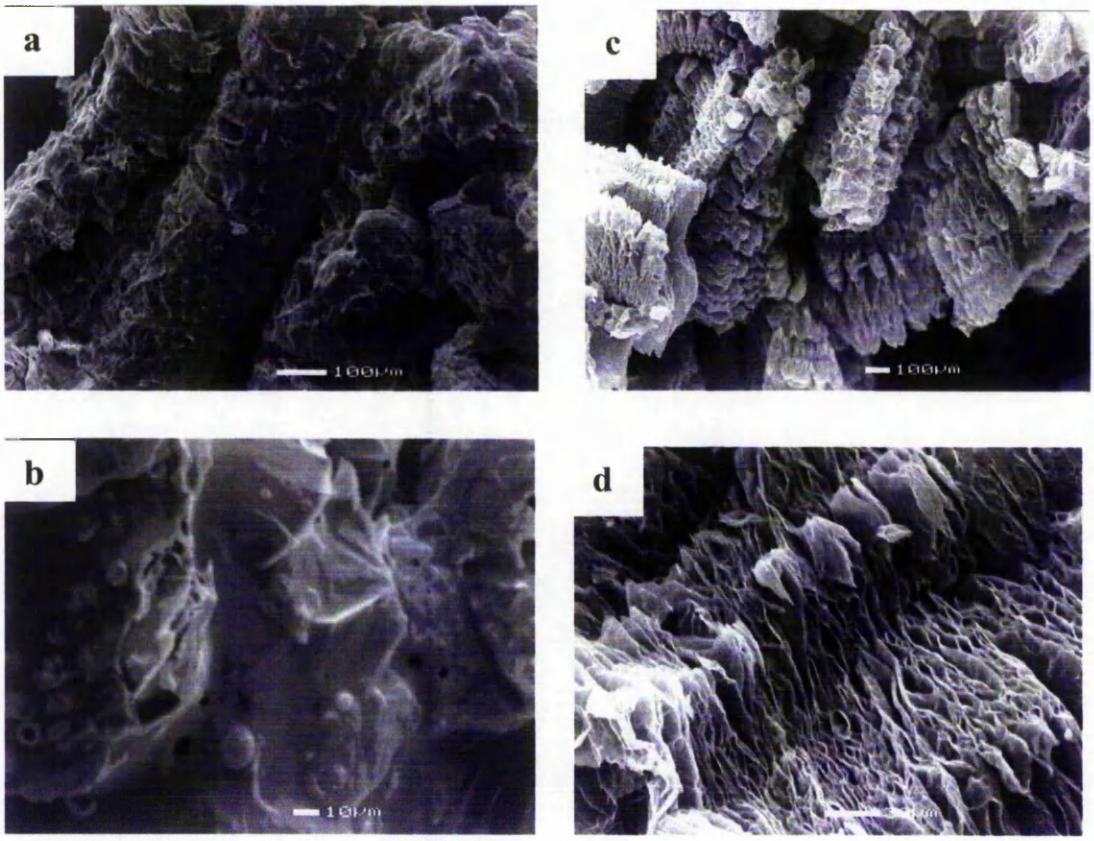

Figure 5.28 SEM images of the rigid polyurethane foam char (a & b) and the PU sheet char (c & d), burnt under load.

Table 5.3 Char properties of the Hilti products

Samples	Natural burning		Burning under load			
	Residue Yield, wt%	Open Porosity, %	Char yield at 600°C, wt.%	Bulk Density of char, kg/M^3	Expan-sion ratio	Durometer Hardness of char
Rigid foam	52.6	83.3	31.8	58.3	1.3	64.7
Flexible foam	57.3	89.7	53.1	277.0	-	-
Sheet	44.5	>95	43.7	28.0	11.7	25.5

The flexible PU foam is not an effective expansion product. Its sample shrinks during burning and cannot withstand external forces without collapsing. In terms of fire stopping, the flexible PU foam can be used only where contraction rather than expansion is needed. Both the rigid foam and the PU sheet expand and form firm chars. The PU sheet expanded much more than the rigid foam, but the formed char is weaker.

These two materials are applicable to where expansion is demanded when subjected to fire.

5.8 Reactivity of chars

Reactivity of chars refers to their reactive ability to oxidizing gases, particularly to the oxygen in air. The better the char can resist to be oxidized, the lower reactivity the char has. Low reactive intumescent chars may exist longer to keep integrity of the chars and protect their underneath.

The oxidation resistance of chars formed during combustion depends on the components and structures of the chars. The chars of the three Hilti products are basically composed of charred PU and inert additives. The PUs in the three products are different from each other. Their charring ability and reactivity of the formed polymer chars vary with the original PU resin. As showed in Chapter 5.6, the PU resin in the rigid foam can form a significant amount of polymer char, and the polymer char formed has an obvious oxidation resistance under the burning conditions. The PU in the sheet forms little char and the char disappears in a short time. The charring ability and oxidation resistance of the PU in the flexible foam are between the other two.

The oxidation resistance of the inert inorganic additives also varies. The inert inorganic additives in the Hilti flexible foam char are mainly glass beads and mica (c.a. 75%), which are not combustible and are oxidation resistant in normal fire situations. The most important inert inorganic additive in the chars of the Hilti rigid foam and sheet is expanded graphite strands. Its oxidation resistance is determined by how the carbons exist in the chars. Carbons in graphite do not oxidize evenly. Selective oxidation occurs at particular sites while other sites remain unaffected. Such active sites are located mainly at the prismatic edges and at defects in the graphite layers. Generally, the larger the graphite crystallites are, the higher the oxidation resistance is, as there are less prismatic edges. [78]

The structure of the expanded graphite strands was investigated using SEM and X-ray diffraction. A SEM micrograph of an expanded graphite strand is shown in Figure 5.29. The graphite flake has expanded in macro-scale. Large gaps exist between the graphite layers, whose thicknesses are in the order of 1-2 μm.

The XRD patterns of the rigid PU foam and its char are shown in Figure 5.30. Both XRD patterns have 002 peak of graphite at close to 2□=26.54° (0.3354 nm). This indicates that the expanded graphite strands still have the same crystal structure as they had prior to their expansion, even though the volume of the expanded graphite had increased dramatically. The calculation using Sherrer Equations[78] (Equations 3.9 and 3.10) indicates that the stacking width and height of graphite crystallites are: La=1.6 nm, Lc= 0.8 nm in the foam; and La=0.8 nm Lc=0.4 nm in the char.

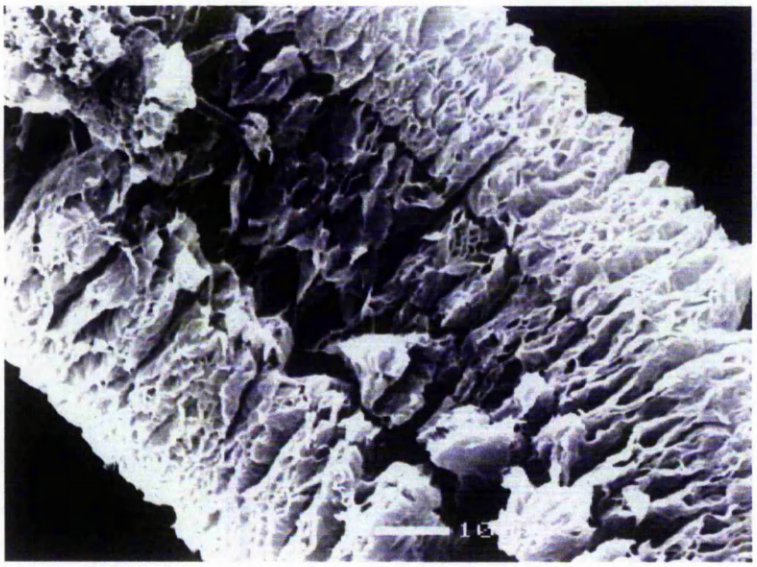

Figure 5.29 A SEM micrograph of an expanded graphite strand

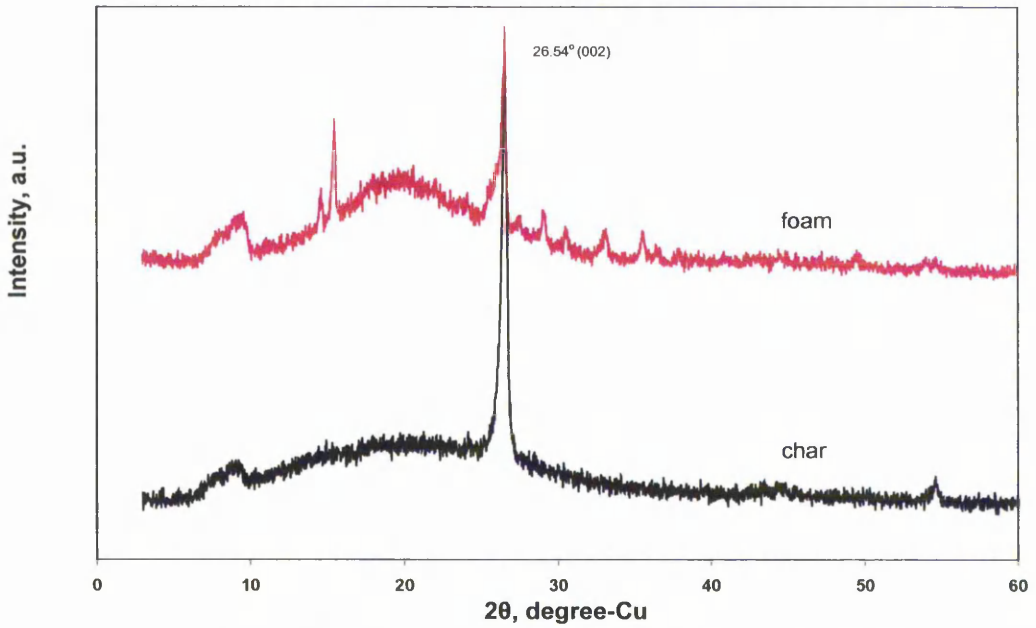

Figure 5.30 XRD patterns of the Hilti rigid foam and its char

The results show that the expansion of expandable graphite results in a decrease in size of the graphite crystallites. The interlayer spacing of the graphite sheets, either expanded in macro- or micro-scale, is not changed. These changes decrease the oxidation resistance of expanded graphite but not significantly, as it is caused by increased surface area of the graphite. The XRD pattern of the char also shows that the charred PU is amorphous, which has higher reactivity than graphite.

5.9 Protective efficiency of the intumescent chars

The differences in char yields between the natural burning test and furnace burning test under load for 30minutes were studied for the protective efficiency of the intumescent chars formed by natural burning. The differences were found to be 20.8%, 4.2% and 0.8% for the Hilti rigid foam, the flexible foam and the sheet, respectively. This data indicates that the char of the rigid foam is a more effective barrier in protecting the underneath polymer during the natural burning test than those of the other two products.

The data in Table 5.3 also shows that the difference in char yields increases as the open porosity decreases in the char produced by the natural burning test. This is consistent with the results from the PU173-PU1476 samples (Chapter 4). The data from these two groups of samples produce the same graph, as shown in Figure 5.31. It can be predicted from the graph that the decrease in the open porosity of the char, for example, to less than 80%, will dramatically increase the natural burning char yield and provide better protection. This appears to be independent of the additives in the polymer systems.

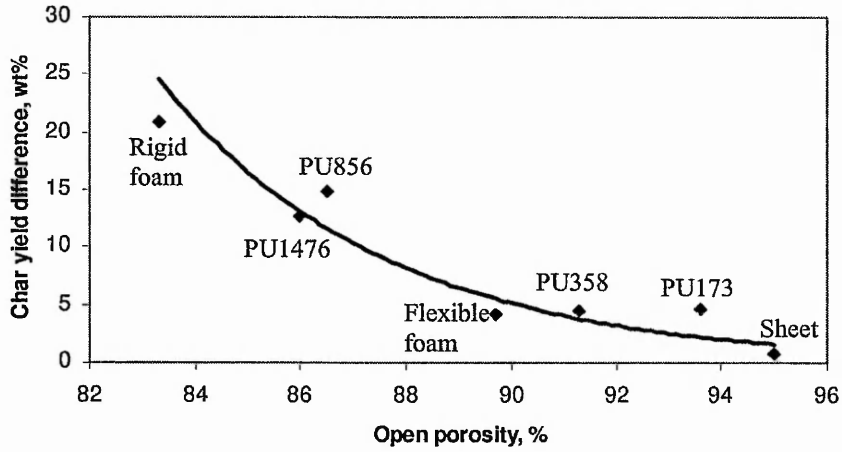

Figure 5.31 The difference in char yields between natural burning and furnace burning *vs* the open porosity of the natural burnt chars

In terms of fire retarding efficiency, an ideal char should be integrated and have low gas permeability, that is, low open porosity, high thermal stability and strength. To produce low porosity chars with the required thermal and mechanical properties, the graphite polymer nanocomposite approach is promising.

5.10 Summary remarks

Three commercial intumescent fire-retarded polyurethane products were studied for their intumescent mechanisms. The three products were the Hilti rigid foam, the Hilti flexible foam and the Hilti sheet. They contain significant amounts of inert inorganic additives besides fire retardants. The rigid foam has expandable graphite flakes, the sheet has expandable graphite flakes and white fibers and the flexible foam has mica and glass beads. They are protected by fire retardants or/and graphite additives so that they self-extinguish immediately once external heat flame is removed from the sample in a fire situation.

The samples of all the three products form a layer of 20-30mm thickly saturated porous char by the natural burning method. The rigid foam and the sheet form chars by dramatic expansion of the expandable graphite flakes. In contrast, the flexible foam char is shorter than its original sample. All the saturated char layers protect the underneath polymer from further burning. The integrity and thickness of the chars are more important than the sample expansion and char yield in intumescent fire-retarding situations.

The study of the intumescent chars shows that the inert inorganic additives, especially expandable graphite, act in a similar manner to charring promoters and blowing agents in conventional intumescent systems. The charred polymer coats the inert inorganic additives, which allows an integrated and reinforced char to form. To obtain highly effective and strong intumescent chars, the charred polymer and the inorganic additives must be combined more intimately, so that they adhere together with minimum porosity. To achieve this ideal structure, the requirements for the polymer are that it flows to wet the additive surfaces before forming a solid polymer char. Sufficient polymer char has to be formed and has low oxidative reactivity so that it will not burn out in a fire in order to maintain the integrity and strength of the chars. The amount and

type of PU in a fire retarding PU system govern the integrity and strength of the char formed and its oxidation resistance.

The saturated char thickness for a given intumescent polymer system is a function of the open porosity of the char formed. The lower the open porosity, the thinner a saturated char is needed to stop further burning. The protective efficiency of a char is correlated with its gas permeability. The less permeable the char is, the better protection the char gives to the polymer underneath.

Expansion of the materials to occupy constrained spaces is required in fire stopping applications, to stop the propagation of fires. Expandable graphite is ideal in this situation as the space constraint is conducive to producing expanded chars with low porosity and high strength due to extensive entanglement of the expanded graphite strands.

Chapter 6

The Development of Nano-Structured Graphite

6.1 Introduction

To synthesise graphite/polymer nanocomposites, it is necessary to modify the graphite, because the interlayer spacing of the graphite aromatic sheets is too small to insert the polymer chains in and the surfaces of the aromatic sheets are incompatible to polymers. Modifying graphite into nano-structured graphite, which is suitable for the synthesis of graphite/polymer nanocomposites, requires the expansion of the interlayer spacing of graphite sheets and introduction of some polar functional groups onto the graphite sheets to increase the compatibility between nano-structured graphite and polymers. Such nano-structured graphite will accommodate polymer chains under suitable reaction conditions.

Two possible methods can be applied to increase the interlayer spacing of graphitic sheets. One is by the intercalation of chemicals into the graphite galleries, and the other is by oxidation. The earliest and most-studied chemical used in intercalation of graphite is potassium. Potassium intercalated graphite compounds have different stages, which indicate the insertion frequency of the potassium. When the potassium inserts itself into the galleries between every individual graphite sheet, the intercalation compound formed has a 1st-stage structure. The 1st stage potassium intercalated graphite compound, formulated as C_8K, has an interlayer spacing of 0.54 nm. [146] As discussed in Chapter 2.3, the interlayer spacing of the 1st-stage potassium intercalated graphite compound is not sufficiently large for nanocomposite formation, and the interlayer surface is highly hydrophobic and organophobic, which is very similar to that of graphite. These two factors limit the use of potassium-intercalated graphite in the synthesis of polymer nanocomposites.

Modifying graphite by oxidation not only increases the interlayer spacing of graphene sheets but also introduces oxygen-containing functional groups into the graphite sheets. These polar function groups improve the surface compatibility of the modified graphite

with polar polymers. The oxidation method was chosen to produce nano-structured graphite to synthesise of graphite/polyurethane nanocomposites.

In this Chapter, five graphite sources with different flake sizes were screened and oxidised into graphite oxides. The difference in flake sizes will lead to different aspect ratios when the graphene sheets are dispersed in polymer in single layers. Based on the study of the graphites and their graphite oxides, one graphite oxide will be chosen to be further modified by intercalating with the hydrophilic polymers such as polyethylene oxide (PEO), polyethylene glycol (PEG) and polyvinyl pyrrolidone (PVP) to produce organo-graphite oxides. The aim of the intercalation with the polymers is to further increase the interlayer spacing and to improve the intersurface compatibility of the graphene sheets with the polyurethane systems.

6.2 Synthesis of graphite oxide

6.2.1 The graphite sources

The five graphite sources used to produce graphite oxides were the Aldrich-F, Aldrich-P, BDH-P, LUH-P and NGS-P. The Aldrich-F was composed of large flakes and its flake was approximately 150 μm in length. The other four graphites were powders. The morphology of the four powder graphites were investigated using SEM, Figures 6.1 a-d.

The micrographs show that all the graphite fine powders are still in flakes. The micro flakes of the Aldrich-P and BDH-P are larger and thicker than those of the other two. The Aldrich-P has two different lengths of micro flakes: one group were approximately 5 μm and the other approximately 10-15 μm. The BDH-P's particles were mostly about 15 μm; only a small number of particles were smaller. The LUH-P's larger particles were less than 10 μm in length. The larger particles in the NGS-P were approximately 5 μm. The particle length together with the ash content of the graphite samples are in Table 6.1.

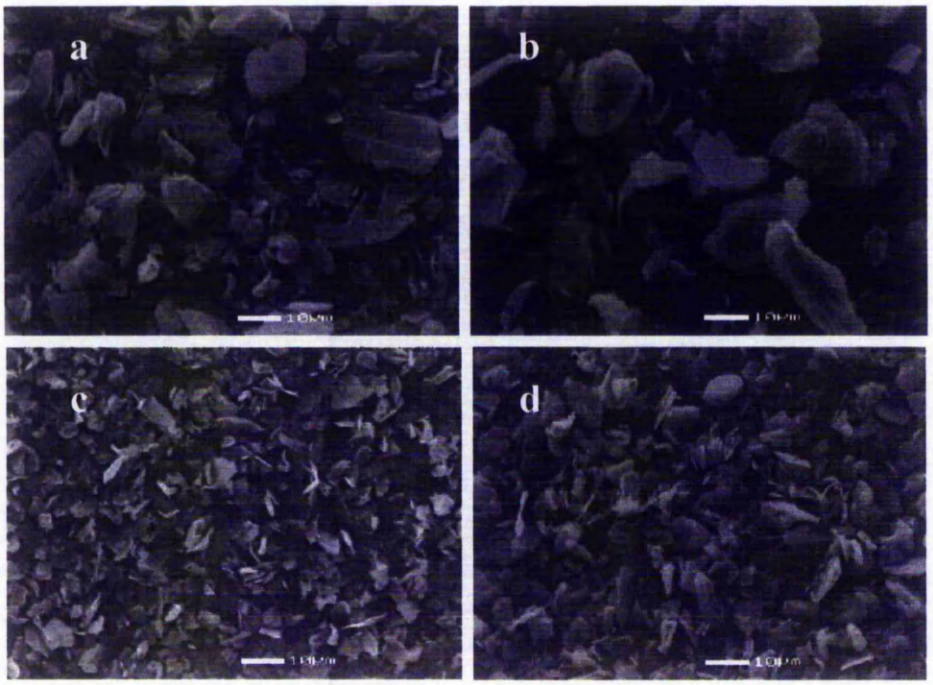

Figure 6.1 SEM images of the graphite powders Aldrich-P (a), BDH-P (b), NGS-P(c) and LUH-P(d)

Table 6.1 Properties of the graphite samples

	Type	Flake length, μm	Ash, wt%
Aldrich-F	Flake	150*	11.7
Aldrich-P	Synthetic	5, 10-15	0.6
BDH-P	Natural	15	0.2
LUH-P	Micronised crystalline	<10	2.6
NGS-P	Micronised flake	5	0.3

* from data sheet.

The ash comes from the mineral impurities in the graphite. Generally, the less the ash content, the purer the graphite is. The Aldrich-F had the highest ash content of 11.7 wt.% and LUH-P produced 2.6 wt.% of ash. The other powders except LUH-P had less than 1 wt.% of ash. The powder graphites have less mineral impurities than the large flake sample.

The five graphite samples were analysed by XRD and they had very similar XRD patterns. As an example, the XRD pattern of the Aldrich-P is shown in Figure 6.2. The strong peak at $2\theta = 26.5^{o}$ is the 002 peak, the characteristic peak of graphite. The 002 peaks indicate the interlayer spacing of the graphite sheets. Other two important peaks

are the 100 at 2θ=42.46° and the 101 at 2θ=44.65°, which indicate the perfection of the graphite sheets. These parameters of the graphite samples are listed in Table 6.2. Due to crystal defects in the graphites and measurement deviation, the peaks are slightly shifted from the corresponding theoretical positions.

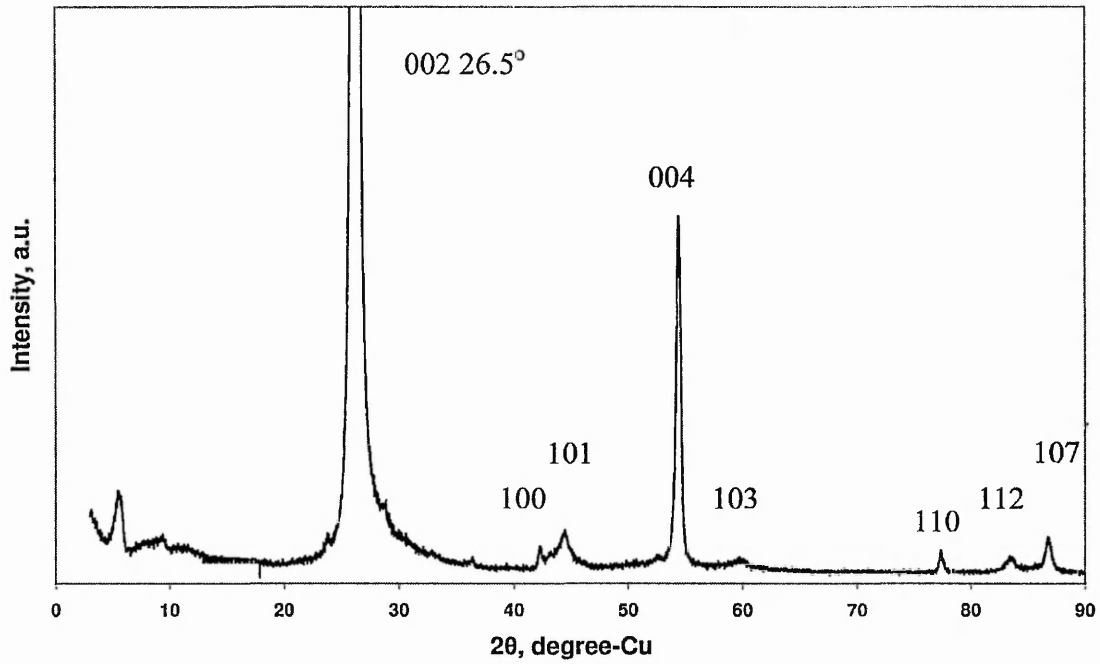

Figure 6.2 XRD pattern of the Aldrich-P

Table 6.2 The XRD data of the graphite samples

Sample	2θ, °			d_{001}, nm
	002	100	101	
Ideal graphite	**26.56**	**42.46**	**44.65**	**0.3354**
Aldrich-P	26.40°	42.36	44.50	0.3373
BDH-P	39.7°*	-	-	0.3370
LUH-P	26.34°	42.26	44.34	0.3380
NGS-P	26.46°	42.34	44.50	0.3364
Aldrich-F	26.32°	42.30	44.42	0.3383

* This sample was examined using Cr as radiation source.

The analyses of the graphites show that the flake length and thickness of the samples decrease in the order of the Aldrich-F, BDH-P, Aldrich-P, LUH-P and NGS-P. Except for the Aldrich-F and LUH-P contain large amounts of minerals, the others have less

than 1% of ash content. The flake length and thickness will influence the mass transfer of oxidants during the graphite modification. Large particles need longer oxidation time to reach a uniform modification. On the other hand, the size of the graphite sheets is important, as their aspect ratios will be different when they are dispersed in polymer nanocomposites. The large aspect ratio of nano fillers will give the nanocomposites better reinforcement and barrier properties.

6.2.2 The effect of the extent of oxidation

The Aldrich-F was oxidised using different oxidants. A mixture of concentrated sulphuric and nitric acids and $KMnO_4$ in concentrated sulphuric acid were used. The oxidation methods are described in Chapter 3. The graphite oxidised by the acid mixture produced expandable graphite (expandable Aldrich-F). The expandable graphite was oxidised in air at 800°C forming expanded graphite (expanded Aldrich-F), which had a specific volume of 239 ml/g. The oxidation of graphite by $KMnO_4$ in concentrated sulphuric acid produced graphite oxide (oxidised Aldrich-F). The XRD patterns of the oxidised Aldrich-F, expandable Aldrich-F, expanded Aldrich-F and the Aldrich-F are shown in Figure 6.3. All of these samples have diffraction peaks at approximately 26° and 54°, which are the 002 and 004 peaks of graphite. The expandable and oxidised Aldrich-F showed the diffraction peak 001 of graphite oxide. The characteristic peaks of the samples are summarised in Table 6.3.

Table 6.3 The characteristic peaks of the Aldrich-F and its products after different oxidation treatments

Sample	Graphitic structure				Graphite oxide
	002	100	101	d_{001}, nm	001
Aldrich-F	26.32°	42.30	44.42	0.3383	N
Expandable Aldrich-F	26.16°	-	-	0.3404	9.76
Expanded Aldrich-F	26.38°	42.46	44.50	0.3376	N
Oxidised Aldrich-F	26.00°	-	-	0.3424	10.36

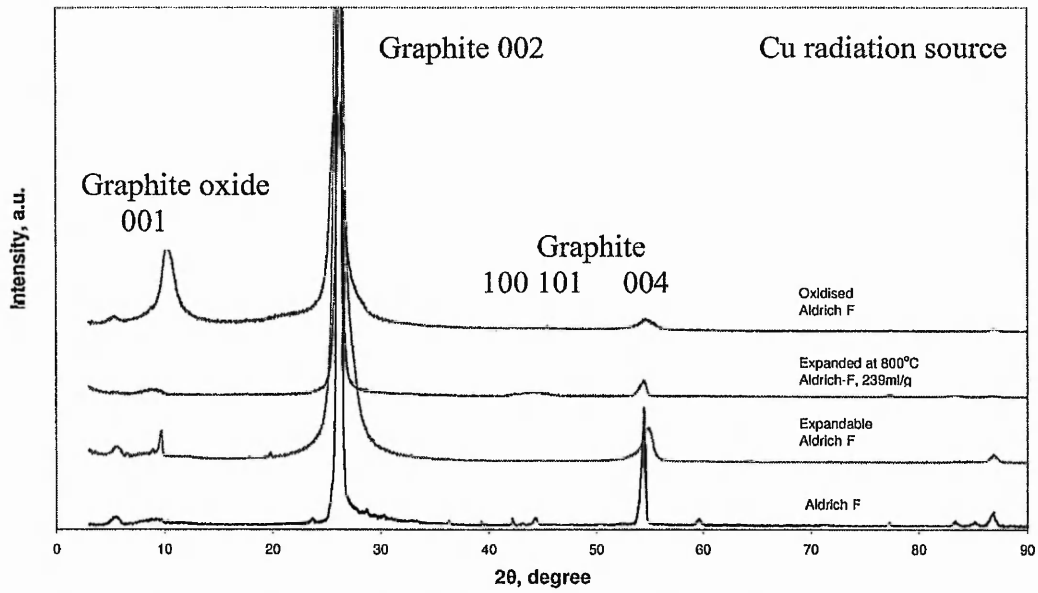

Figure 6.3 XRD patterns of the Aldrich-F, its expandable graphite, expanded graphite and oxidised graphite

The Aldrich-F has a very sharp and strong 002 peak at $2\theta=26.32^{\circ}$, corresponding to an interlayer spacing of the graphite sheets of 0.3383nm. After treatment with a mixture of concentrated acids, the expandable graphite basically keeps the XRD pattern of graphite, but the 002 peak became wider, and the 100 and 101 peaks weakened and were undetectable. The 002 peak centres at 26.16°, indicating an interlayer distance of 0.3404nm, which is greater than that of the original graphite. This XRD pattern indicates that the crystal structure of the graphite is retained in the expandable graphite, but the presence of residues of intercalated H_2SO_4 makes the crystal structure imperfect. Besides the XRD pattern of graphite, the expandable graphite has a small new peak at $2\theta = 9.76^{\circ}$, which should be the 001 peak of graphite oxide. This peak shows that the expandable graphite has a detectable amount of graphite oxide, which was formed by oxidation by the mixed acids of H_2SO_4 and HNO_3.

After the expandable Aldrich-F was further oxidised in air at 800°C for 1 minute, the expanded graphite produced had a better graphite structure. Because the chemicals retained in the expandable graphite were released during heating, which resulted in the restoration of the interlayer spacing of the graphite sheets. The 002 peak moved back from 26.16° to 26.38°, and the 100 and 101 peaks reappeared. The 001 peak at 2θ

=9.76° disappeared, indicating that the corresponding structure had reverted to graphite during the heat treatment.

The oxidised Aldrich-F still had the XRD pattern of graphite, but an extra strong peak occurred at 2θ=10.36°, which is the 001 peak of graphite oxide. This result indicates that the graphite flakes were only partially oxidised into graphite oxide. The amount of the graphite oxide formed is significant, which is shown by the relative intensity of the 001 peak of the graphite oxide to the 002 peak of graphite. The 002 peak of the graphite is located at 26.00°, corresponding to an interlayer distance of 0.3424 nm, which is the largest of all four samples. This is the result of the strong oxidation of the graphite by the active atomic oxygen produced from the $KMnO_4$ in the cooled concentrated H_2SO_4.

The experimental results show that the oxidation of the Aldrich-F by the acid mixture does not change the basic crystal structure of the graphite. The mixed acids are not sufficiently strong to introduce oxygen-containing functional groups into the graphite sheets and to change the whole crystal structure. The reactions occur only at the prismatic and defect areas of the graphite. The expansion of the expandable graphite flakes into the expanded graphite does not alter the basic crystal structure of the graphite either. It only decreases the crystal sizes of the graphite.

The oxidation of the Aldrich-F by $KMnO_4$ in concentrated H_2SO_4 produced a significant amount of graphite oxide, but did not entirely convert the graphite flakes into graphite oxide. This oxidation treatment of the Aldrich-F converts the surface layers into graphite oxide because of the limit in mass transfer of the oxidant during the oxidation. The $KMnO_4$ in concentrated H_2SO_4 is a suitable oxidant to produce graphite oxide, but the large flake graphite is not an ideal graphite source to be modified into nano-structured graphite for the synthesis of graphite/polymer nanocomposites.

6.2.3 The effect of the size of graphite flakes

To further examine the effect of the particle size of graphite sources on the mass transfer during oxidation, the four graphite powders were oxidised by $KMnO_4$ in concentrated H_2SO_4. The graphite oxides produced were coded as Aldrich-GO, BDH-GO, LUH-GO and NGS-GO respectively, and were examined by XRD. Their XRD patterns along with that of the oxidised Aldrich-F (Figure 6.4) show that the 001 peaks of all the graphite oxides are in a very similar position. All the graphite oxides have

identical two-dimensional crystal structures. Their 001 peaks are located between 10.36 and 11.12°, indicating that the interlayer spacing of the graphite oxides is between 0.80 and 0.85 nm.

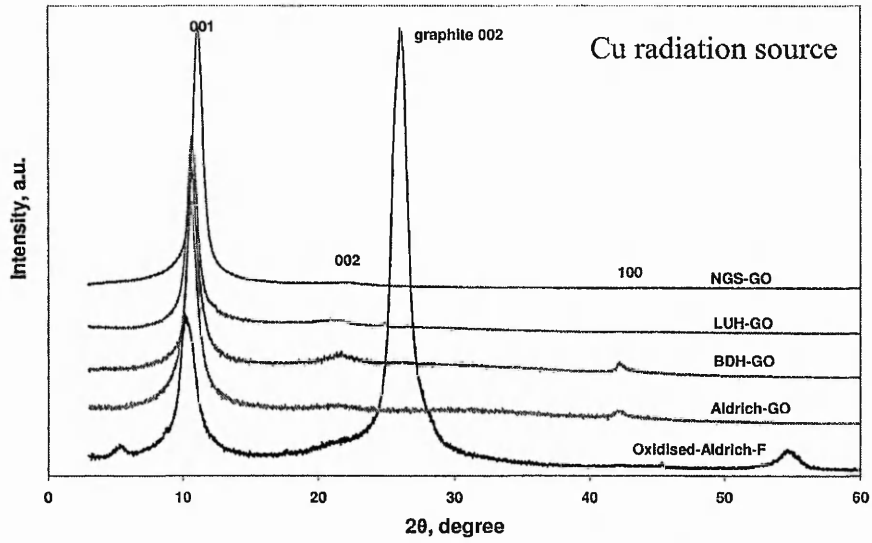

Figure 6.4 XRD patterns of GOs from the graphite samples

The graphite oxides produced from the Aldrich-P and BDH-P have an obvious 100 peak at 2θ=42.4°, whereas those from the LUH-P and NGS-P do not. The Aldrich-GO and BDH-GO were brown in colour in their aqueous suspensions during the synthesis, while the LUH-GO and NGS-GO were bright yellow in colour. The difference both in the XRD 100 peak and in colour of the graphite oxides can be explained by the particle morphology of the graphite powders. The Aldrich-P and BDH-P have larger and thicker particles, which lead to brown graphite oxides. The finer powders of the LUH-P and NGS-P have smaller and thinner particles and can be better oxidised resulting in lighter coloured products, which are yellow. This is because the larger and thicker particles have a higher resistance to mass transfer than the smaller and thinner particles.

The above study indicates that the flake size of the graphites has an influence on the graphite oxides produced. Large flakes like that of the Aldrich–F result in that graphite only partially converted into graphite oxide. When the flake size decreases to the level of the Aldrich-P and BDH-P, the graphite can be entirely oxidised into graphite oxide. As the flake size further reduces to the level of the LUH-P and the NGS-P, the resulting graphite oxide has a lighter colour.

Graphite oxide in general has a uniform two-dimensional layer structure and an interlayer spacing double that of the graphite itself. This is a suitable nano-structured graphite for the synthesis of graphite/polymer nanocomposites. Graphite oxide produced from the Aldrich-P was chosen for further study and surface modification for the synthesis of graphite/polyurethane nanocomposites, because the Aldrich-P could be entirely oxidised into graphite oxide and had larger flake sizes. This allows the nanocomposites synthesised to have better reinforcement and barrier properties because of larger aspect ratios of the graphite sheets.

6.2.4 The effect of moisture

Chemical structure studies of graphite oxide have suggested that the oxygen-containing groups in the graphite oxide are hydroxyl and ether-like oxygen bridges between 1 and 3 carbon atoms.[147,148] These oxygen-containing groups make graphite oxide hydrophilic. Depending on the amount of water contained in the GO, the interlayer distance varies in the range from 0.6 to 1.1nm. [126] Due to the synthesis of polyurethane being very water sensitive, the water content, the water absorbing rate of the graphite oxide and the variation of the interlayer distance of the graphite oxide with water content were investigated.

The Aldrich-GO was dried at 50°C and then pressed into a plate and its XRD pattern measured. This was defined as the water balanced GO. The plate was then dried in a vacuum oven at 105°C for 24 hours. The sample was weighed before and after drying and was found to contain 18.87% of water before drying. The sample had its XRD measured at time of 0, 2.3, 4 and 22 hours after exposure to ambient atomsphere. A wet Aldrich–GO sample also had its XRD examined. This material was taken from the filter cake after being washed by 5% HCl aqueous solution. The XRD patterns of the Aldrich-GO with different water contents are presented in Figure 6.5.

The 001 peak of the wet graphite oxide is at $2\theta=9.06^{\circ}$, corresponding to an interlayer spacing of 0.98 nm. The interlayer spacing decreases to 0.83 nm after drying in the vacuum oven at 50°C. Further drying at 105°C for 24 hours does not change the crystal structure of the graphite oxide, but decreases the interlayer spacing to 0.64 nm. After exposure to the air, the interlayer spacing increased due to absorbance of moisture from

the atmosphere. When the exposure time was 22 hours, the interlayer spacing increased to 0.73 nm.

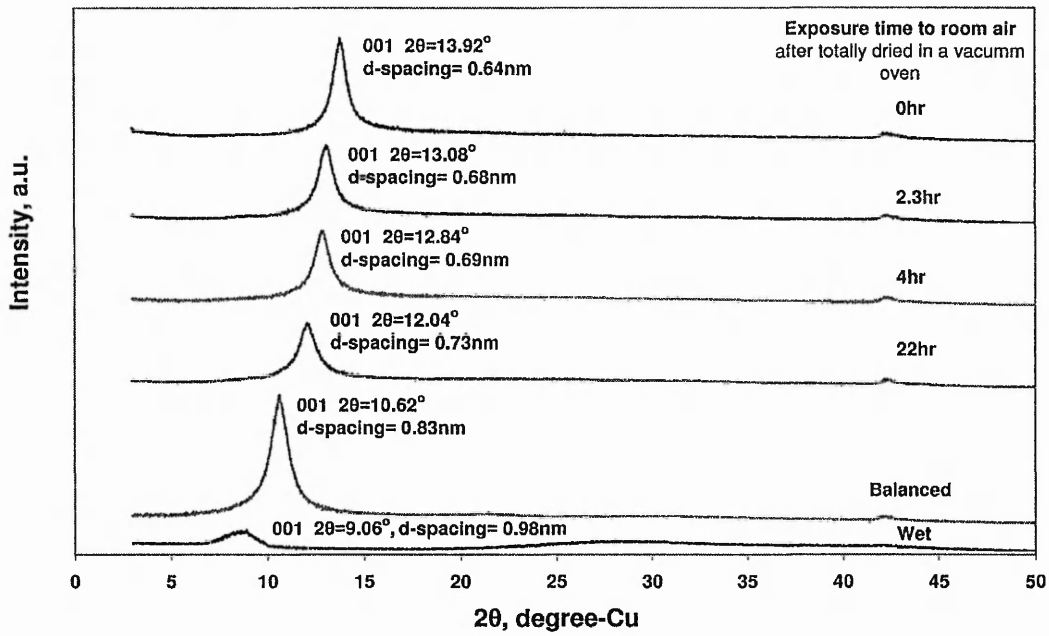

Figure 6.5 XRD patterns of the Aldrich-GO after drying and absorbing water

Larger interlayer spacings are conducive to the synthesis of graphite/polymer nanocomposites. For non-water sensitive polymers, water is a very good solvent for the synthesis of their nanocomposites with graphite oxide. However, the polymerisation of polyurethanes is very sensitive to water due to the reaction of isocyanate functional groups with water. Therefore, water needs to be controlled in the synthesis of polyurethane nanocomposites. The water in graphite oxide may be used as blowing agent or removed by drying. The change in the interlayer distance with the water absorbing time shows that the absorbance of water can be ignored by using the GO immediately after drying.

6.2.7 Thermostability of graphite oxide

The water removed from graphite oxide is in two states: mobile water and strongly bound water. The mobile water is physically bonded to the GO and can be removed without affecting the chemical structure of the GO, while the strongly bound water is chemically bonded to the GO and cannot be removed without altering the chemical structure of the GO.[149,150] The hydroxyl groups in graphite oxide, for example, may be

removed as water by heat treatment, meanwhile the gases CO, CO_2 and H_2 are released.[151] These reactions result in a significantly less ordered structure in the graphite oxide.[149] The influence of water content and effects of heat treatment on the chemical and crystal structure of graphite oxide is not clear.

The Aldrich-GO, dried at 50°C in vacuum, was analysed by thermogravimetric analysis in an inert atmosphere to investigate its dehydrating and decomposing processes and thermal stability. The weight change of the graphite oxide with temperature is shown in Figure 6.6.

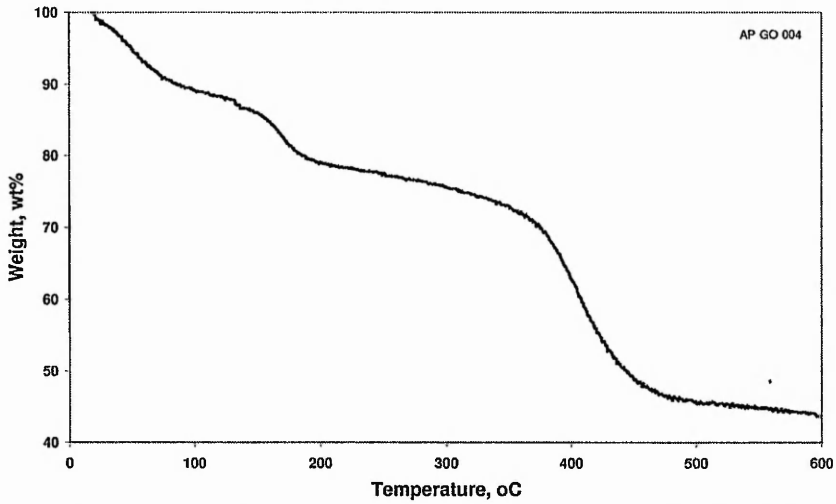

Figure 6.6 Thermo-gravimetric analysis of the Aldrich-GO

The weight loss curve shows that the graphite oxide loses its weight readily at room temperatures in a dried inert atmosphere. The weight loss process can be divided into two phases. Between room temperatures and approximately 200°C, about 20% weight is lost, which is virtually the amount of water eliminated in drying at 105°C (18.87%). The weight loss may predominantly be removal of the mobile water. From 200°C to 500°C the sample loses approximately 35% of its weight. This weight loss should be caused by the decomposing of graphite oxide. A XRD pattern of the Aldrich-GO heated at 600°C for 2 minutes in a Muffle furnace is shown in Figure 6.7. Heating up to this temperature, the crystal structure of the graphite oxide has been destroyed, and the resulting structure is like that of graphite, having a 002 peak at 25° and a 100 peak at 42.6°.

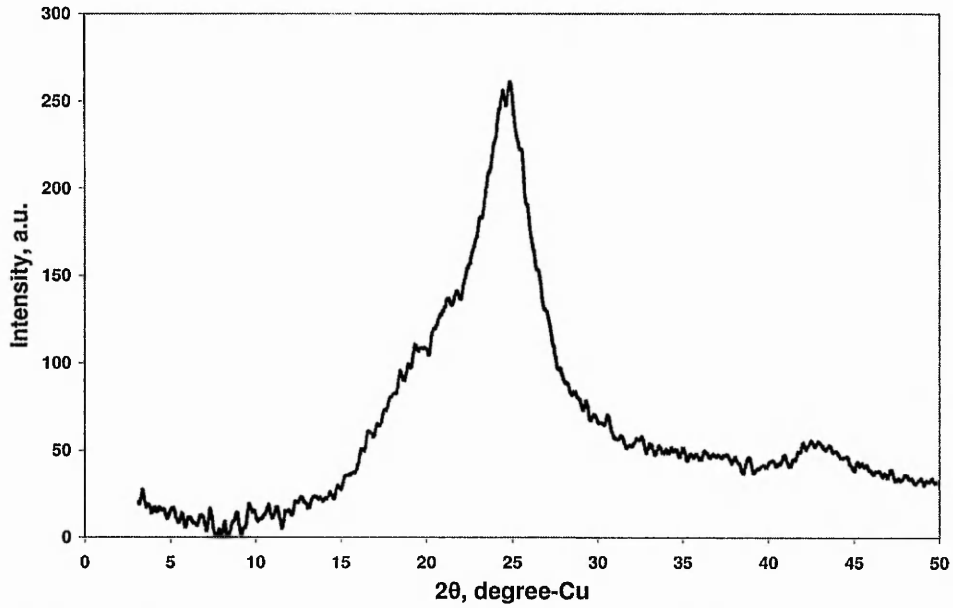

Figure 6.7 XRD pattern of the Aldrich-GO after heated at 600°C for 2 minutes.

The study of the thermal stability of the graphite oxide indicates that the graphite oxide is much more thermally sensitive than graphite. To keep the two dimensional crystal structure, the graphite oxide should be treated at lower temperatures, for example less than 105°C. The decomposing of graphite oxide results in graphite-like materials. This property may be used to improve the char of its polymer nanocomposites.

6.3 Surface modification of graphite oxide

Due to the presence of a large amount of oxygen-containing functional groups, graphite oxide is hydrophilic and is easy to disperse in water and forms hydrogen bonds with other polar function groups. To further modify the graphite oxide, it was intercalated with the hydrophilic polymers PEO, PEG and PVP to produce organo graphite oxides. This work aimed to further expand the interlayer distance of graphene sheets of the graphite oxide and to modify the interlayer surface of the graphite oxide from highly hydrophilic to organophilic. These organo-graphite oxides have potential to be graphene sources for the synthesis of graphite/polyurethane nanocomposites.

6.3.1 Intercalation of polyethylene oxide

Polyethylene oxide (PEO) has been extensively studied by intercalating with clays to form nanocomposites.[152-155] It also has a very similar chemical structure with

polyethylene glycols, which are a group of polyols used for the synthesis of polyurethanes. A PEO with a number average molecular weight of 600,000 was chosen to intercalate with the Aldrich-GO to study the nanocomposite formation and the charring properties of GO/polymer nanocomposites. The latter will be discussed in the Chapter 7.

The graphite oxide and the PEO were separately dispersed or dissolved in water. The aqueous solution of the PEO was then added to the GO suspension. The mixture was sonicated for 30 minutes and stirred for 24 hours. The suspensions, with the GO loadings of 0.5 wt.%, 1 wt.%, 3 wt.% or 5 wt.% in the final composites are shown in Figure 6.8. These suspensions had been left overnight with no agitation.

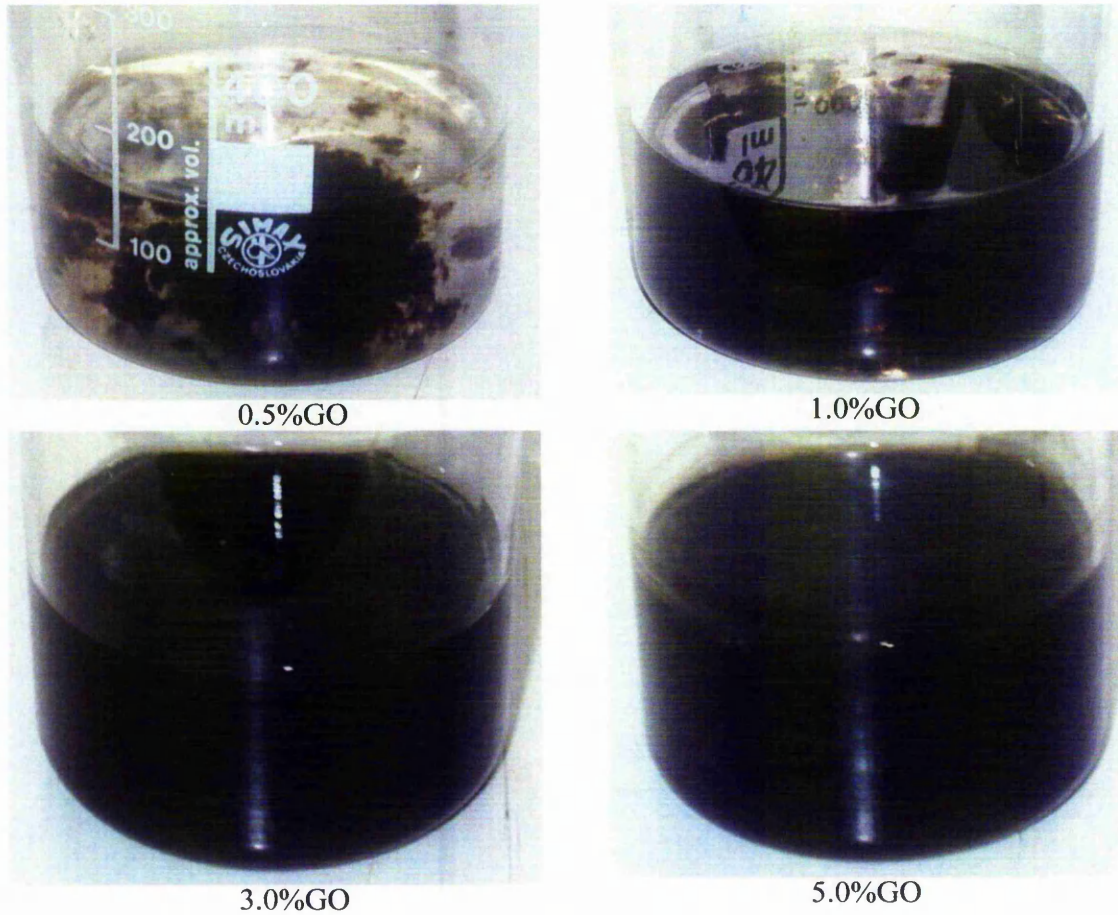

Figure 6.8 The suspensions of PEO intercalated with 0.5-5.0 wt.% of the Aldrich-GO. The amounts of GO and PEO in the suspensions are 5:995mg, 10:990mg, 30:970mg and 50:950mg, respectively.

The graphite oxide in the suspensions aggregated together as brown floccules, which could be re-dispersed easily by stirring. In the suspension with a GO loading of 0.5 wt.%, the brown floccules were clearly suspended in a transparent aqueous solution. When the GO loading increased, the number of floccules increased and the colour of the suspensions became darker. The observation under a stereomicroscope showed that the GO floccules were still suspended in transparent liquid even when the GO loading was 5.0 wt.%.

This phenomenon together with the dispersion of GO in water indicates that the interactions between PEO and GO are stronger than those between water and GO. The interaction between the PEO and the GO results in coagulated particles.

The PEO intercalated GO blends were cast into films by allowing the water to evaporate naturally. The films were flexible. The film with 0.5 wt% of the GO was not uniform, Figure 6.9. Some parts of the film were not brown due to the very low concentration of the GO. The 0.5 wt.% of graphite oxide was not sufficient for all the PEO to be intercalated between the graphene sheets. All other films were black.

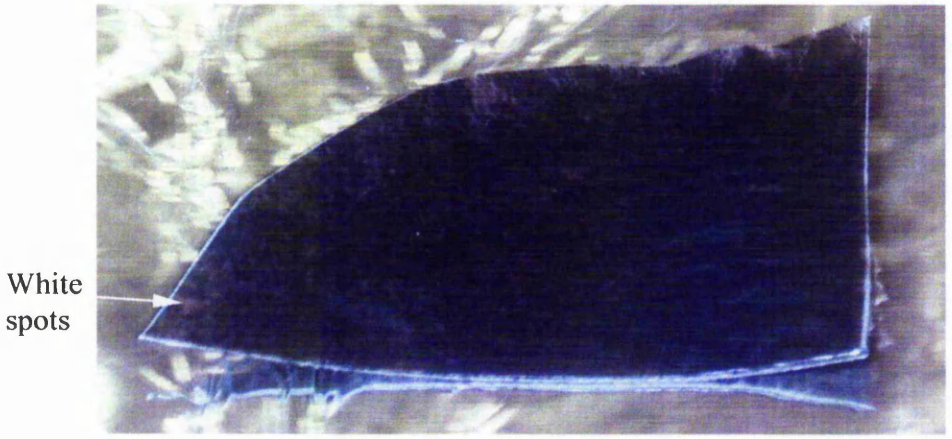

Figure 6.9 The PEO intercalated GO film with 0.5 wt% of the GO

The XRD patterns of the PEO intercalated GO with the GO loadings of 0.5 wt.%, 1.0 wt.%, 3.0 wt.%, 5.0 wt.% and 50 wt.% are shown in Figure 6.10. The samples with the GO loading of 0.5 wt.% and 1.0 wt.% have no obvious diffraction peak of the graphene sheets. When the loading increased to 3.0 wt.%, a diffraction peak occurred at 7.24°. The peak position did not shift when the GO loading increased up to 50%. These XRD patterns indicate that the PEO has intercalated into the graphite oxide. The interlayer

spacing of the graphene sheets increases from 0.8 nm to 1.22 nm. The expansion of graphite oxide is independent of its loading.

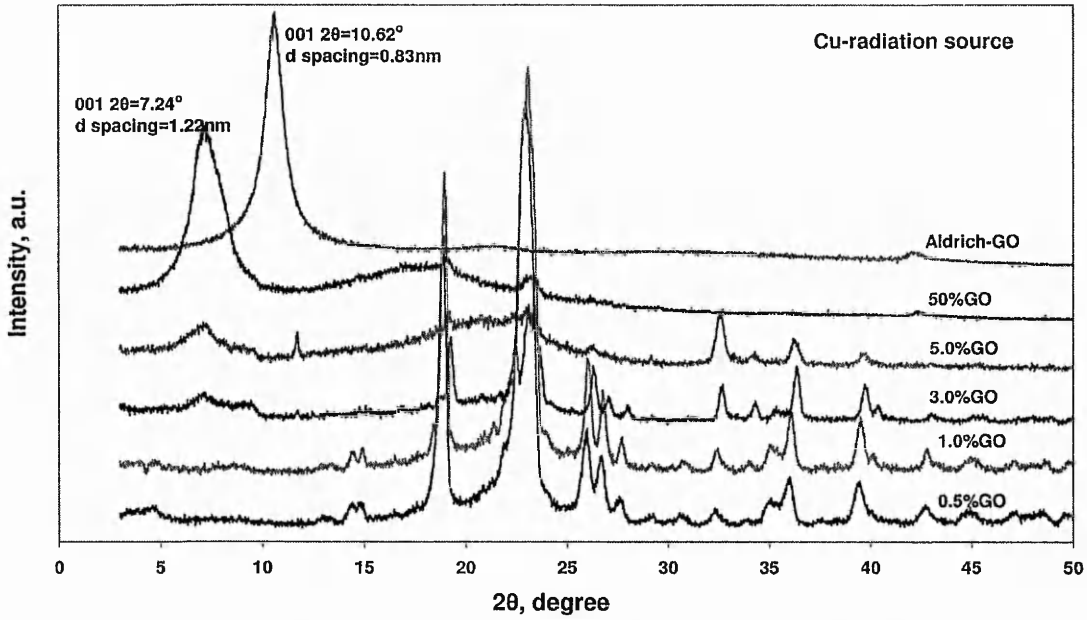

Figure 6.10 XRD patterns of the PEO intercalated Aldrich-GOs

PEO is a crystalline polymer. With graphite oxide loadings lower than 3%, the XRD patterns show strong diffraction peaks of PEO, indicating that the PEO exists in the crystalline form. When the GO loading increases to 5.0 wt.% the intensity of the diffraction peaks of the PEO decreased and could barely be seen, indicating that most of the PEO has effectively intercalated into the galleries of the graphite oxide and has a confined crystal structure, which is much smaller in size than those in bulk PEO. [156]

6.3.2 Intercalation of polyethylene glycol

A polyethylene glycol with a number average molecular weight of 1500 (PEG1500) was chosen to intercalate with the Aldrich-GO to prepare organo-graphite oxides for the synthesis of graphite/polyurethane nanocomposites. The PEG1500 is a suitable polyol for the production of rigid polyurethane foams. It has a linear molecular structure, which is very similar to that of PEO except it has two hydroxyl groups at both ends of the polymer chains, and is readily to be dissolved in water.

The PEG1500 and the Aldrich-GO were dissolved or dispersed in distilled water respectively. The PEG1500 aqueous solution was then stirred into the GO aqueous

suspension. The PEG1500 intercalated GOs were cast into films as the water evaporated naturally. The films were soft. The PEG1500 intercalated GOs with 10 wt.% and 50 wt.% of GO were synthesised and examined using XRD, as shown in Figure 6.11.

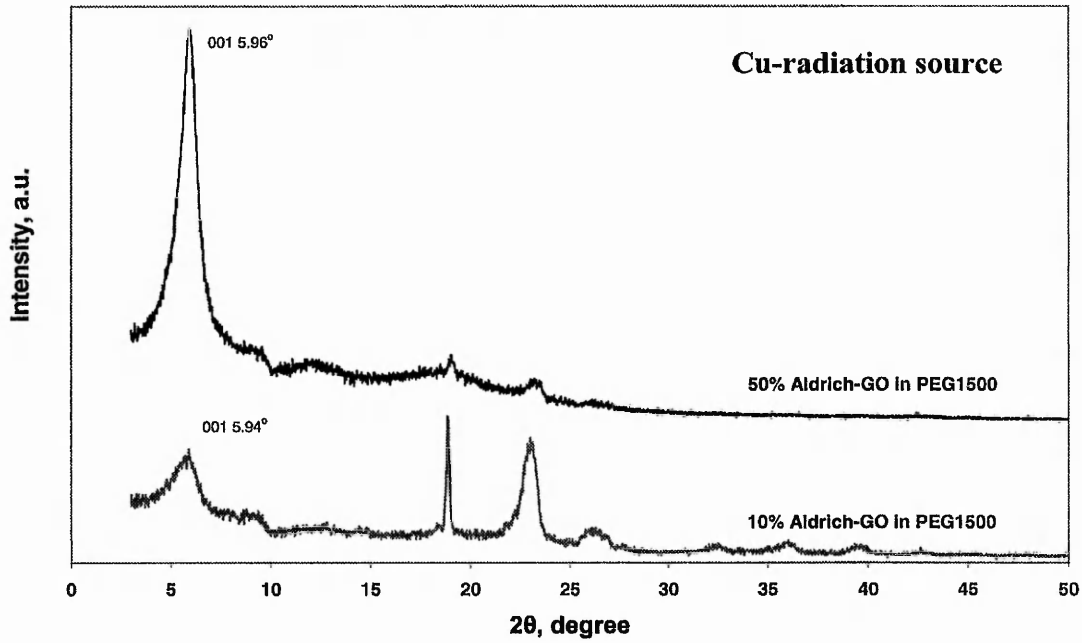

Figure 6.11 XRD patterns of the PEG1500 intercalated Aldrich-GOs

The XRD patterns show that the PEG1500 intercalated GOs with both 10 wt.% and 50 wt.% of GO have diffraction peak 001 at the same position, 2θ = 5.94-5.96°. This indicates that the PEG has very similar intercalation manner to the PEO. The interlayer expansion of the GO is independent of its loading. The 001 peak position corresponds to an interlayer distance of the graphene sheets of 1.48 nm, which is slightly larger than that of the PEO intercalated GOs. This may be caused by the relatively much shorter molecular chains and much more hydroxyl end groups of the PEG1500 compared to those of the PEO 600,000.

6.3.3 Intercalation of polyvinyl pyrrolidone

Polyvinyl pyrrolidone is also a water-soluble polymer and has been found to have a synergistic effect on expanding the interlayer spacing of clays.[157] In this project, a PVP with a number average molecular weight of 55,000 was used to intercalate with the Aldrich-GO to make an organo-graphite oxide for the synthesis of graphite/ polyurethane nanocomposites.

The GO and the PVP were separately dissolved or dispersed in distilled water. The PVP aqueous solution was then added into the GO suspension. The PVP/GO organo-graphite oxides were synthesised with GO loadings of between 10-90 wt.% and cast into films. All the films were very brittle and could be easily ground into powders. The brittleness comes from the PVP, because a pure PVP film is more brittle than its composites with the GO.

The XRD studies of the PVP intercalated GOs indicate that the PVP has intercalated into the interlayer galleries of the GO, Figure 6.12. The interlayer spacing of the graphene sheets in the intercalated compounds varies with the GO content. When 90 wt.% of GO was dispersed in the PVP, the interlayer spacing of the graphene sheets was 0.75 nm, which was smaller than that of the graphite oxide, 0.83nm. This indicates that the PVP has substituted the water molecules existing in the graphite oxide. As the GO loading decreased to 80 wt.%, the interlayer spacing of graphene sheets expanded to 1.37 nm. At GO loadings of 50 wt.% and 10 wt.%, the interlayer spacings increased to 2.23 nm and 3.71 nm, respectively. The interlayer spacings of the graphene sheets increase linearly as the GO loading decreases.

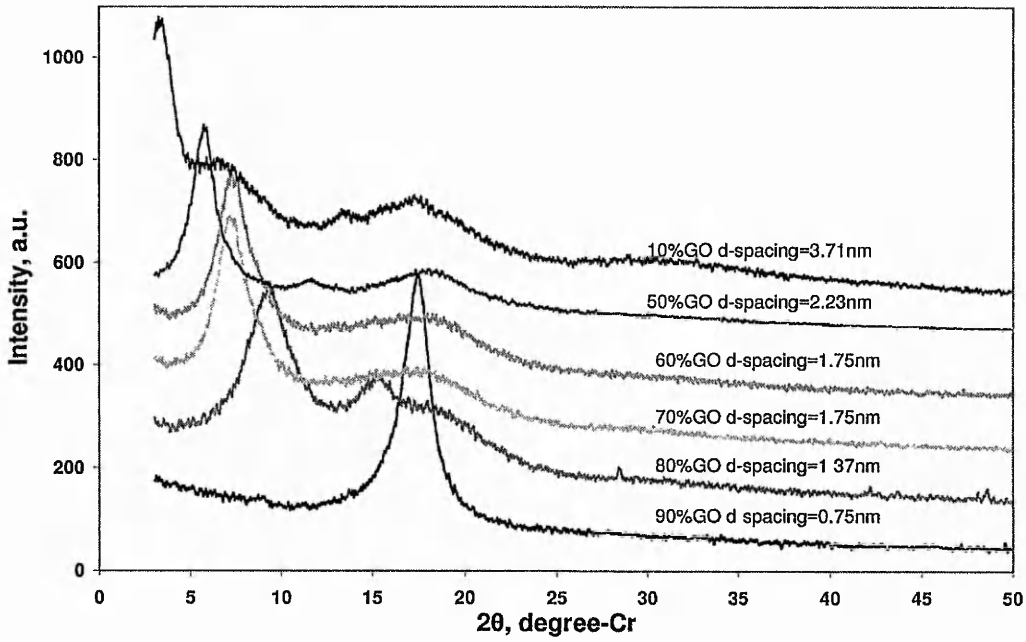

Figure 6.12 The XRD patterns the PVP intercalated GO

Alternatively, the interlayer distance of the PVP intercalated GO linearly increases as the PVP concentration rises, as shown in Figure 6.13. This phenomenon indicates that the PVP exists in the interlayer galleries of the GO not simply in a manner of single layer or multiple layers like that of PEO. The amorphous PVP as a matrix has the graphene sheets of GO uniformly dispersed in it.

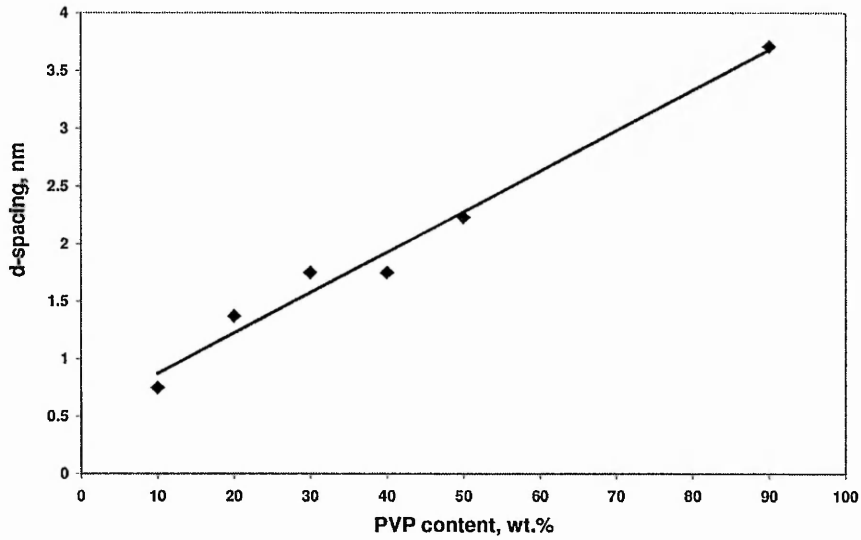

Figure 6.13 The interlayer spacings of the PVP intercalated GOs *vs* the PVP contents

Large interlayer spacings of the graphene sheets are preferred to the synthesis of graphite polyurethane nanocomposites. But the PVP intercalated GO with a low GO loading would add too much PVP into polyurethanes to reach a required loading of graphene sheets. The large amount of the PVP in polyurethanes will result in very brittle final products due to the brittleness of PVP. Thus, a 50:50 formulation of the GO to PVP was used to produce an organo-graphite oxide, which had an interlayer spacing of 2.23 nm.

6.3.4 Organo-graphite oxides

The PEG1500 and PVP intercalated Aldrich-GOs with a polymer GO ratio of 50:50, by weight, were prepared as organo graphite oxides to be used in the synthesis of graphite polyurethane nanocomposites. The PEG1500 has two hydroxyl groups to take part in the polymerisation of polyurethanes, while the PVP has no active hydrogen to take part in the reactions of polyurethanes. The organo graphite oxides were denoted as 50%GO +PEG1500 and 50%GO+PVP, respectively. The interlayer spacings were 1.48 nm for the 50%GO +PEG1500 and 2.23 nm for the 50%GO+PVP. The organo graphite oxides

were further studied using SEM and thermo-gravimetric analysis for their morphology and thermal stability, respectively.

The microphotographs of a torn cross-section of the 50%GO+PEG1500 film are shown in Figures 6.14 a & b. The organo GO has a uniform structure in micro scale. The graphene sheets of the GO dispersed in water as single layers and formed the intercalated compound by piling up with the polymer chains between them, resulting in layered-structured composite. The presence of harder graphene sheets resulted in saw-toothed structure in the torn surface (Figure 6.14 b). This agrees with the XRD results.

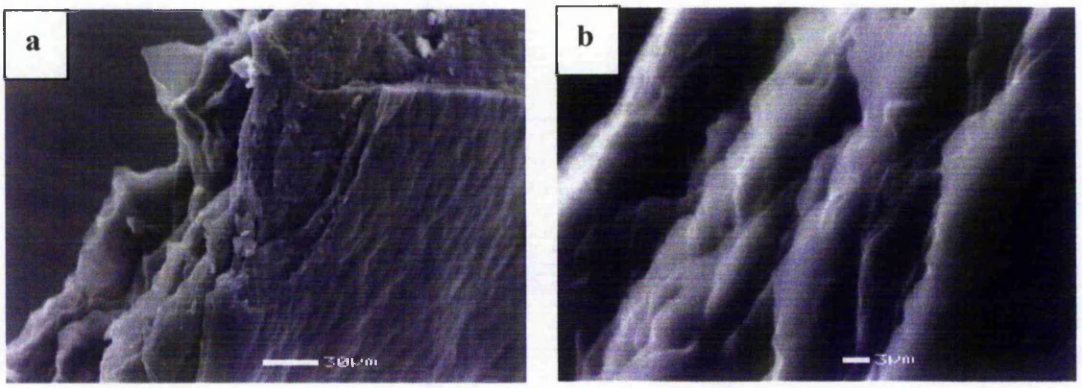

Figure 6.14 SEM images of the 50% GO+PEG1500

The thermal stability of both organo graphite oxides was investigated by thermo-gravimetric analysis. The TGA curves are shown in Figure 6.15. The TGA results show that the 50% PEG1500 intercalated GO has a lower thermal stability than that of the GO. The main onset temperature of weight loss is approximately 250°C, about 100°C lower than that of the GO. The PEG1500 is a waxy like material, and has a melting point of 45°C. The intercalation has significantly improved the thermal stability of the PEG1500. The intercalated composite did not melt when heated at 100°C under vacuum. In contrast, the PVP intercalated GO has significantly higher thermal stability than that of the GO. Its main degradation started at approximately 450°C, it was approximately 100°C higher than that of the GO. When heated to 600°C, the 50%GO+PVP has a slightly higher amount of residue than the GO, approximately 42%, while the 50%GO+PEG1500 has a residue yield 2-3% less than the GO. These results indicate that the intercalated GOs have improved thermal stability compared to the pure polymers from which they are made.

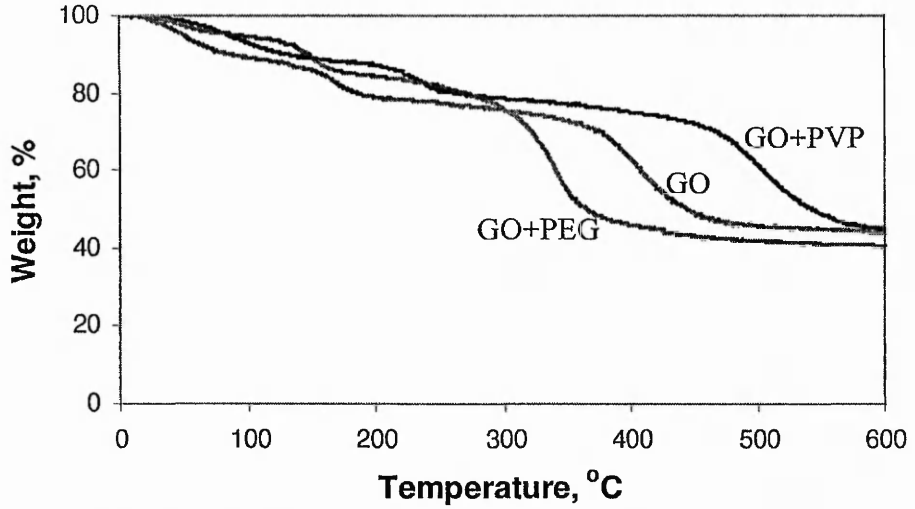

Figure 6.15 Thermo-gravimetric analysis of the Aldrich-GO, 50%GO+PEG1500 and 50%GO+PVP

6.4 Summary remarks

Five graphite sources with different flake sizes were screened to produce nano-structured graphites by oxidation. By the modified Hummers and Offemen method, large graphite flakes (ca. 150 μm) could only partially be oxidised into graphite oxide, but the small graphite flakes (less than ca. 15 μm) were oxidised evenly into graphite oxides, which had interlayer distances of approximately 0.8 nm. Among the four powders studied, the Aldrich-P graphite powder was chosen for further study, because of its relatively large flake length. The larger flake length will lead to larger aspect ratios when the graphene sheets are dispersed in single layers in polymers. The higher aspect ratio should lead to better improved mechanical and barrier properties of nanocomposites produced.

The Aldrich-GO was further modified into organo graphite oxides by intercalating with the hydrophilic polymers PEO, PEG1500 and PVP in water. The intercalations increased the interlayer spacing of the graphene sheets and modified the surface of the graphene sheets. The interlayer spacings of the PEO and the PEG1500 intercalated GOs are independent of the concentration of the polymers, which are 1.22 nm for the PEO and 1.48 nm for the PEG1500. However, the interlayer spacing of the PVP intercalated GO linearly increases as the PVP concentration rises.

Two organo graphite oxides were prepared for the synthesis of graphite polyurethane nanocomposites. They are 50%PVP intercalated GO and 50%PEG1500 intercalated GO. The interlayer spacing of the graphene sheets in the former is 2.23 nm, in the later is 1.48 nm. The organo graphite oxides have improved thermal stability compared to the corresponding pure polymers.

Chapter 7
The Development of Graphite /Polyurethane Nanocomposites

7.1 Introduction

Graphite/polymer nanocomposites contain graphite in single sheets dispersed in the polymer. Due to the graphite sheets being dispersed in single layers, they have potential to improve not only mechanical properties, but also thermal stability and barrier properties of the polymer. The improved thermal stability and barrier properties may improve fire retardancy of graphite/polymer nanocomposites in a similar way to clay/nylon-6 nanocomposites. The clay/nylon-6 nanocomposites form a layer of integrated char on the burning surface at an early stage of burning, which results in slow and gentle burning and significantly decreased peak heat release rates compared to the pure nylon-6. [6, 134] Different from clay layers, graphite sheets themselves are composed of carbon and hence may act as charring nucleation agent to promote char formation of graphite/polymer nanocomposites.

In this chapter, three nano-structured graphites developed in Chapter 6 were used in the synthesis of graphite/polyurethane nanocomposites. They were the Aldrich-GO and its two organo graphite oxides, that is, the 50%GO + PVP and 50%GO + PEG1500. The fire retardancy of the organo graphite oxides and the graphite/polyurethane nano-composites synthesised were investigated by burning tests. The fire retardancy of the PEO intercalated GOs with GO loadings ranging from 0.5 wt.% to 5.0 wt.%, produced in Chapter 6, were also studied to gain an understanding of the effect of graphene loadings and nano-structure on the flammability in order to explore the prospect of commercial application of graphite/polymer nanocomposites.

7.2 The polyurethane nanocomposite based on graphite oxide

A polyurethane foam system detailed in Table 7.1 was chosen for this study. A tolylene diisocyanate (TDI) mixture was used as the diisocyanate component, and a polyethylene

glycol with a number average molecular weight of 300 (PEG300) as the polyol component. The blowing agent and catalyst used were water and 1,4-diadabicylo[2,2,2]octane, respectively. The isocyanate index of the foams was 105.

Table 7.1 The formulation of the polyurethane foams

Component	Chemicals
Diisocyanate:	98% Tolylene diisocyanate 80/20
Polyol:	Polyethylene glycol Mn300
Blowing agent:	Water, 3% based on polyol weight
Isocyanate Index:	105
Catalyst:	1,4-Diadabicylo[2,2,2]octane, 0.1-0.2% based on polyol weight
Additives:	5% of GO or equivalent based on final foam weight

A 5.0 wt.% loading of GO was used in the synthesis of polyurethane nanocomposite foam. The GO were dried in the vacuum oven at 50°C for 24 hours. The water contained in the GO after the drying was calculated and used as the foaming agent.

Due to the cross-linking feature of the foam, an *in situ* polymerisation method was developed to synthesise graphite/polyurethane nanocomposites. Before the polymerisation reactions, the graphite oxide may be dispersed in either the diisocyanate or the polyol. The isocyanate is very sensitive to active hydrogen and readily reacts with water producing unstable carbanicacids which then decompose to amines and carbon dioxide (Reaction 2.7). The amines formed react further with isocyanate groups forming biurets (Reaction 2.8). The carbon dioxide liberated causes foaming. If the graphite oxide is dispersed in the diisocyanate component, the isocyanate groups will react with the water or hydroxyl groups in graphite oxide before being mixed with the polyol, resulting in changes in the polymerisation system. Graphite/polyurethane nanocomposites, therefore, were synthesised via the route of dispersing the nano-structured graphites into the polyol and then polymerising with the diisocyanate.

A graphite/polyurethane composite foam with 5.0 wt% of GO was synthesised using the above described method. A pure PU foam and a foam with 5.0 wt.% of graphite powder (Aldrich-P) were also synthesised for comparison. The three foams were investigated by

XRD for their nanostructures. The XRD patterns in Figure 7.1 show that the pure polyurethane has an amorphous structure. The polyurethane in the other foams shows very similar diffraction patterns except the filler peaks. The foam containing 5.0 wt.% of graphite powder has a strong 002 peak of graphite, indicating the polyurethane chains did not intercalate into the interlayer galleries of the graphite. The foam containing 5.0 wt.% of GO has the 001 peak at an angle lower than that of graphite oxide. It locates at $2\theta=7.0^{\circ}$, which indicates that the interlayer spacing of the graphite oxide has increased from 0.83 nm to 1.26 nm. The extent of the interlayer expansion is the same as that of

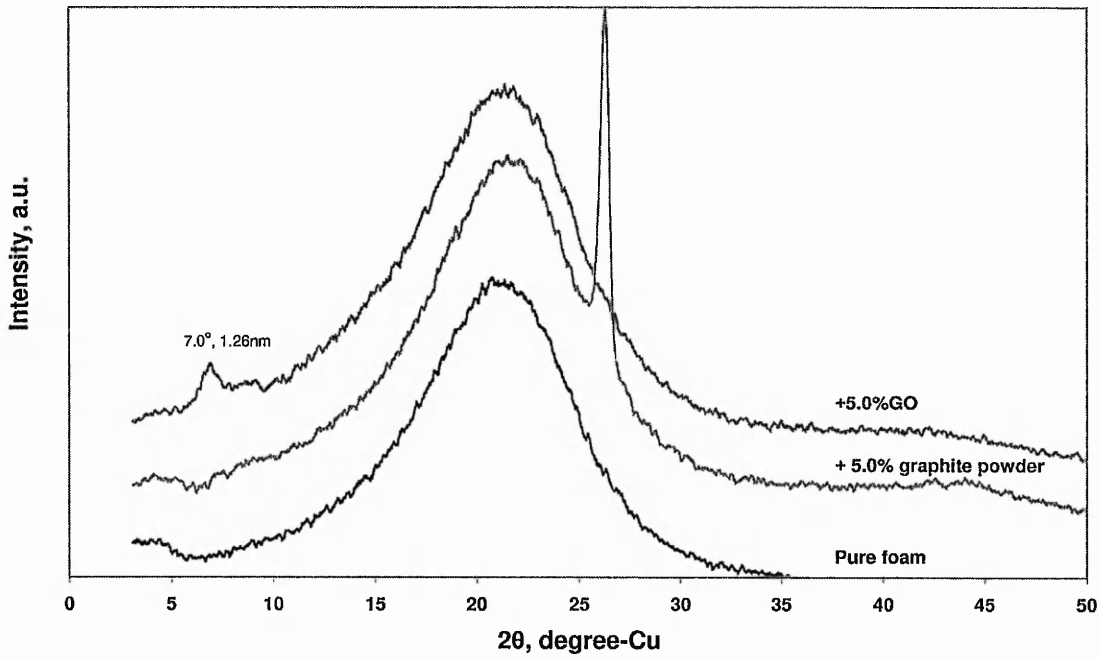

the GO intercalated by PEO (1.22 nm).

Figure 7.1 XRD patterns of the pure PU and the PU foams with 5.0 wt.% of graphite powder or GO

7.3 The polyurethane nanocomposites based on the organo graphite oxides

The organo graphite oxides (50%GO+PEG1500 and 50%GO+PVP) were also used to synthesise polyurethane foams in the same way as that of the GO. The loading of organo GOs was 10.0 wt.% based on the foam weight, which is equivalent to 5.0 wt.% of GO. The PEG1500 in the 50%GO+PEG1500 was calculated as a part of the polyol

component. The foams synthesised were analysed by XRD for their nano-structures, as shown in Figure 7.2. The 001 peaks are located at $2\theta = 3.8^{o}$ for the foam containing 10.0 wt.% of 50%GO+PVP and $2\theta = 7.2^{o}$ for the foam containing 10.0 wt.% of 50%GO+PEG1500. The interlayer distances of the graphene sheets are 2.32 nm for the former and 1.26 nm for the latter.

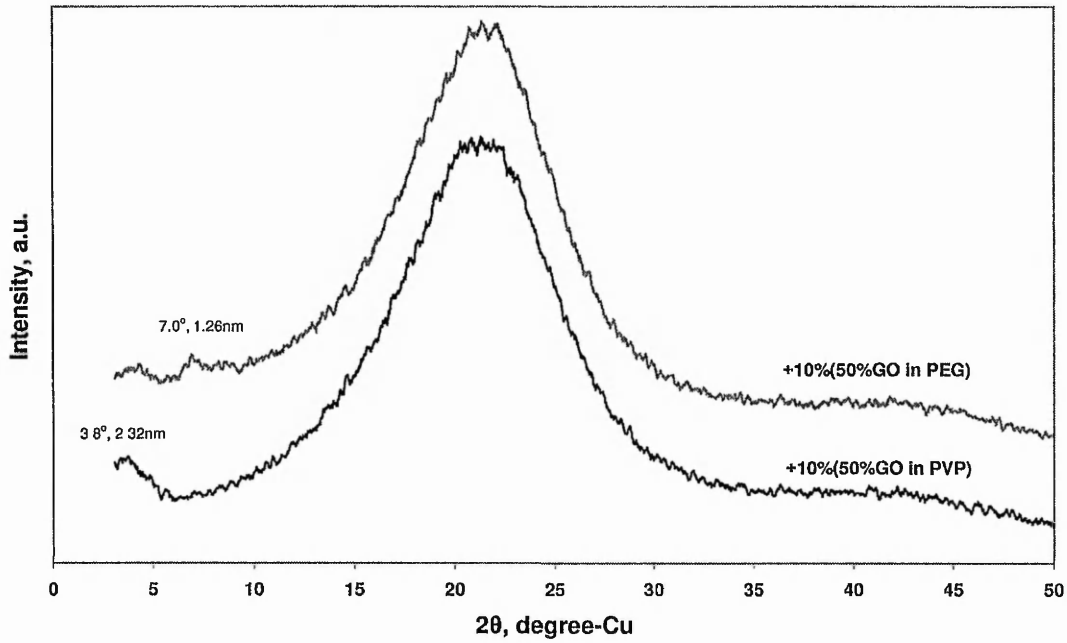

Figure 7.2 XRD patterns of the polyurethane foams with 10.0 wt.% of 50%GO+PVP and 50%GO+PEG1500

The interlayer spacing of the graphene sheets in the foam containing 50%GO+PEG1500 was smaller than that of 50%GO+PEG1500, and was the same as those in the foam made from the graphite oxide. There was no further interlayer expansion of the graphene sheets in the foam containing 50%GO+PVP. These results may indicate that the strong interactions formed between the pre-intercalated polymers and the graphene sheets are of the same order as those formed between the PEG300 and the graphene sheets, so that the PEG300 cannot further insert or substitute the pre-intercalated polymers. The added polymers are probably bound with the graphene sheets in hydrogen bonds.

The interlayer spacings of the graphene sheets in the nano-structured graphites and the polyurethane nanocomposites are summarized in Table 7.2. The comparison shows that the PEG1500 and PVP are not ideal to be used for the surface modification of graphite

oxide for the synthesis of polyurethane nanocomposites, because their interactions with the graphene sheets of GO are similar to those between the polyol such as PEG300 and the graphene sheets, so that the polyol can not insert itself or substitute the pre-intercalated polymer to connect with the graphene sheets. The ideal chemicals for the surface modification of graphite oxide should have weaker interactions with the graphene sheets than the polyol.

Table 7.2 The interlayer spacings of the graphene sheets in the polyurethane nanocomposites

Prior to foaming		d-spacing of the graphene sheets in the PU foams, nm
Fillers	d-spacing, nm	
Graphite powder	0.33	0.34
GO	0.83	1.26
50%GO+PEG1500	1.48	1.26
50%GO+PVP	2.23	2.32

In summary, the three polyurethane nanocomposites synthesized have dispersed graphene sheets in nano scale. More work needs to be carried out to study the polymers existing in the interlayer galleries of the graphene sheets.

7.4 The fire retardancy of graphite/polymer nanocomposites

The fire retardancy of three categories of graphite/polymer nanocomposites was investigated using burning tests. The chars formed during combustion were also investigated. The three categories of the nanocomposites are the two organo GOs, the three graphite/polyurethane nanocomposites and the PEO intercalated GOs with GO loadings ranging from 0.5 wt.% to 5.0 wt.%.

7.4.1 The organo graphite oxides

The fire retardancy of the 50%GO+PEG1500 and 50%GO+PVP were investigated by the burning tests, because they, as organo GOs, were used in the synthesis of graphite/polyurethane nanocomposites. The samples were in the form of film and were burnt using the natural burning and the Muffle furnace burning methods.

The films were easy to ignite with a Bunsen flame and self sustained the burning until the sample burnt out. During the burning there were no melting of the polymers observed. The burning gave rise to highly integrated chars, as shown in Figures 7.3 a & b, which retained the geometrical shapes of the original samples. After the flame died, smouldering was observed on the char of the PEG1500 intercalated GO, which changed the colour of the char from silver to black (Figure 7.3a). As a slow, low-temperature, flameless form of combustion, smouldering is sustained by the heat evolved when oxygen directly attacks the surface of a condensed-phase fuel. The smouldering observed indicates that a part of the char formed in the combustion of the PEG1500 intercalated GO has low oxidation resistance.

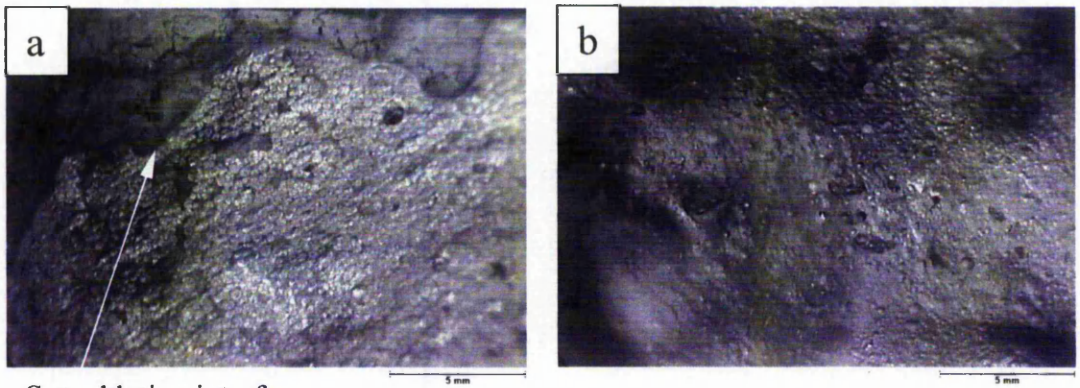

Figure 7.3 The chars of the 50%GO+PEG1500 (a) and the 50%GO+PVP (b). by the natural burning test

When the samples were placed in the Muffle furnace, both films cracked at the beginning as they were burning, and the sound was louder in the case of the PVP intercalated compound. This may be caused by the rapidly releasing of decomposed gases. After being burnt at 600°C for 2 minutes, the chars of the both samples retained their original geometrical shapes. It is different from the graphite oxide itself. The graphite oxide exploded when subjected to Bunsen flame.

A SEM image of the char of 50%GO + PEG1500 is shown in Figure 7.4. The char shows a layered net-work structure. The layered structure was composed of the graphene sheets of the intercalated GO, because only a limited amount of the char was formed from the PEG1500. This will be discussed in next paragraph. The fissures were left between the layered structures after the PEG1500 was burnt out. This micrograph indicates that the graphene sheets have dispersed well in the intercalated compound.

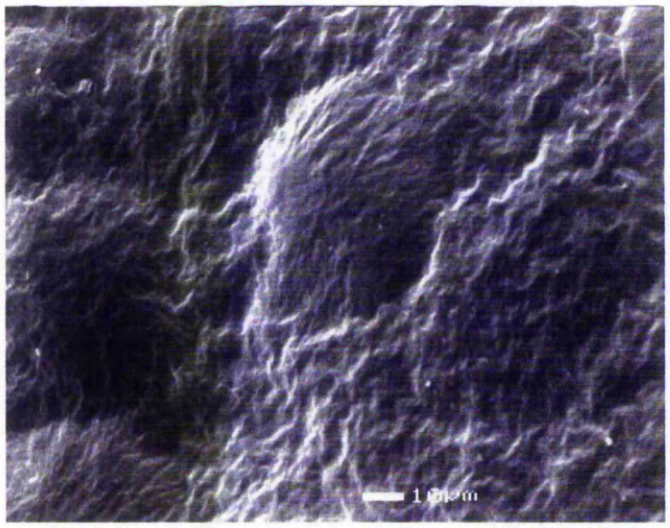

Figure 7.4 A SEM image of the char of 50%GO+PEG1500

The char yields of the samples burnt by natural burning and in the Muffle furnace are given in Table 7.3. The natural burning tests produced more chars than the burning in the Muffle furnace tests because a protective char layer formed above the sample resulting in incomplete burning, and the oxidation condition in the Muffle furnace was stronger than that of natural burning. The 50%GO + PEG1500 had a char yield of 27.8 wt.% by natural burning and 23.8 wt.% by burning in the Muffle furnace. The GO itself when heated in an inert atmosphere decreased in weight from 100 wt.% to 42.6 wt.% at 600°C (see Figure 6.17). Subtracting the char yield formed from the GO itself in TGA experiment from the figure for the 50%GO+PEG1500, the yield of char attributable to the PEG is 6.5 wt.% and 1.5 wt.% for natural burning and furnace test, respectively. These results show that there is a slight improvement in char yields when the PEG is intercalated between the graphene sheets.

Table 7.3 Char yields of natural and Muffle furnace burning

Sample	**Char Yield, wt%**					
	Natural Burning			**Muffle**		
	Total	**from GO**	**from polymer**	**Total**	**from GO**	**from Polymer**
PEG 1500	---	---	---	0	---	0
50%GO + PEG 1500	27.8	21.3	6.5	22.8	21.3	1.5
PVP	---	---	---	1.6	---	1.6
50%GO + PVP	49.6	21.3	27.3	35.7	21.3	14.4

The 50%GO+PVP produced significantly more char than the 50%GO+PEG1500. The char yields were 49.6% and 35.7% by natural burning and furnace burning, respectively. Taking out 21.3% of the char formed from the GO, 28.3% out of the char yield of natural burning and 14.4% out of the char yield of the Muffle furnace test were formed from the PVP. A further 0.8% can be subtracted due to the char formed when the PVP being burnt on its own, Table 7.3, resulting in char yields attributable to the PVP due to the nano-structure formation are 27.5% for natural burning and 13.6% for the furnace test. These results show that the intercalation of the PVP between the graphene sheets significantly improves the char forming ability

Both the PEG1500 and PVP intercalated GOs did not melt during burning and produced integrated chars. The char produced from the PVP intercalated GO is stronger and has a significantly higher yield. The difference in the char yields of the PEG and PVP intercalated GOs might be caused by their difference in the melting points and the molecular structures of the polymers. The PEG1500 has a very low melting point of 45°C, which results in the PEG1500 having a limited retentive time in the galleries of the graphene sheets during burning, and PEG has a linear molecular structure and forms little char on its own. In contrast, the PVP has not only much higher melting point (about 250°C) but also a heterocyclic structure. This may allow the PVP to remain for a longer time in the galleries of the graphene sheets to have a better opportunity to form char. These results indicate that the char formation of the graphite/polymer nanocomposites is dependent on the organic species intercalated between the graphite sheets.

7.4.2 The graphite/polyurethane nanocomposites

The synthesised graphite/polyurethane nanocomposites were investigated by the natural burning method. The original samples and their corresponding chars are shown in Figures 7.5 a to e. The pure polyurethane foam melted and flowed away during combustion. The residue had a random shape due to the flowing of the sample during combustion (Figure 7.5a). The foam containing 5.0 wt.% of graphite powder showed a similar burning behaviour to the pure PU foam, it also melted and flowed during combustion (Figure 7.5b). The original shape of both samples cannot be retained.

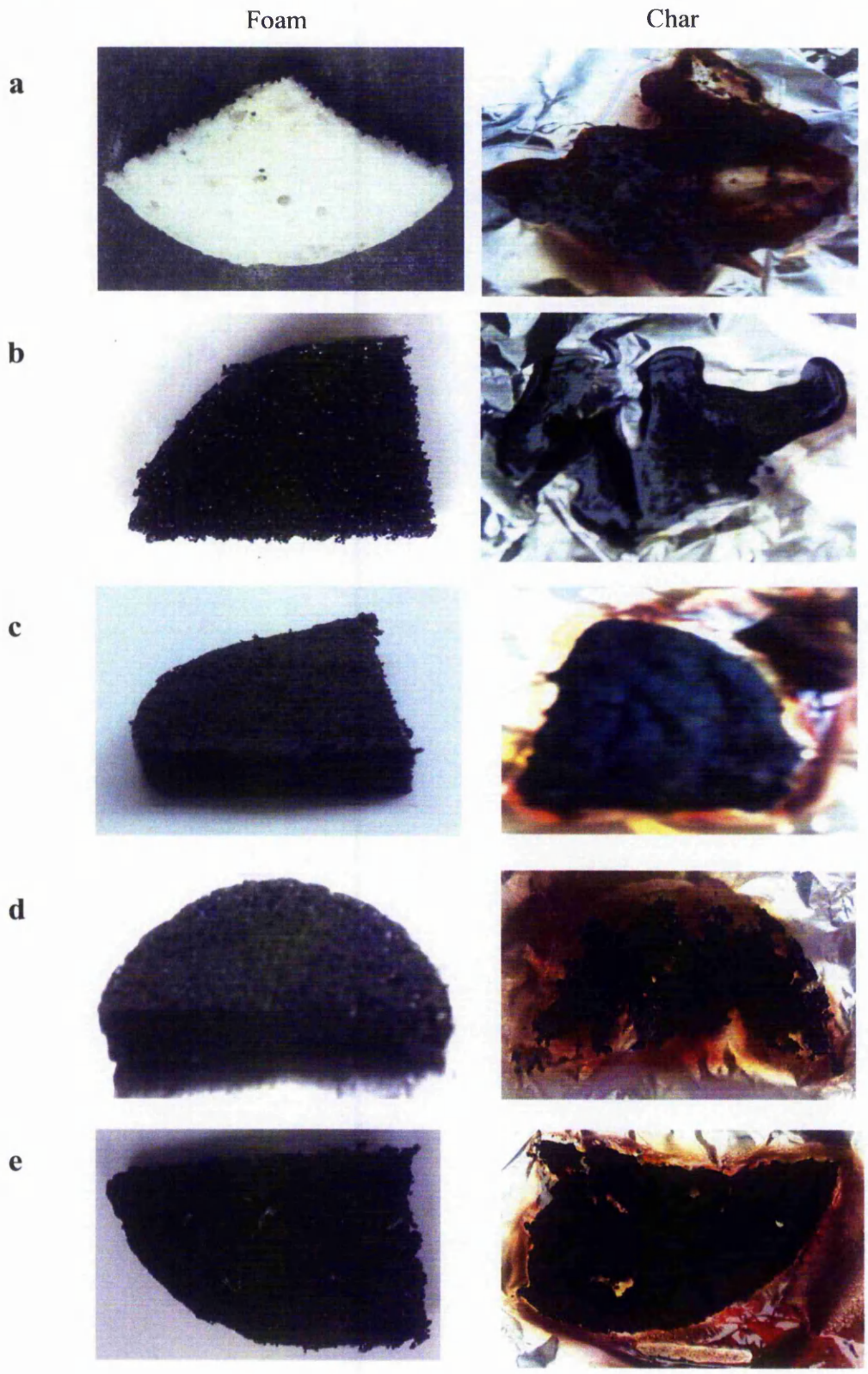

Figure 7.5 Nanocomposite foams and their natural burnt chars: (a) pure foam, (b) with 5% of graphite powder, (c) with 5.0 wt.% of GO, (d) with 10.0 wt.% of 50%GO+ PVP, (e) with 10.0 wt.% of 50%GO+PEG1500.

The nanocomposite foams exhibited different burning behaviour. They were easier to ignite with a Bunsen flame than the pure foam, and then slowly burned until the flame died away. The burning went on without any dripping and gave rise to integrated chars that had similar geometrical shapes to the original foams (Figures 7.5 c-e). The relatively easy ignition and slow burning process of the graphite/polyurethane nanocomposites are similar to the results of clay/polymer nanocomposites. [158,159] The nanocomposites formed solid chars at an early stage during the burning, which resulted in a slow and gentle, especially, non-dripping burning process.

The three nanocomposite foams yielded a large amount of chars by the natural burning test. The char yields were between 35.7% and 41.3%, as shown in Table 7.4. The chars produced from the foams containing 5.0 wt.% of GO and 10.0 wt.% of 50%GO+PVP were of significant bulk strength. The durometer hardness is 42A for the former and the 51A for the latter. The char made from the foam containing 10.0 wt.% of the 50%GO+PEG1500 was weaker. The char was left with holes made by the indentor after the durometer hardness measurement.

Table 7.4 Char yields of the synthesised PU foams

Foams	Natural burning		Muffle.
	Char Yield, wt.%	Duro Hardness	Char Yield, Wt.%
Pure PU300 II105			4.8
+ 5%PVP			5.1
+ 5% PEG1500			4.7
+ 5%Aldrich-P			8.2
+5%GO	41.3	42A	9.2
+ 10%(50%GO + PVP)	35.7	51A	11.3
+10%(50%GO+PEG1500)	36.9	20A(broken)	8.5

In general, the polyurethane nanocomposite foams were easier to ignite than the pure foam. But they formed a layer of char at the early stage of burning, which resulted in a slow and non-dripping burning process. The fire retarding mechanism is similar to that of some phosphorous-containing fire retardants in polyurethane systems, which decompose at lower temperatures than the pure polymer but form a layer of char at an early stage of burning resulting in fire retarding.[42] However, a 5.0 wt.% of GO in the polyurethane is sufficient to prevent the burning polymer from dripping and instead to form a layer of integrated rigid char.

The addition of the GO, 50%GO+PVP and 50%GO+PEG1500 improved the char morphology, char strength of the nanocomposite foams when tested by natural burning. The natural burning test is carried out under a less strong oxidation condition than furnace burning at high temperatures. Also the char formed in the natural burning test protects its underneath. To examine the char formation and char yields in a strong burning and oxidation circumstance, the PU foam samples were burned in a Muffle furnace at 600°C for 2 minutes. The char yields are also tabulated in Table 7.4. The data shows that the pure foam produced 4.8% of char after 2 minutes burning. The foam with 5.0 wt.% of Aldrich-P produced 8.2% of char. The char yield was 3.4% higher than that of the pure foam. This indicates that the added graphite powder did not entirely retain in the char and the addition of the graphite powder did not promote the char formation of the polyurethane.

The nanocomposite foams yielded approximately 10% of char. When the weight loss of the graphite oxide itself is taken into account, the equivalent amount of graphite in the foam is about 2.2%. Based on this calculation, the net increases in char yield are 2.2% for the foam with 5.0 wt.% of GO, 4.0% for the foam with 10.0 wt.% of 50%GO+PVP and 1.6% for the foam with 10.0 wt.% of 50%GO+PEG1500 after being burnt for 2 minutes. This increase in the char yield was due to the formation of the nanocomposite, because the addition of 5.0 wt.% of PEG1500 or PVP did not cause obvious changes in the char yields (Table 7.4).

The charring results of these foams indicate that the addition of the graphite powder does not alter the charring ability of the polyurethane foam. However, the addition of nano-structured graphites not only alters the char morphology, but also improves the char yield by 40% for 5.0 wt.% of GO and 10.0 wt.% of 50%GO+PEG1500; by 78%

for 10.0 wt.% of 50%GO+PVP compared to the char yields of the pure polyurethane foams, respectively.

The char of the PU foam with 5.0 wt.% of GO was examined by XRD and showed a XRD pattern of a graphitised carbon, Figure 7.6. The XRD pattern indicates that the polymer intercalated GO has changed back to a graphite structure after being heated at 600°C for 2 minutes. The 002 peak at 2θ=25.82° and the 100 peak at 2θ=43.02° indicate that the graphitisation of the char is not complete.

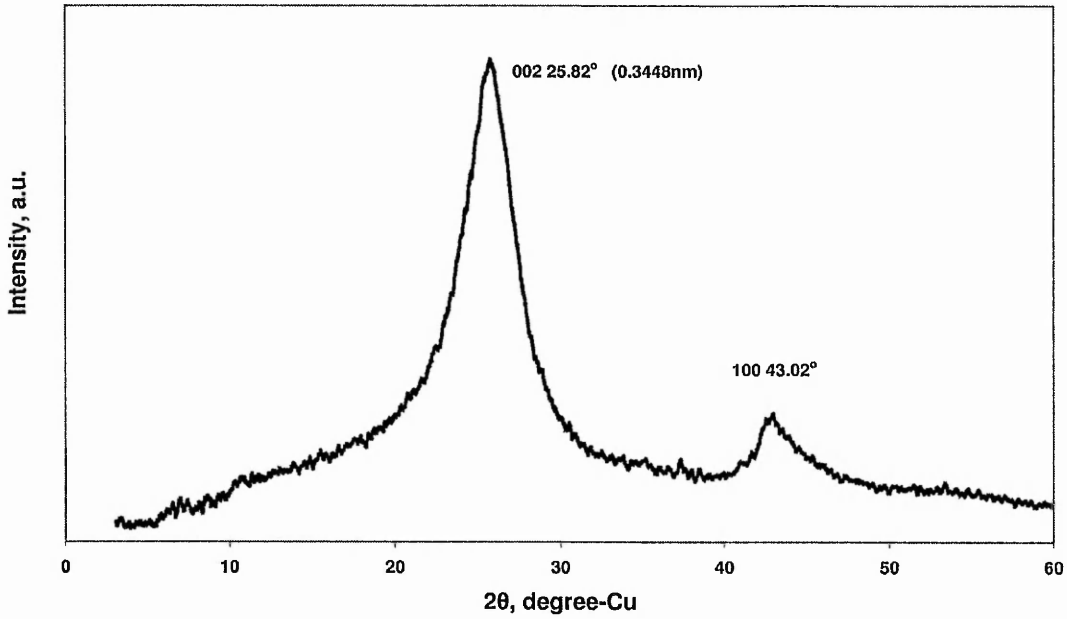

Figure 7.6 The XRD pattern of the char of the PU foam with 5 wt.% of GO, burnt at 600°C for two minutes.

7.4.3 The PEO intercalated graphite oxides

The PEO intercalated GOs with low GO loadings were cast into films in Chapter 6. The film samples have simpler morphology than samples in the form of foam. They are used to investigate the loading effect of the graphene sheets on the char formation of graphite/polymer nanocomposites in order to decrease influence factors.

The PEO films, which were intercalated with 0.5 wt.%, 1.0 wt.%, 3.0 wt.% or 5.0 wt.% of GO, were studied by natural burning. All the films experienced a similar burning

process. They ignited easily with a Bunsen flame and then self sustained the burning. After the burning flame died away, they produced black chars, which had similar geometries to those of the original films. The films and their chars are shown in Figures 7.7 a to d.

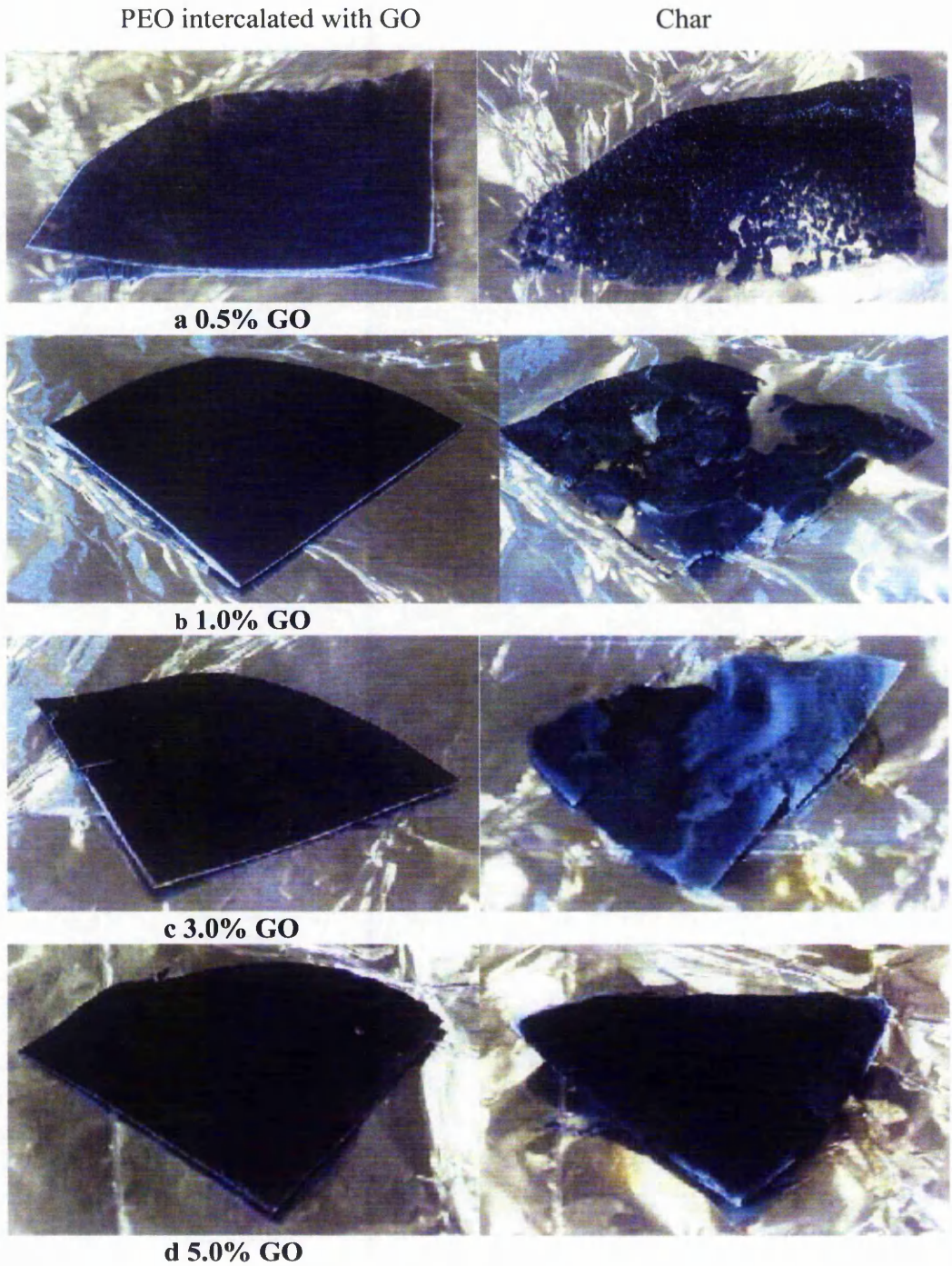

Figure 7.7 The PEO intercalated GO films and their naturally burnt chars

Besides the similarities in burning process, the GO loading affected solid phase reactions during the burning and the quality of the chars formed. During the burning, the PEO in the film with 0.5 wt.% of GO melted. Decomposed gases could be clearly observed bubbling out. The molten PEO did not drip. The char formed was disconnected (Figure 7.7a). When the GO loading increased to 1.0 wt.%, no melting and bubbling were observed during the burning. A piece of char with large cracks (Figure 7.7b) was produced. Compared to the char formed from the PEO film with 0.5 wt.% of GO, this char was better integrated. When the GO loading increased to 3.0 wt.% and 5.0 wt.%, the films burnt without any melting and bubbling. The chars produced were integrated (Figures 7.7 c & d). The char formed from the film with 3.0 wt.% of GO was fragile, while the char formed from the film with 5.0 wt.% of the GO was rigid and had a durometer hardness of 66.3A.

From the burning tests it can be seen that 1.0 wt.% of graphite oxide content is the threshold for preventing melting during combustion. The quality of chars was improved as the graphite oxide loading increased. A loading of 5.0 wt% of GO is sufficient to produce an integrated char with strength. This result is consistent with that of the graphite polyurethane nanocomposites, and can be used to formulate commercial fire retarding polymer nanocomposites.

7.5 Summary remarks

Graphite/polyurethane nanocomposites were synthesised via a route of dispersing nano-structured graphites in the polyol PEG300, and then polymerised with the diisocyanate TDI. The graphite/polyurethane nanocomposites synthesised combusted slowly without any dripping and produced integrated chars. The chars formed not only have identical geometrical shapes to the original samples, but also have strength and graphite-like structure. These properties are valuable in the design of a new generation of intumescent fire retarding polymer systems.

The study of the effect of graphite oxide loading on char formation shows that the threshold loading of graphite oxide is 1.0 wt.% to prevent polymer melting during combustion. A 5.0 wt.% graphite oxide loading is sufficient for producing an integrated intumescent char with strength.

The study of the charring ability of polymers in their graphite nanocomposites shows that the PVP produces significantly amount of char during burning, while the PEG1500 produces only a small amount of char. The charring ability of polymers in nanocomposites is dependent on the structure and properties of polymers.

Chapter 8

Conclusions and Suggestions for Future Work

8.1 Conclusions

Intumescent fire retardancy has been more and more widely applied in manufacturing commercial fire retardant polymer systems. It is more effective and environmentally friendly than other conventional fire retardancies. However, very little work has been done in the field of intumescent chars. Although there are some general characteristic techniques available, none was considered suitable for assessing the quality of intumescent chars in terms of fire retarding efficiency. The relationship between fire retarding efficiency and the char quality has not been established. These situations have hindered the further development of intumescent fire retarding polymer systems. Furthermore, to form an intumescent char, a large quantity of intumescent fire retardants has to be added into the polymer. Consequently, there is a significant reduction in the mechanical properties. This contradiction may be overcome by dispersing single graphite sheets in polymers to form graphite/polymer nanocomposites, which may improve polymer materials in both fire retardancy and mechanical properties.

In this research work, an intumescent mechanism study has been carried out based on the development of a number of characterisation techniques for intumescent chars. The characterisation techniques included an open porosity technique to characterise the gas permeability of chars, a durometry technique to assess the bulk strength of chars, microscopic methods to gain the information on char structures and X-ray diffraction analysis to characterise the carbon structure in the chars for their reactivity. A single direction well-ventilated natural burning method was also developed to produce intumescent chars that may map the whole charring process during burning. This burning method shows that the thickly saturated intumescent chars formed protect the underlying polymer. The protection efficiency of intumescent chars is evaluated by the difference between the char yields of natural burning and furnace burning.

The intumescent mechanism study of three commercial fire retarding polyurethane products showed that the three products contained inert inorganic additives, which were expandable graphite flakes, mica, glass beads and glass fibres. The inert inorganic additives, especially expandable graphite, act in a similar manner to charring promoters and blowing agents in conventional intumescent formulations. The charred polymer coats the inert inorganic additives, which allows an integrated and reinforced char to form. To obtain highly effective and strong intumescent chars, the charred polymer and the inorganic additives must be more intimately combined to have minimum porosity. The open porosity of intumescent chars determines the protection efficiency and strength of the char. The lower the open porosity, the better protection and strength the char has.

The protection efficiency-open porosity relationship shows that a char having an open porosity of less than 80% will have a high-level protection. While the products studied produced chars with open porosities ranging from 83% to 95%. The high open porosity is the char weakness of the current commercial products, which results in both lower protection efficiencies and strength of the intumescent chars. This may be improved either by optimizing the polyurethane structure and concentration in the products or by applying graphite/polymer nanocomposites. The optimized polymer system or graphite/ polymer nanocomposites should allow the charring polymer to coat the inorganic additives and to form a strengthened integrated char.

Graphite/polyurethane nanocomposites were synthesized and studied. Graphite is not suitable to be directly used in the nanocomposite synthesis due to its narrow interlayer spacing of graphite sheets and incompatible surface to polymers. Graphite was oxidized into graphite oxide to expand the interlayer distance of graphite sheets and to introduce some polar functional groups onto the graphite sheets to improve the compatibility between the modified graphite and polyurethanes. Five graphite sources with different flake lengths were studied and oxidized into graphite oxides by a modified Hummers and Offemen method. The different flake lengths of the graphites will result in different aspect ratios when the graphene sheets are dispersed in single sheets in polymers. Large graphite flakes (ca. 150 μm) were only partially oxidized into graphite oxides. Four graphite powder samples (with flake size less than ca. 15 μm) were oxidized evenly into graphite oxides. Among the four graphite powders studied, the Aldrich-P graphite

powder was chosen to produce graphite oxide for further study, because its flake lengths are relatively large, it may result in a larger aspect ratio of the graphene sheets when nanocomposites formed. The graphite oxide produced from the Aldrich-P was further modified into organo graphite oxide by intercalating with 50% of PEG1500 or 50% of PVP, which were coded as 50%GO+PEG1500, 50%GO+PVP, respectively. The graphite oxide and the two organo graphite oxides, together called nano-structured graphites, were used in the synthesis of graphite/polyurethane nanocomposites. The interlayer spacings of the nano-structured graphites were 0.83 nm for the graphite oxide, 1.48 nm for the 50%GO+PEG1500 and 2.23 nm for the 50%GO+PVP.

The graphite/polyurethane nanocomposites were synthesized by dispersing the nano-structured graphites in the polyol PEG300, and then polymerized with the diisocyanate TDI. The nanostructure of the polyurethane nanocomposite produced from the graphite oxide showed that the interlayer spacing of the graphene sheets increased to 1.26 nm. The polyurethane nanocomposites containing the organo graphite oxides did not further increase the interlayer spacing of the graphene sheets.

The fire retardancy of the organo graphite oxides and the three synthesised polyurethane nanocomposites was studied. Both organo graphite oxides produced integrated chars, and the chars had identical morphologies to the original samples. The study of their char yields indicated that the PVP intercalated graphite oxide produced a significant amount of char from the PVP, while the PEG1500 intercalated graphite oxide produced only a little char from the PEG1500. The polyurethane nanocomposites did not flow during burning and produced more char than the pure polyurethane. The chars formed had good continuity, strength and graphitic structures. These properties indicate a new generation of intumescent fire retarding polymer materials are possible.

A study of the effect of graphene sheet loading on the fire retardancy of its nanocomposites was carried out on a group of polyethylene oxide intercalated graphite oxides, whose graphite oxide loadings were ranged from 0.5 wt.% to 5.0 wt.%. The results showed that a 1.0 wt.% graphite oxide loading could avoid the nanocomposite melting. A 5.0 wt.% graphite oxide loading is sufficient to form an integrated char with strength.

8.2 Suggestions for future work

This research on graphite/polymer nanocomposites has demonstrated that all the synthesised nanocomposites with 5.0 wt.% of graphite oxide or equivalent or more not only have retarded burning behaviour, but also form strong integrated chars during burning. These fire retardant properties can be applied to formulate environmentally friendly commercial fire retarding products for various applications without affecting the mechanical properties. Polyurethanes are widely used commodity polymer materials. Graphite/polyurethane nanocomposites were synthesised via the intercalation of a polyol with graphite oxide. The investigation was only carried out on a polyethylene glycol Mn300 and tolylene diisocyanate polyurethane foam system. To commercialise graphite/polyurethane nanocomposites, following aspects should be studied.

- Intercalation of different types of polyol such as polyether polyols, polyester polyols, linear polyols or short-branched polyols into graphite oxide
- Intercalation of graphite oxide with polyols in solvent. It can be applied when directly intercalating polyol into graphite oxide is not applicable.
- Polymerisation of polyols that intercalated or partially intercalated with graphite oxide with either TDI or MDI or polymeric MDI to produce various polyurethane products

It is very attractive to synthesise non-porous graphite/polyurethane nanocomposites to study the improvement in strength, stiffness and fire retardancy at the same time. The effect of aspect ratio of graphene sheets on the improvement of mechanical properties and barrier properties is also a very important issue.

References

1. D. W. Van Krevelen, *Properties of Polymers, Chapter 26B, Flammability of Polymers*, Elsevier Scientific, NY, 1976
2. W. Bassett, *Proc. Fire Retardant Chemical Association Meeting*, San Antonio, TX, March, p.12, 1989
3. J. W. Gilman, S. M. Lomakin, T. Kashiwagi, D. L. VanderHart, and V. Nagy, *Fire and Materials* 22: 61, 1998
4. J. W. Gilman, S. M. Lomakin, T. Kashiwagi, D. L. VanderHart, and V. Nagy, *NIST Annual Conference on Fire Research*, Gaithersburg, MD, p.133, 1996
5. A. R. Horrocks and D. Price, *Fire Retardant Materials*, Woodhead Publishing/ CRC Press, 2001
6. A. Usuki, M. Kawasumi, Y. Kojima, A. Okada, T. Kutauchi and O. Kamigaito, *J. Material Research* 8: 1174, 1993
7. F. Gao, *Polymer Engineering Centre* [Online]. UK: The Nottingham Trent University. Available at http://www.facct.ntu.ac.uk/research/groups/pec/ [accessed 15 December 2000]
8. C. J. Hilado, *Flammability Handbook for Plastics*, 3rd edition, Westport, Conn.: Technomic, 1982
9. S. M. Lomakin and G. E. Zaikov, *Ecological Aspects of Flame Retardancy*, VSP International Science Publishers, Zeist, Netherlands, 1999
10. R. Rothon, *Particulate-Filled Polymer Composites*, Longman Scientific & Technical, 1995
11. J. W. Lyons, *The Chemistry and Uses of Fire Retardants*, Wiley, New York, 1970
12. QUALITEST™, Advanced Testing Technologies: *Limiting Oxygen Index Chamber* [Online]. Available at http://www.qualitest-inc.com/loi.htm [accessed 10 May 2004]
13. A. R. Horrocks, M. Tunc and D. Price, *Textile Progress* 18(1-3): 1, 1989
14. M. Nelson, *Short Articles on Combustion of Polymers*: *Oxygen-Index Methods* [online]. Australia: University of Wollongong. Available at: http://www.uow.edu.au/~mnelson/review.dir/oxygen.html [accessed 10 May 2004]
15. V. Babrauskas, *Fire and Material* 8(2): 81, 1984
16. V. Babrauskas and W. J. Parker, *Fire and Materials* 11:31, 1987
17. V. Babrauskas, *Ten Years of Heat Release Research with Cone Calorimeter* [online]. Fire Science and Technology Inc.. Available at http://www.doctorfire.com/cone.html [accessed 10 May 2004]
18. C. F. Cullis and M. M. Hirschler, *The Combustion of Organic Polymers*, Clarendon Press, Oxford, 1981

19. W. Watt and J. Green, *Carbon Fibres: Their composites and Applications, Plastics &Polymers Conference Supplement No. 5*, p23, Proceedings of the International Conference organised by the Plastics Institute, London, 2-4 February 1971

20. G. Woods, *The ICI polyurethanes book*, 2nd edition, Chichester - New York, ICI Polyurethanes and John Wiley & Sons, 1990

21. M. Szycher, *Szycher's Handbook of Polyurethane*, CRC press, 1999

22. N. M. K. Lamba, K. A. Woodhouse and S. L. Cooper, *Polyurethanes in Biomedical Applications,* CRC Press, 1998

23. W. D. Woolley, *Britain Polymer J.* 4: 27, 1972

24. W. D. Woolley, *J. Fire and Flame Combustion Toxicity* 1: 259, 1974

25. J. D. Ingham and N. S. Rapp, *J. Polymer Science.* A. 2: 4941, 1964

26. L. P. Rumao and K. C. Frisch, *J. Polymer Science* A. 10: 1499, 1972

27. S. T. Marks and E. Metcalfe, *Combustion and Flame* 107: 260, 1996

28. M. Ravey and Eli M. Pearce, *J. of Applied Polymer Science* 63: 47, 1997

29. M. Ravey, E. D. Weil, I. Keidar and E. M. Pearce, *J. of Applied Polymer Science* 68: 217, 1998

30. S. Foti, M. Giuffrida, P. Maravigna and G. Montaudo, *J. of Polymer Science: Polymer Chemistry Edition* 21: 1567, 1983

31. S. Foti, M. Giuffrida, P. Maravigna and G. Montaudo, *J. of Polymer Science: Polymer Chemistry Edition* 21: 1583, 1983

32. A. Ballistreri, S. Forti, P. Maravigna, G. Montaudo and E. Scamporrino, *J. of Polymer Science: Polymer Chemistry Edition* 21: 1923, 1983

33. S. Foti, M. Giuffrida, P. Maravigna and G. Montaudo, *J. of Polymer Science: Polymer Chemistry Edition* 19: 1679, 1981

34. F. Gao, D. Price, G. J. Milnes, B. Eling, C. I. Lindsay and P. T. McGrail, *J. of Analytical and Applied Pyrolysis* 40-41: 217, 1997

35. S. Tsuge and H. Ohtani, *Polymer Degradation and Stability* 58: 109, 1997

36. N. Grassie and A. P. Mendoza, *Polymer Degradation and Stability* 9: 155, 1984

37. K. J. Voorhees, S. F. Baugh and D. N. Stevenson, *J. Analytical and Applied Pyrolysis* 30: 47, 1994

38. C. Dick, E. Dominguez-Rosado, B. Eling, J. J. Liggat, C. I. Lindsay, S. C. Martin, M. H. Mohammed, G. Seeley and C. E. Snape, *Polymer* 42: 913, 2001

39. D.W. Krevelen, *Polymer* 16: 615, 1975

40. J. K. Backus, W. C. Darr, P. G. Gemeinhardt and J. H. Saunders, *J. Cellular Plastics* 1: 178, 1965

41. J. E. Kresta and K. C. Frisch, *J. of Cellular Plastics* 11: 68, 1975

42. K. C. Frisch and S. L. Reegen, *Flame Retardant Polymeric Materials*, Plenum Press NYS London, 1975

43. M. Ravey, E. D. Weil, I. Keidar and E. M. Pearce, *J. of applied Polymer Science* 68: 231, 1998

44. A. J. Papa and W. R. Proops, *J of applied Polymer Science* 16: 113, 1972
45. P. W. Wang, W.Y. Chiu, L. W. Chen, B. L. Deng, T. M. Don and Y. S. Chiu, *Polymer Degradation and Stability* 66: 307, 1999
46. T. C. Chang, Y. S. Chiu, H. B. Chen and S. Y. Ho, *Polymer degradation and stability* 49: 375, 1995
47. T. C. Chang, W. Y. Shen, Y. S. Chiu, H. B. Chen and S. Y. Ho, *J. of polymer Research* 1: 353,1994
48. T. C. Chang, W. Y. Shen, Y. S. Chiu and S. Y. Ho, *Polymer Degradation and Stability* 49: 353, 1995
49. N. Grassie and D. H. Mackerron, *European Polymer Journal* 16: 113, 1980
50. N. Grassie and D. H. Mackerron, *Polymer Degradation and Stability* 5: 43, 1983
51. N. Grassie and D. H. Mackerron, *Polymer Degradation and Stability* 5: 89, 1983
52. H. Piechota, *J. Cellular Plastics* 1: 186, 1965
53. N. Grassie and G. Scott, *Polymer Degradation and Stability*, Cambridge University Press, 1985
54. J. W. Gilman, T. Kashiwagi, R. H. Harris, Jr. S. Lomakin, J. D. Lichtenhan, A. Bolf and P. Jones, *Chemistry and Technology of polymer Additives*, Editored by M.A. Malden, S. AK-Malaika, A. Golovoy, C.A. Wilkie, Blackwell Science Inc., 1999
55. J. W. Gilman(n.d.), *PCT Int. Appl. PCT/US97/06440*
56. K. M. Butler, *ACS Symposium Series 66,* p 214, American Chemical Society, Washington, DC, 1997.
57. K. M. Butler, H. R. Baum and T. Kashiwagi, *International Association for Fire Safety Science. Fire Safety Science. Proceedings. Fifth (5th) International Symposium.* March 3-7, 1997, Melbourne, Australia, Intl. Assoc. for Fire Safety Science, Boston, MA, Y. Hasemi, Editor(s), p 523, 1997
58. E. D. Weil, R. H. Hansen, and N. Patel, *ACS Symposium Series 425*, p.97, American Chemical Society, Washington, DC 1990
59. A. R. Horrocks, *Polymer Degradation and Stability* 54: 143, 1996
60. A. R. Horrocks, S. C. Anand and B. J. Hill, *US Patent 5645926,* 1997
61. R. Delobel , N. Ouassou, M. Le Bras and J. M. Leroy, *Polymer Degradation and Stability* 30: 41, 1990
62. S. Bourbigot, M. Le Bras and R. Delobel, *Carbon* 31: 1219, 1993
63. S. Bourbigot, M. Le Bras and R. Delobel, *Carbon* 33: 283, 1995
64. S. V. Levchik, L. Costa and G. Camino, *Polymer Degradation and Stability* 36: 229, 1992
65. S. Duquesne, M. Le Bras, C. Jama, E.D. Weil and L. Gengembre, *Polymer Degradation and Stability* 77: 203, 2002
66. X. Almeras, M. Le Bras, P. Hornsby, S. Bourbigot, Gy. Marosi, S. Keszei and F. Poutch, *Polymer Degradation and Stability* 82: 325, 2003

67. T. Kashiwagi, J. W. Gilman, K. M. Butler, R. H. Harris, J. R. Shields and A. Asano, *Fire and Materials* 24: 277, 2000

68. S. Duquesne, M. Le Bras, S. Bourbigot, R. Delobel, G. Camino, B. Eling, C. Lindsay and T. Roels, *Polymer Degradation and Stability* 74: 493, 2001

69. S. Duquesne, R. Delobel, M. Le Bra and G. Camino, *Polymer Degradation and Stability* 77: 333, 2002

70. M. Bugajny, M. Le Bras and S. Bourbigot, *J. of Fire Sciences* 17: 494, 1999

71. M. Bugajny, M. Le Bras and S. Bourbigot, *J. of Fire Sciences* 18: 7, 2000

72. M. Bugajny, M. Le Bras, A. Noël and S. Bourbigot, *J. of Fire Sciences* 18: 104, 2000

73. H. D. Lutter, R. Zschiesche, H. J. Gabbert, V. Hasse and K. Fimmel, *US005739173A, Apr.14,* 1998

74. A. W. Atkinson, M. J. Walsh and J. A. Cooper, *GB2 226 033 A,* 1990

75. S. Duquesne, M. Le Bras, S. Bourbigot, R. Delobel, G. Camino, B. Eling, C. Lindsay and T. Roels, *Polymer Degradation and Stability* 74: 493, 2001

76. M. Modesti, A. Lorenzetti, F. Simioni and G. Camino, *Polymer Degradation and Stability* 77: 195, 2002

77. M. Modesti and A. Lorenzetti, *European polymer J.* 39: 263, 2003

78. H. Marsh, *Introduction to Carbon Science*, Butterworths, 1989

79. S. Reshetnikov, A. N. Garashchenko and V. L. Strekhov, *Polymer Advance Technology* 11: 392, 2000

80. S. Reshetnikov, M. Yu. Yablokova, E. V. Potapova, N. A. Khalturinskij, V. Ya. Chernyh and L. N. Mashlyakovskii, *J. of Aapplied Polymer Sciences* 67: 1827, 1988

81. B. Xiao, *PhD thesis*, University of Newcastle upon Tyne, 2004

82. H. O. Pierson, *Handbook of Carbon, Graphite, Diamond and Fullerenes*, William Andrew Publishing/Noyes, 1993

83. G.M. Jenkins and K. Lawamura, *Polymeric Carbons- Carbon Fibre, Glass and Char*, Cambridge University Press, 1976

84. F. N. Cogswell, *Thermoplastic aromatic polymer composites*, Butterworth Heinemann Ltd, 1992

85. F. Gao, *Nanocomposites 2002*, Sheraton San Diego Hotel & Marina San Diego, California, USA, September 23, 2002

86. B. Z. Jang, *Advanced Polymer Composites*: *Priuciples and Applications*, ASM International, 1994

87. S.V. Levchik, G. Camino, L. Costa and M. P. Luda, *Polymer Degradation and Stability* 54: 317, 1996

88. R. Tothon, *Particulate-Filled polymer composites*, Longman Scientific & Techanical, 1995

89. M. Alexander and P. Dubois, *Materials Science and Engineering* 28: 1, 2000

90. H. L. Cox, Britain, *J. of Application Physics* 3: 72, 1952

91. A. Kelly and W.R. Tyson, *High Strength Materials*, John Wiley &Sons, 1965

92. P. C. LeBaron, Z. Wang and T. J. Pinnavaia, *Applied Clay Science* 15: 11, 1999

93. G. D. Parfitt, *Dispersion of Powders in Liquids*, Applied Science Publisher, NJ, 1981

94. M. Rosoff, *Nano-Surface Chemistry*, Marcel Dekker, Inc. 2002

95. R. A. Vaia and E. P. Giannelis, *Macromolecules* 30: 7990, 1997

96. R. A. Vaia and E. P. Giannelis, *Macromolecules* 30: 8000, 1997

97. A. C. Balazes, C. Singh and E. Zhulina, *Macromolecules* 31: 8370, 1998

98. E. Manias, A. Touny, L. Wu, K. Strawhecker, B. Lu and T.C. Chung, *Chem. Mater.* 13: 3516, 2001

99. F. Gao, S. Chen and J. B. Hull, *J. of Materials Science Letters* 20: 1807, 2001

100. A. Usuki, M. Kawasumi, Y. Kojima, A. Okada, T. Kurauchi and O. Kamigaito, *J. Material Research* 8: 1174, 1993

101. A. Usuki, Y. Kojima, M. Kawasumi, A. Okada, Y. Fukushima, T. Kurauchi and O. Kamigaito, *J. Material Research* 8: 1179, 1993

102. Y. Kojima, A. Usuki, M. Kawasumi, A. Okada, T. Kurauchi and O. Kamigaito, *J. Polymer Science Part A: Polymer Chemistry* 31: 983, 1993

103. Y. Kojima, A. Usuki, M. Kawasumi, A. Okada, T. Kurauchi, O. Kamigaito and K. Kajik, *J. of Polymer Science Part B: Polymer Physics* 32: 625, 1994

104. Y. Kojima, A. Usuki, M. Kawasumi, A. Okada, Y. Fukushima, T. Kurauchi and O. Kamigaito, *J. of Materials Research* 8: 1185, 1993

105. Y. Kojima, A. Usuki, M. Kawasumi, A. Okada, T. Kurauchi and O. Kamigaito, *J. of Applied Polymer Science* 49: 1259, 1993

106. R. A. Vaia, H. Ishii and E. P. Giannelis, *Chem Mater* 5: 1694, 1993

107. R. A. Vaia, K. D. Jandt, E. J. Kramer and E. P. Giannelis, *Macromolecules* 28: 8080, 1995

108. R. A. Vaia, K. D. Jandt, E. J. Kramer and E. P. Giannelis, *Chem Mater* 8: 2628, 1996

109. L. M. Liu, Z. N. Qi and X.G. Zhu, *J. of Applied Polymer Science* 71: 1133, 1999

110. T. D Fornes, P. J. Yoon, D. L. Hunter, H. Keskkula and D. R. Paul, *Polymer* 43: 5915, 2002

111. A. Usuki, A. Koiwai, Y. Kojima, M. Kawasumi, A. Okada, T. Kurauchi and O. Kamigaito, *J. of Applied Polymer Science* 55: 119, 1995

112. Y. Kojima, T. Matsuoka, H. Takahashi and T. Kurachi, *J. of Applied Polymer Science* 51: 683, 1994

113. L. J. Mathias, R. D. Davis and W. L. Jarrett, *Macromolecules* 32: 7958, 1999

114. T. X. Liu, Z. H. Liu, K. X. Ma, L. Shen, K. Y. Zeng and C. B. He, *Composites Science and Technology* 63: 331, 2003

115. M. Ito, K. Mizuochi and T. Kanamoto, *Polymer* 39: 4593, 1998

116. H. R. Dennis, D. L. Hunter, D. Chang, S. Kim, J. L. White, J. W. Cho and D. R. Paul, *Polymer* 42: 9513, 2001

117. Y. X. Pan, Z. Z. Yu, Y. C. Ou and G. H. Hu, *J. Polymer Science Part B: Polymer Physics* 38: 1626, 2000

118. G. H. Chen, D. J. Wu, W. G. Wang and W. L. Yan, *J. of Applied Polymer Science* 82: 2506, 2001

119. W. G. Zheng, S. C. Wong and H. J. Sue, *Polymer* 73: 6767, 2002

120. W. G. Zheng and S. C. Wong, *Composites Science and Technology* 63: 225, 2003

121. G. H. Chen, D. J. Wu, W. G. Weng, B. He and W. L. Yan, *Polymer International* 50: 980, 2001

122. G. H. Chen, C. L. Wu, W. G. Weng, D. J. Wu and W. L. Yan, *Polymer* 44: 1781, 2003

123. G. H. Chen, D. J. Wu, W. G. Weng, and W. L. Yan, *Polymer Engineering Science* 4: 2148, 2001

124. F. M. Uhl and C. A. Wilkie, *Polymer Degradation and Stability* 76: 111, 2002

125. M. Xiao, L. Y. Sun, J. J. Liu, Y. Li and K. C. Gong, *Polymer* 43: 2245, 2002

126. U. Hofmann and A. Frenzel, *Z. Elektrochem.* 37: 613, 1931

127. Y. Matsuo, K. Tahara and Y. Sugie, *Carbon* 34: 672, 1996

128. Y. Matsuo, K. Tahara and Y. Sugie, *Carbon* 35: 113, 1997

129. Y. Matsuo, K. Tahara and Y. Sugie, *Chem. Mater.* 10: 2266, 1998

130. J. Y. Xu, Y. Hu, L. Song, Q. A. Wang, W. C. Fan, G. X. Liao and Z.Y. Chen, *Polymer Degradation and Stability* 73: 29, 2001

131. P. Xiao, M. Xiao, P. G. Liu and K. C. Gong, *Carbon* 38: 626, 2002

132. J. Y. Xu, Y. Hu, L. Song, Q. A. Wang and W. C. Fan, *Material Research Bulletin* 36: 1833, 2001

133. J. Y. Xu, Y. Hu, L. Song, Q. A. Wang and W. C. Fan, *Carbon* 40: 2961, 2002

134. J. W. Gilman, T. Kashiwagi and J. D. Lichtenhan, *SAMPE Journal*, 33: 40, 1997

135. J. W. Gilman and T. Kashiwagi, In: Polymer-clay nanocomposites. T. J. Pinnavaia and G. W. Beall editors. New York: John Wiley & Sons; pp193-206, 2000

136. J. W. Gilman, T. Kashiwagi, S. Lomakin, E. P. Giannelis, E. Manias, J. D. Lichtenhan and P. Jones, In fire retardancy of polymers: the use of intumescence pp.203, The Royal Society of Chemistry, Cambridge, 1998

137. J. Lee and E. Giannelis, *Polymer Preprints*, 38: 688, 1997

138. P. B. Messersmith and E. Giannelis, *Chem. Mater.* 6: 1719, 1994

139. J. Zhu, F. M. Uhl, A. B. Morgan and C. A. Wilkie, *Chem. Mater.*, 12: 4649, 2001

140. J. Wang, J. Du, J. Zhu and C. A. Wilkie, *Polymer Degradation and Stability*, 77: 249, 2002

141. J. Du, J. Zhu, C. A. Wilkie and J. Wang, *Polymer Degradation and Stability* 77: 377, 2002

142. J. Du, D. Wang, C. A. Wilkie and J. Wang, *Polymer Degradation and Stability* 79: 319, 2003

143. J. W. Gilman, T. Kashiwagi, M. Nyden, J. E. T. Brown, C. L. Jackson, S. Lomakin, E. P. Giannelis and E. Manias, *Chemistry and Technology of Polymer Additives*, Blackwell Science Inc. p249, 1999

144. H. Lipson and H. Steeple, *Interpretation of X-ray powder diffraction patterns*, London, Macmillan, 1970

145. W. S. Hummers and R. E. Offeman, *J. of Amer. Chem. Soc.*, 1339 (1958)

146. M. S. Dresselhaus, *Festkoerperprobleme* xxv p21, 1985

147. G. L. Ruess, *Kolloid J.* 110: 17, 1945

148. A. Clauss, R. Plass, H. P. Boehm and U. Hofmann, *Z. Anorg. Chem.* 291: 14, 1957

149. A. Lerf, H. He, M. Forster and J. Klinowski, *J. Phys. Chem.* B 102: 4477, 1998

150. F. Aragón and J. M. Cowley, *Nature* 196: 468, 1962

151. S. S. Barton, G. L. Boulton and B. H. Harrison, *Carbon* 10: 395, 1971

152. N. Ogata, S. Kawakage and T. Ogihara, *J. Applied Polymer Science* 66: 573, 1997

153. R. L. Parfitt and D. J. Greenland, *Clay Mineral* 8: 305, 1970

154. X. Zhao, K. Urano and S. Ogasawara, *Colloid Polymer Science* 267: 903, 1989

155. E. Ruiz-Hitzky, P. Aranda, B. Casal and J.C. Galván, *Advanced Materials* 7: 1995

156. E. P. Giannelis, R. Krishnamoorti and E. Manias, *Advances in Polymer Science*, Vol. 138, Polymers in confined environments. 1999, p 107-147

157. D. Majumdar, T. N. Blanton and D. W. Schwark, *ECM proceedings, Nanocomposites 2001*, June 25-27, 2001 Chicago, Illinois USA

158. J. W. Gilman, T. Kashiwagi and J.D. Lichtenhan, *Sample Journal* 33: 40, 1997

159. J. W. Gilman, *Applied Clay Science* 15: 31-49, 1999